

Measuring Short-range Forces Using Levitated Nano-particles

O. Abbas¹, N. Bagherzahed Akbari¹, A. Breabout¹, P. Brown¹, A. Groth¹, J. Nasiruddin¹, D. Nasrollahi Shirazi¹, and M. Raees Usman¹

¹ *Dept. of Physics & Astronomy, University College London, Gower St, Kings Cross, London WC1E 6BT*

October 7, 2020

Contents

I EXECUTIVE SUMMARY	4
II GROUP METHODOLOGY	5
III BACKGROUND	7
1 Introduction	7
2 The Vacuum	7
2.1 The Vacuum in Modern Quantum Field Theory	7
2.2 Vacuum Catastrophe/Cosmological Constant Problem	7
3 Macroscopic Forces from a Microscopic Perspective	8
4 The Casimir Force	9
4.1 Attractive vs Repulsive Casimir Force	11
4.2 Drude and Plasma Models	11
4.3 Thermal Casimir Force	12
4.4 Applications of the Casimir Force	12
5 Casimir Force Past Experiments	14
5.1 Experimental Considerations for the Casimir Force	14
5.2 Initial measurements	16
5.3 Investigations into different geometries and the resultant Casimir Force	21
5.4 Novel Methods of Force Detection: Optical Levitation	27
5.5 Summary	30
6 Non-Newtonian Gravitational Force	31
6.1 Measurement of the Non-Newtonian Gravitational Force	31
6.2 Using Casimir Forces to Measure Non-Newtonian Gravitational Force	31
7 Optically Trapped Levitated Nanoparticles	32
7.1 Optical Traps	32
7.2 Levitated Nanoparticles for Casimir Force Experiments	32
IV SIMULATIONS: SETTING THE TRAP	33
1 The Motivation	33
1.1 The Basis of the Simulation	33
V EXPLORING COLLISIONS	38
1 Introduction	38
2 Field Ionisation of molecules	38
2.1 Dielectric Barrier Discharges	40
2.2 Sharp Point Electric Fields	41
3 Calculations	42
3.1 Particle Collisions	42
3.2 Trapped Nanoparticle	42
3.3 Incoming Particles	43
3.4 Final Particle Chosen	44
3.5 Simulating Gas Collisions	44
3.6 Simulating Projectile Collisions	46
3.7 Assumptions and Approximations of the Simulation	47
4 Conclusion of Findings So Far	48
VI REPULSIVE CASIMIR EXPERIMENT	48
1 The apparatus	49
2 Preliminary Procedure: Trapping the Nanoparticle	50
3 Casimir Force Experiment	51
4 Experimental Problems	51
4.1 Probability of trapping the particle	51
4.2 Mounting the pinhole plates	51
4.3 Electrostatic Patches	52
4.4 Risk of Gold Melting	52

VII COMPARISON OF CALCULATIONS AND SIMULATIONS	53
1 Simulating the Casimir Potential	53
2 Experimental Data	54
3 Comparison	54
VIII Data Analysis	54
1 Data Gathered	54
2 Power Spectral Density	55
3 Signal Problems	57
4 Band Filters	57
IX FINAL SUMMARY	59
X APPENDICES	68
1 Code	68
2 Finances	76
3 Contingency Plan	76
4 Risk Assessment	77
5 Safety Certificates	81
6 Agenda and minutes	89
XI ACKNOWLEDGMENTS	118

I EXECUTIVE SUMMARY

The project brief was to measure short range forces that can be investigated using 100 nm nanoparticles levitated in high vacuum. A thorough survey of literature was conducted to understand the origin of short range dispersion forces (e.g. the Casimir force) as well as the non-Newtonian gravity force. The experimental considerations for a variety short range forces were investigated to aid in choosing which to explore further, leading us to eventually focus on the measurement of the Casimir force. The use and operation of optical tweezers to trap nanoparticles and the theory behind nanoparticle levitation was researched to enhance the understanding and eventual employment of these principles.

By splitting up the team into two groups; concerned with calculations and simulations respectively, the group explored one avenue of investigating short ranged forces which was the calculating momentum and energy changes in collisions between a levitated nanoparticle and a range of projectile particles. While several particles were considered as candidates for the projectile particles, the calculations, simulations and practical considerations supported the use of alpha (α) particles and Sulfur Hexafluorine (SF_6) molecules, as they would produce a measurable perturbations to the nanoparticles oscillation.

A simulation was created with an initial aim to investigate the response of an optically trapped nanoparticle's oscillations to these collisions. This was accomplished by creating a dynamical animation of how the nanoparticle oscillates along three independent axes of motion, due to the three dimensional harmonic potential formed by the optical tweezers. Numerical integration in the form of the velocity Verlet scheme [1] was used to extract this oscillatory motion from the classical equations of motion within Python. The behaviour of the nanoparticle was analysed graphically in real time, to visually see the effects of the collisions with the incoming particles through position and velocity-time graphs. This confirmed that the method of optical trapping was sensitive enough to detect such small scale forces.

Subsequently, stochastic background gas collisions were introduced to the simulation in addition to a driving term due to thermal forces, and a damping term was also implemented. A decay of the amplitude of oscillations on each of the three independent axes was observed, with a characteristic envelope determined by the damping term as predicted. Also, the thermal driving term implemented provided a floor to the amplitude of motion. This Brownian motion induced by background collisions can be used to calibrate short range forces.

The next step was to review experimental set-ups used to measure the Casimir force specifically. After consideration, the group selected the 'The Repulsive Casimir Force with Metallic Ellipsoid Structure' [2] experiment to carry out due to its favourable geometry that lends itself to the measurement of both the attractive, and repulsive Casimir force. The experiment was split into two distinctive sections 1) trapping the nanoparticle 2) measurement of the repulsive Casimir force.

The simulation was then modified to implement the Casimir force. This was accomplished by isolating experimental Casimir force-distance data from previous experiments [2] and then using a regression model to fit a polynomial representing the force as a function of distance to the data. This expression for the repulsive Casimir force was implemented into the simulation.

After conducting the first segment of the experiment, a power spectral density was derived from the experimental nanoparticle position and frequency data. (TALK ABOUT HOW SIMULATION PSD WAS DERIVED). Comparisons between the experimental and simulated power spectral densities (COMPARE)

Due to the outbreak of the corona-virus, the group was unable to conduct the second part of the experiment for the measurement of the repulsive Casimir force which has had a significant adverse impact on the project.

II GROUP METHODOLOGY

Omar Abbas:

- Communications officer
- Experimental - helped conduct experiment
- Writing of 'Field Ionisation of Molecules'
- Writing of 'Chosen Experiment' except from: 'Electrostatic Patches' & 'Risk of Gold Melting'
- Writing of 'Final Summary'
- Lead poster creation

Nima Akbari:

- Experimental- helped conduct experiment
- Writing of 'Casimir Force Past Experiments'
- Edited, formatted and supervised all LaTex code written
- Compiled References in BibTex
- Lead poster creation
- Edited and proof read final report

Arthur Breabout:

- Main Minute Taker
- Experimental logistics - helping acquire source materials required for experiment
- Writing of 'Applications of the Casimir Force'
- Writing of 'Electrostatic Patches' & 'Risk of Gold Melting'
- Compiling of appendices
- Lead poster design

Peter Brown:

- Chief Programmer and Head of Simulations
- Writing of 'Simulations' section
- Lead poster creation
- Edited and proof read final report

Alex Groth:

- Collision calculations
- Casimir & Optical potential data and plotting
- Writing of 'Optical Traps'
- Writing of 'Calculations'
- Writing of 'Final Summary'
- Poster writing

Yanek Nasiruddin:

- Collision calculations

- Data analysis of experimental results
- Writing of 'Comparison of Calculations and Simulations'
- Poster writing

Dorsa Nasrollahi Shirazi:

- Agendas and chairing of meetings
- Co-ordinating and supervising delegation of tasks and group organisation
- Collision calculations
- Experimental - helped conduct the experiment
- Final report outline
- Writing of 'Background' except from: 'Applications of the Casimir Force', 'Optical Traps' and 'Levitated Nanoparticles'
- Writing of 'Executive Summary'
- Lead poster creation
- Edited and proof read final report

Muhammad Raees Usman:

- Simulations
- Writing of 'Simulations'
- Writing of 'Executive Summary'
- Poster review

III BACKGROUND

1 Introduction

The exploration of small and short ranged forces is essential in further understanding areas such as nanotechnology, aeronautics, detection of forces such as gravity at short separations, as well as dark energy candidates [3]. The short-ranged force dominant in the context of charged particles is the attractive electrostatic Coulomb force, arising from the interaction of a charged particle near a surface with its image charge [4]. This survey of literature will be concerned with forces many orders of magnitude below this; mainly the different forms of dispersion forces and gravity at sub-millimetre length scales. Furthermore, the use and operation of optical traps as well as the levitation of nanoparticles will be explored.

2 The Vacuum

2.1 The Vacuum in Modern Quantum Field Theory

According to quantum field theory predictions, the vacuum is not empty of matter and exempt of fluctuations despite previous assumptions. It in fact reflects properties of all particles since these are just excitations of quanta fields [5]. Each point in the field can be considered as a simple harmonic oscillator (SHO), and after quantization, a quantum harmonic oscillator (QHO).

The classical perception that a vacuum was empty space had already come under question following the dawn of statistical mechanics, proposing that space is filled with black body radiation which exerts pressure on cavity boundaries [3]. In 1900, Max Planck published his first quantum law intended to provide an explanation for the properties of this thermal radiation. His law gave the energy per electromagnetic mode as $E = n\hbar w$ where $n = \frac{1}{e^{\frac{\hbar w}{k_B T}} - 1}$ is the number of photons per mode, \hbar the reduced Planck's constant, w the angular frequency, k_B the Boltzmann's constant and T the temperature. Note that $\hbar w$ is the energy per photon [6].

Planck published a revised version of the equation in 1911 after conducting a deeper examination of the interaction between matter and radiation. This equation included an extra term ($\frac{\hbar w}{2}$) eluding to the 'zero-point' energy present in the black body radiation, which is simply the lowest energy a QHO can have, such that now [6]:

$$E = \left(\frac{1}{2} + n \right) \hbar w \quad (1)$$

The significance of this equation can be understood by examining its form when $T = 0$, where the thermal fluctuation term disappears, leaving only the zero-point energy. This difference in energy between the laws is due to vacuum fluctuations [6].

These fluctuations can be considered real electromagnetic fields propagating in space with the speed of light. They continuously fluctuate around the mean zero-point energy $\frac{\hbar w}{2}$.

The assumptions used in Planck's derivation would not hold today. However, in 1912 Einstein and Stern produced what can now be credited as the first satisfactory argument, in a paper exhibiting how Planck's second law was consistent with the classical limit at high temperatures [7].

2.2 Vacuum Catastrophe/Cosmological Constant Problem

Nernst was the first to highlight that vacuum fluctuations should exist for all field modes in a paper published in 1916, remarking that the classical notion of being able to attain empty space in principle by removing all matter, and setting $T = 0$ must be dismissed. Additionally, he commented that the existence of this zero-point energy would be challenging for gravitation theory [8].

Although there is no problem with the sum of the vacuum energy over all field modes being infinite, a problem arises when it is noted that the finite sum attained after introducing a cut-off frequency is still much larger than what is observed through gravitational phenomena. In fact, any value set as the frequency cut-off produces the same difficulty [9].

This led the respectable scientist Pauli to question the existence of vacuum fluctuations in his book *Wave mechanics*. It cannot be denied that these fluctuation energies do not contribute to gravity in an ordinary way, otherwise, the observable universe would not be recognisable. However, through various atomic and subatomic experiments it is known they can be emitted, absorbed and scattered [9].

Since 1916 there has been an ongoing discrepancy between quantum theories and the classical theory of general relativity, which saw Einstein introduce the cosmological constant to explain the acceleration of the universe's expansion [10]. This has yet to be resolved and is termed the vacuum catastrophe/cosmological constant problem [6].

3 Macroscopic Forces from a Microscopic Perspective

Van der Waals forces are the attractive forces amongst atoms, and between components of two bodies separated by R , at microscopic length scales [11].

Using a quantum mechanical approach, London showed in 1930 that these occur due to the non-retarded (non-relativistic) dipole-dipole interactions, with a $1/R^6$ law for energy interaction at large distances [12]. The force arises when a spontaneous dipole moment p_1 of an atom produces a dipole electric field, which in turn induces a dipole moment p_2 in an adjacent atom. Depending on the orientation of the dipoles, this produces attraction between the atoms as shown in Fig. 1a.

Van der Waals forces assume two essential approximations which are not always valid [13]:

- **Quasi-static approximation**

This assumes that the induced polarization takes place instantaneously, an assumption only valid if the separation is significantly smaller than the wavelength of the fluctuating fields. At distances larger than this wavelength, the effect of the finite wave propagation speed c (retardation effects) must be considered.

- **Ignoring multiple scattering effects**

This approximation ignores the effect of multiple scattering events between particles. When there are two or more atoms, there will be numerous dipole electric fields and hence induced polarizations, as depicted in Fig. 1b.

Consideration of the retardation effects and application of QED led to the treatment of the Casimir-Polder force published in 1948, which altered London's law to $1/R^7$ for large separations. In the same paper, they completed calculations with a macroscopic body by measuring the force between a polarized atom and perfect metal plate [14].

In 1948, Casimir extended this macroscopic force to calculations of vacuum fluctuation pressure between two conductive plates [15]. This force includes the effects of multiple scatterings, shown in Fig. 1c, since they become substantial in the limit of the many atoms in two solid bodies. Therefore, there is no two-body relation that can be summed over all atoms to give the total effect, making these forces non-additive.

The Casimir and van der Waals force can be used interchangeably since the latter constitutes the regime where bodies are close enough to each other that the speed of light is effectively infinite [16]. These forces are collectively known as dispersion forces [17]. Specifically, the Casimir-polder and Casimir forces are termed 'long-ranged retarded dispersion van der Waals forces' [18].

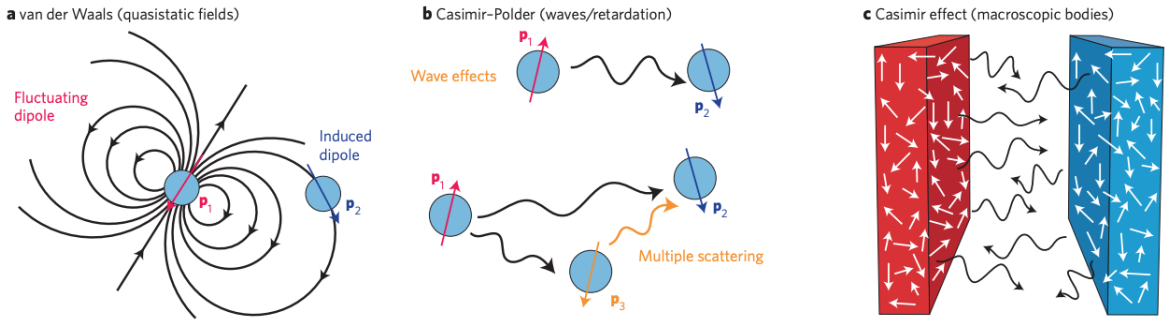


Figure 1: **a)** This image depicts van der Waals forces between two atoms after one fluctuating dipole p_1 , creates an electromagnetic dipole field, which subsequently induces a fluctuating dipole p_2 in an adjacent atom. **b)** At larger atom separations, the wave retardation effects must be considered, leading to the Casimir-Polder force. When more than two atoms are involved, the multiple scattering effects explains its non-additive nature. **c)** When macroscopic bodies are involved, the Casimir force arises between them due to the interaction of many fluctuating dipoles in the bodies. Reproduced from [13, Fig. 1]

In 1955, Evgeny Lifshitz developed the most generalised relativistic form of the van der Waals interaction, applicable to a body at any finite temperature and with any dielectric properties [19]. Lifshitz derived the Casimir force for real metals and not just ideal metals. He also predicted that this force can be repulsive, a topic which will be discussed further in the review.

4 The Casimir Force

This well-defined notion of the vacuum being filled with permanent vacuum fluctuations at all frequencies has several observable manifestations in microscopic and macroscopic physics [20]. The Casimir force, arising from the radiation pressure exerted when they are ‘contained’ between two perfect metal plates, is the most accessible experimental macroscopic consequence [21]. It is the dominant force between two neutral non-magnetic plates.

As discussed, there are difficulties associated with the intersection of quantum and gravitation physics due to the existence of quantum fluctuations. Therefore, it is of utmost importance that the consequence of these fluctuations is measured to a high degree of accuracy. Fig. 2 displays vacuum oscillations between two ideal metal plates where the boundary conditions have selected the oscillations.

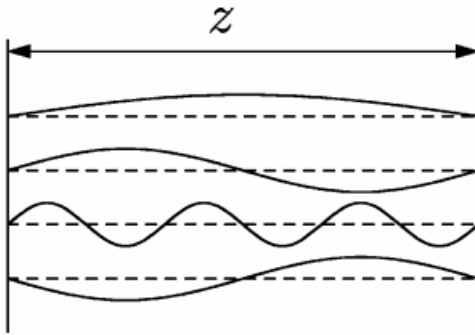


Figure 2: This image depicts vacuum oscillations between two metal plates. There are less electromagnetic modes inside rather than outside the plates, meaning the radiation pushes the plates together. The only electromagnetic modes that can exist within the cavity are those which have nodes on both walls. Reproduced from [22, Fig. 2]

The aggregate of these oscillations is equal to infinity, which itself does not pose any difficulties. In all fields of physics, apart from gravitation, energies are defined until an additive constant.

It is commonly accepted that physical energies are measured from the top of this infinite well. Therefore, to compute physical energies, the infinite vacuum energy of space must be subtracted from the infinite result. The Casimir force is the negative derivative of this finite energy with respect to separation [22].

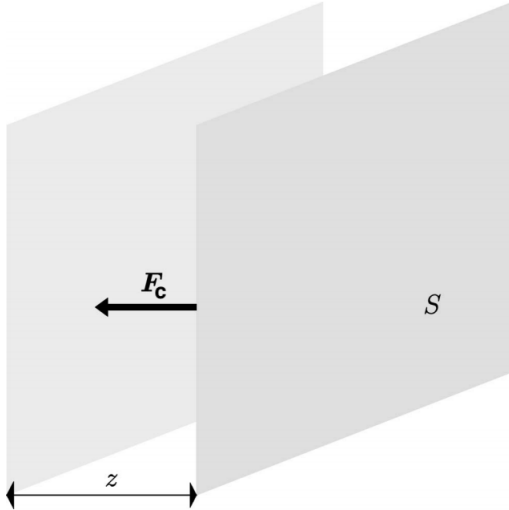


Figure 3: Image showing the Casimir force F_C acting on two perfectly reflective, non-magnetic, parallel plates with surface area S in a vacuum at $T = 0$ separated by distance z . Edited from [22, Fig. 1]

The energy (E_c) per unit area Casimir predicted in 1948 by summing the electromagnetic field modes of a cavity between two neutrally charged, perfectly reflective parallel metallic plates with separation z in a vacuum at $T = 0$ takes the form [21]:

$$E_c = \frac{\hbar c \pi^2 S}{720 z^3} \quad (2)$$

The force per unit area between the plates is (F_c):

$$F_c = -\frac{dE_c}{dz} = \frac{\hbar c \pi^2 S}{240 z^4} \quad (3)$$

where c is the speed of light and S the surface area of the plates. The area of the plates is assumed to be much larger than the separation ($S \gg z$). It is worth noting that the sign convention used is the reverse of thermodynamic conventions to ensure the quantities are positive: a negative pressure corresponds to a positive force [20].

By assessing the above equation, it can be inferred that the Casimir force is a quantum and relativistic phenomena due to the dependence on \hbar and c respectively. The unusual property of this force emerges when it is noted that in classical electrodynamics, no net force is predicted to act between uncharged conducting plates.

Both classically, and in the quantum realm, all forces are dependent on charges or an interaction constant. For instance, the gravitational force depends on mass whilst the electric force depends on charge. The Casimir force in contrast depends only on the fundamental constants mentioned, and the geometrical parameter z . The magnitude of this force is indicative of the macroscopic scale with $z = 1 \mu\text{m}$ producing pressure $P = 1.3 \text{ mPa}$ [22]. Moreover, the force is independent of the fine structure constant present in the van der Waals force expression, a property derived from the perfect reflection assumption made during the derivation by Casimir [21].

The action of the vacuum resulting in the force acting between two bodies is the static Casimir effect [23], whilst the Casimir effect in the presence of accelerated boundaries is known as the dynamic Casimir effect [24].

The reference to the vacuum energy when discussing the Casimir force is merely a calculation

aid and an effective macroscopic description of the force. The only correct formulation is the one computed using van der Waals forces given it is the true origin of the force [25]. Thus, it must be emphasised that the Casimir force cannot be taken as evidence for the existence of vacuum fluctuations [26].

4.1 Attractive vs Repulsive Casimir Force

The most common form of the Casimir force is when it is attractive and corresponds to negative radiation pressure between two metallic plates separated by a vacuum [20]. For an identical configuration but with dielectric half-spaces divided by a vacuum, the force is similarly always attractive.

To assess the possibility of the repulsive Casimir force, the key is to focus on the dielectric permittivity of the medias. If these dielectric permittivities are different, the force can be repulsive. More specifically, the dielectric of one plate must be higher than a surrounding liquid, whilst the other plates' dielectric should be lower than the surrounding. Simply put, the ordering of dielectric properties of materials as opposed to their shape determines whether the force is negative or not [17].

Another way of observing the repulsive Casimir force is by changing the geometry of the experiment. One experiment that demonstrates this uses a metallic needle-like particle above a metal plate with a hole [27], and will be discussed in more detail later.

4.2 Drude and Plasma Models

This section assesses the question: what model of the dielectric constant dispersion should be used to calculate the Casimir force?

Since metal plates are commonly used in short-range force experiments, it is instructive to note that their force is dependent on the optical properties of the reflective surface, which in turn alters based on the dielectric function. These dielectric functions are written at imaginary frequencies $w = i\xi$, and can be understood as a sum of conduction band electrons and inter-band transition contributions [9].

$$\epsilon(w) = \hat{\epsilon}(w) - \frac{\sigma(w)}{iw} \quad (4)$$

where $\hat{\epsilon}(w)$ represents the inter-band contribution. The conduction band electron contribution is described by the frequency contingent metal conductivity [28]:

$$\sigma(w) = \frac{w_p^2}{\gamma - iw} \quad (5)$$

where w_p is the plasma frequency and γ the Drude damping constant.

For good metals (e.g. gold), the value of γ is substantially smaller than w_p , so the lossless limit $\gamma \rightarrow 0$ is used to exemplify its imperfect reflection. This simplified case is known as the Plasma model [9]. However, a non-zero value of gamma ($\gamma \neq 0$) provides a better fit with the collected data, and serves as a more accurate description. This case is known as the dissipative Drude model and successfully fulfils the essential condition that metals such as gold have a finite static conductivity [28]:

$$\sigma_0 = \frac{w_p^2}{\gamma} \quad (6)$$

In contrast, the Plasma model suggests infinite static conductivity. When imperfect reflection is accounted for, the Casimir force is reduced at all distances for $T = 0$. The reduction factor η_F , which varies between 0 and 1, is given by an expression containing the real measured force (F) and the ideal force (F_c) [9]:

$$\eta_F = \frac{F}{F_c} \quad (7)$$

Plasma Model

In this model, there is only one characteristic length scale: the plasma wavelength $\lambda_p = \frac{2\pi c}{w_p}$, which is typically in the ultraviolet region for metals (136nm for gold) [9]. At large distances ($z \gg \lambda_p$), the Casimir force is recovered ($\eta_F \rightarrow 1$), explicable given that metals are perfect reflectors at low frequencies ($w \ll w_p$).

Conversely, at short distances, there is a substantial reduction in the force ($\eta_F \ll 1$) scaling as $\frac{z}{\lambda_p}$ due to metals being bad reflectors at high frequencies ($w \gg w_p$). Clearly the power law of the change of force with distance varies. Physically this can be understood to be a result of the coulomb reaction between surface plasmons present on both interfaces [9].

Drude Model

At distances z larger than the thermal wavelength $\lambda_T = \frac{\hbar c}{k_B T}$ ($z \gg \lambda_T$), a few microns at room temperature, a significant thermal correction to the force must be made [21]. Boström and Sernelius were the first to note that although γ has a small value, it has a significant effect on the force at non-zero temperatures. It is also important to emphasise that unlike the Plasma model, the Drude model leads to negative Casimir interaction entropy contributions. However, this does not violate any thermodynamic laws since the contribution amounts to the difference in entropies [29].

At large distances ($z \gg \lambda_T$) or temperatures, there is a ratio of 2 between values calculated using the Plasma and Drude assumptions [28].

In cases where the experiment is conducted at small distances (below $0.75 \mu\text{m}$), the thermal contribution and effects of γ are not large, so the Plasma model provides a close fit to the data. On the other hand, when the distances involved are notable, the difference between the two models is large. In these cases, the Drude model provides a more accurate prediction that encompasses the thermal corrections [9]. The relevance of this will be seen in the '*Thermal Casimir Force*' section.

Not many experiments have explored the large distance/temperature regions so they tend to favour the less accurate plasma model. This may seem counter-intuitive since unlike the Plasma model, the Drude model explains the static conductivity of metals. The origin of this discrepancy may be due to inaccuracies in calculations or experimental conduct [29].

4.3 Thermal Casimir Force

The thermal Casimir force is due to thermal instead of quantum fluctuations of the electromagnetic field at a finite temperature.

An experiment was carried out over the separation range $0.7 \mu\text{m} - 7 \mu\text{m}$ and at $T = 300 \text{ K}$ to investigate this effect at Yale university [30]. The chosen geometry was a gold-coated sphere and plate for reasons discussed in '*Experimental Considerations for Casimir Force*'. The flat surface was mounted in a torsional pendulum configuration; on a horizontal beam suspended from its centre by a wire. As the sphere was slowly brought towards the plate, the pendulum twisted towards the sphere because of the Casimir force. The sphere was moved between the selected separation range whilst the electrostatic force that had to be applied to the other half of the pendulum to balance the beam was recorded. Due to the presence of electrostatic patches (discussed later), corrections were applied before data analysis.

At separations below $1 \mu\text{m}$, the zero-point Casimir force dominated. However, at distances greater than $3 \mu\text{m}$ the $T = 0$ Casimir force decayed as $\frac{1}{z^3}$, whilst another measured force i.e thermal Casimir force dropped off as $\frac{T}{z^2}$. In this region, it was deduced that the thermal Casimir force was dominant. Furthermore, the plasma model was ruled out for the ($0.7 \mu\text{m} - 7 \mu\text{m}$) range according to the experimental findings, serving as a confirmation of the Drude model.

4.4 Applications of the Casimir Force

Most of the research being conducted to find applications of the Casimir force aims towards manipulating and neutralizing the Casimir forces in experimental systems.

Levitating nanospheres using the Casimir force

A team at MIT, led by Alejandro Rodriguez, hypothesized that combining different shapes and different materials could lead to the observation of a Casimir force [31]. Consequently, they showed that the repulsive and attractive forces caused by the Casimir effect could be balanced out, obtaining what was dubbed a “Casimir molecule”.

An application was placing Teflon nanospheres immersed in ethanol above an infinite slab of silicon nanospheres [32]. The Casimir force between the nanoparticles was found to be repulsive below 100 nm, but attractive above this distance. By choosing a suitable radii for the Teflon nanospheres, they were able to suspend the spheres above the slab against the force of Gravity.

Nanotechnology applications of the Casimir force

Another application was to use this tool to reduce the combined stick and friction created by the Casimir effect, effectively acting as a lubricant of some sort [33]. This tool would be most useful in accelerometers, gyroscopes and other micro-electro-mechanical system chips, also known as (MEMS) chips [34].

The Casimir force can be controlled by inserting an ellipsoid plunger into a flat plate through a complementary hole. Modifying the position of the plunger would cause the Casimir force to repel, reducing the amount of stiction [33].

This idea was developed further by a joint research team of Hong Kong University of Science and Technology, and Princeton University [35]. In order to measure the Casimir force between interpenetrating periodic silicon structures, they successfully designed and built an integrated actuator-measurement apparatus. Similar to the experiment mentioned previously, a fluctuation between repulsive and attractive Casimir forces was observed as the silicon structures were brought together. The particularity of this experiment is that the complete setup was carved out of a single silicon chip. Putting both plates on a single lithographic plate resolves alignment issues between plates, which become increasingly important as the plates gets closer. The high degree of parallelism allowed the team to obtain separation distances between 10 nm – 100 nm.

This experiment opens the possibility for compact Casimir force measurements, and creating practical nanodevices through machining of specific shapes directly onto the lithographic plate [36].

Engineering applications of the Casimir force

The Casimir force has also been considered in drastically different areas, such as interstellar travel. The concept stems from a paper written in 1984 by Robert L. L. [37], which puts forward the idea of a “vacuum-fluctuation battery”, where the Casimir force is applied to a stack of charged conducting plates. Each conducting plate has a charge of the same polarity, resulting in the creation of a repulsive electrostatic force opposing the Casimir force. Due to the attractive nature of the Casimir force, the plates will converge if the repulsive electrostatic force is set to be weaker than the Casimir force. As a result, the electric field between the plates will receive energy from the Casimir force. Increasing the electrostatic force would separate the plates and allow for a new cycle.

The energy reservoir for this type of battery would be the vacuum itself, which is available in quasi-limitless supply in space. The battery could then be used to power a spaceship engine. Research for a ‘space drive’ powered on vacuum fluctuations is still mainly theoretical, but several groups are actively researching its viability [38].

Dark energy and the Casimir force

Various research has been conducted around the link between the Casimir force and dark matter. The gravitational force is known to display a Casimir effect [39].

Applying the Casimir effect to the entire universe results in measurements that are analogous to dark energy [40]. However the magnitude of the Casimir force is extremely high compared to the observed values for dark matter [41]. Research is underway to try and justify this discrepancy. The boundary conditions of the universe are not yet known and could provide an insight [42]. Research is also being led into precisely calculating the quantum gravitational effect [43], which is an attempt to quantify the gravitational field using the Casimir effect.

5 Casimir Force Past Experiments

5.1 Experimental Considerations for the Casimir Force

After the publication of the two 1948 papers by Casimir and Polder, investigations into fundamental questions about quantum field theory and the configuration of the vacuum began [18]. The 1990s marked the advent of precision experiments of the Casimir force, sparking renewed interest in this broad subject, both theoretically and experimentally [30]. Despite sometimes being claimed, the Casimir force has yet to be measured at the 1% level [28]. Below are outlined some of the general difficulties associated with experimentation:

1. Non-additive Nature

The non-additive nature of the force, due to reasons outlined in *Macroscopic Forces from a Microscopic Perspective*, produces a challenge during experimentation [3]. Since the fluctuating polarizations between atoms cannot be summed to give the total macroscopic force between two bodies, more complex computational methods must be employed [13].

2. Electrostatic Force

It is appropriate to avoid using charged particles in these experiments since their dispersion force is much smaller than the electrostatic image force. Bearing in mind these forces are already difficult to measure due to their small magnitudes, this is greatly unfavourable. Residual electrostatic forces could be cancelled out by applying a reverse voltage with the same magnitude [13]. It may be necessary to subtract effects of the electrostatic force to deduce the Casimir force [44].

3. Static Electric Charges

Likewise, it should also be ensured that any residual charge that may manifest as an electromagnetic interaction (electrostatic patches) is negligible [28]. If the cleaning procedure involves rubbing surfaces, insulator surfaces may become charged, but this rarely induces an attractive electrostatic force due to the ‘mosaic’ effect distributing the charges evenly. Despite this, to avoid difficulties, insulator surfaces can be made conductive - for example, by using a radioactive agent or ionising the surfaces. Alternatively, a conductive material can instead be chosen [45].

4. Different Surface Potentials

Regardless of plates being made from the same material, there is a difference in surface potential. If charge can be transferred from one plate to another due to this gradient, an attractive force can be generated. Therefore, the area between the plates must be prevented from being conductive if this is to be avoided i.e a radioactive agent should not be used on insulator surfaces and they should not be ionised. Typically, the difference of surface potentials between two plates of the same metal ranges between 5 mV – 25 mV [45].

5. Keeping Bodies Parallel and at Small Separations

Maintaining these macroscopic bodies at distances below 1 μm and parallel is a difficulty [22]. Since each plate has a large surface area, it is difficult to measure any angle of inclination to ensure the plates remain parallel.

6. Measuring Small Separations

Determining distances of this magnitude to high precision is another obstacle [22]. If separation cannot be measured through optical methods due to choices in metal, a capacity method can be employed; the capacitance formed by the test subject can be used to measure distance [45]. However, it must be noted that this determines only the average distance between the two plates.

7. Accurate knowledge of the dielectric constant $\epsilon(w)$

As described in [Drude and Plasma Models](#), the force between metallic surfaces is dependent on their optical properties, and hence $\epsilon(w)$. Consequently, accurate knowledge of the value of $\epsilon(w)$ over a wide range of w is required. The available data is composed of measurements taken using different samples and processes from a range scientists, making it an inconsistent

source. In addition to this, the uncertainties in the value of $\epsilon(w)$ lead to large uncertainties in the calculation of F_C as well [13].

Clearly, points 3 and 4 are mutually exclusive for non-conductive surfaces, pointing to why using conductive surfaces can be advantageous. Further in the report, this will influence the choice of chosen nanoparticle.

The original formula proposed by Casimir is for ideal conditions and does not consider the effects of imperfect reflection, thermal fluctuations, geometry and corrections coming from surface physics, so it must be amended as such. [28] Here are possible corrections that must be made to account for the following:

- **Imperfect Reflection**

Casmir's original derivation assumed perfect reflection, so experiments are usually conducted with metal plates since these most closely reproduce this behaviour. At frequencies below the plasma frequency w_p , which is contingent on the metal's conduction electrons, they behave nearly perfectly. [21]. As previously discussed, the Casimir force only follows its theoretical trajectory at distances much larger than the plasma wavelength ($z \gg \lambda_p$) corresponding to low frequencies ($w \ll w_p$).

At distances shorter than a few plasma wavelengths (e.g $0.3 \mu\text{m}$ for gold), the finite conductivity must be accounted for and the force deviates from ideal predictions [20]. Consequently, precise knowledge of frequency dependency is crucial for reliable theoretical predictions [9].

The newly deviated Casimir force can be evaluated using scattering amplitudes which are dependent on the frequency, polarizability and wave vector to describe the imperfectly reflecting surfaces [20]. This scattering approach for calculating the Casimir force between non-perfect reflectors is also the current best solution for use in arbitrary geometries [9].

- **Thermal Fluctuations**

Many of the real experiments are not undertaken at $T = 0$, so the thermal fluctuations will be superimposed with the vacuum fluctuations; a correction must be formulated for these thermal effects (thermal Casimir force) [21]. At room temperature and low frequencies i.e $\hbar w < k_B T$, there is a significant number of thermal photons, so at large distances (usually above $3 \mu\text{m}$ at room T) a considerable thermal correction must be made. Since most precise measurements are made below $0.5 \mu\text{m}$, this correction is below 1% [20].

- **Geometry**

Although early theoretical predictions were applicable for infinite planar geometries, the first precise measurements were made between a sphere and plate due to the challenge of keeping plates parallel during an experiment [16]. The Proximity Force Approximation (PFA), in which the surfaces are approximated as infinitesimal parallel plates, had to be applied to allow for comparison of theory and experimental Casimir force [46]. It is only valid in the limit that the radius of curvature of the spherical plate is much larger than separation ($R \gg Z$) [9]. Despite the imperfection of it failing to capture curvature, it worked well for many experiments. The equation is as follows [30]:

$$F_{PFA} = \frac{2\hbar c \pi^3 R}{720 z^3} \quad (8)$$

where z is the distance between the flat plate and closest point on the spherical plate.

- **Surface Roughness**

Surfaces are not perfectly smooth and are bound to be covered in roughness, dust or chemical impurities. This makes surface properties different to bulk material properties. To account for surface roughness, the PFA is used again [21]. Conversely, the surface profile can be mapped using interferometric methods, and used to obtain a statistical model for surface roughness used to make corrections to F_C [13]. These corrections only play a large role at the same distances as for thermal fluctuations [20].

- **Electrostatic Patches**

Patches, due to varying potentials of the plate surfaces, caused by impurities/oxides or changes in crystalline structure (surface properties) are composed of micro-crystallites with

different work functions. This effect must be accounted for in the final Casimir force equation [30].

These corrections can be examined in theory-experimental comparisons. Given that thermal fluctuation and surface roughness effects are only substantial in measurements below $0.5 \mu\text{m}$, they have not been experimentally tested as much [20].

The following is a review of experimental methods covering the initial sophisticated measurements used to measure the Casimir force using electromechanical methods such as torsion pendulums, to more modern and novel methods that achieve more precise measurements. Representing a relatively new area of physics, a lot of new and exciting developments have been made in the past 20 years in the measurement of the Casimir force predicted in 1948 [15].

5.2 Initial measurements

Measurement of attractive forces between flat plates

In 1958, an attempt was made to measure the Casimir force proposed 10 years earlier [45]. M.J. Spernaay introduced an era of Casimir force experimentation that would not reach fruition for several more years. Spernaay's experiment is successful, very interesting, and if not limited by technology, helpful.

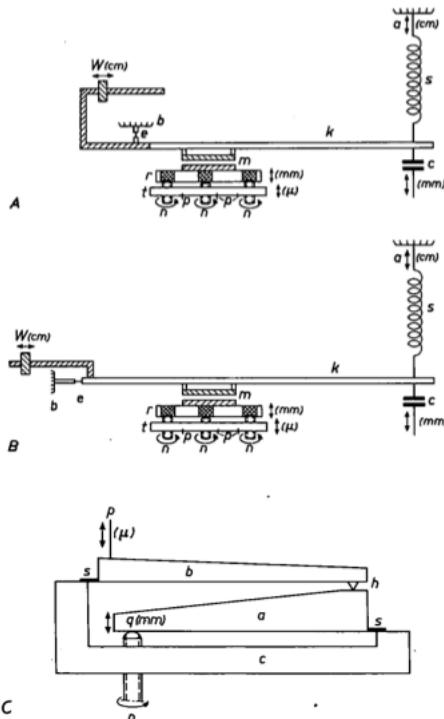


Figure 4: A and B are the two balances used where counter weight W can be moved to keep the lever arm k in balance. C is one of three lever systems used to decrease the interplate space. This is done by turning the screw n . Reproduced from [45, Fig. 2].

This experiment used a lever system, shown in Fig. 4, where an attractive force between the plates m displaces the aluminium (Al) beam k , and results in a change in the capacitance of the two plates. A spring S and counterbalances were used to establish an equilibrium. The apparatus was contained in a glass container with air pumped out and replaced with dust free nitrogen before a vacuum of 10^{-2} mmHg ($\sim 1.3 \times 10^{-5} \text{ mbar}$) was obtained. The plates were chosen by considering the oxide layers that would form on their surfaces. The author notes that chromium (Cr) steel and Cr oxide layers are only $5\text{-}50 \text{ \AA}$ in thickness, and therefore suitable. Al turned on a lathe, so that maximum protrusions were less than 200 \AA , was also used. Besides the oxide layer, a mechanical cleaning procedure was used to clear dirt from the surfaces of each material.

The lever system C in Fig. 4 shows one of three used to change the interplate spacing as the screw n is turned. The plates were both insulated, and their alignment was determined only by eye, a rather crude method that resulted in a large uncertainty. Another factor that increased the uncertainty was the capacitance measurement that was limited in precision thanks to the vibration of the system. Having three independent lever systems was also an issue as the parallelism of the plates had to be continually reassessed. It was also not possible to make the system dust free, a further source of uncertainty.

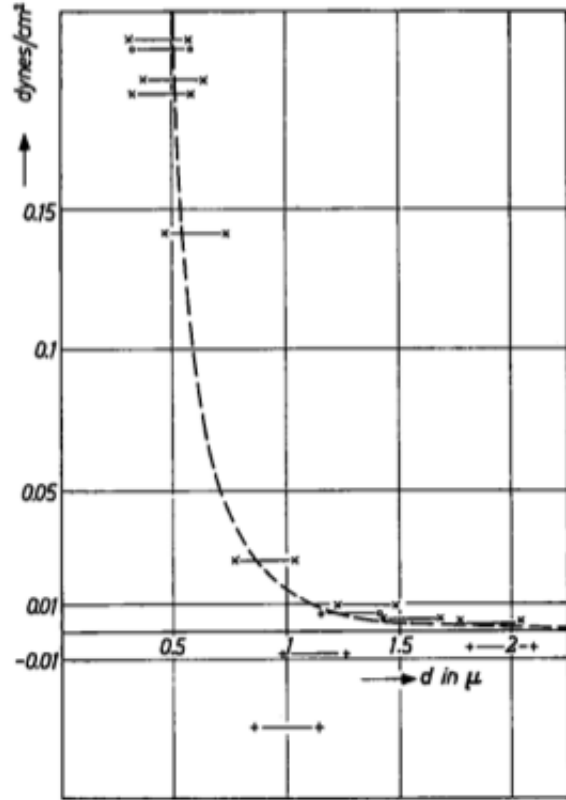


Figure 5: The Force resulting from the experiment for chromium steel \times — \times , chromium \circ — \circ and, aluminium $+$ — $+$ plates. The uncertainty in the distance is represented in the width of the lines. Reproduced from [45, Fig.4].

The results represented in Fig. 5 for Cr steel, and Cr are closest to Casimir's predictions, though the attractive force is too large. This large attractive force could be due to the substantial variation in the angle of the two plates relative to each other. Not being parallel contributed to the large uncertainty in mean distance, illustrated in Fig. 5 by the large horizontal lines representing each measurement.

Further uncertainty was contributed by the Al plates, where Sparnaay found that at distances smaller than $2\text{-}3 \mu\text{m}$, there was a small repulsive force between the two plates that contradicted the theoretical predictions. The author attributes this to a build up of Al oxide after the removal of the dust particles, which could not be done in a vacuum.

Due to the large uncertainty in the distance, and the various other difficulties with this experiment, it was not considered unambiguous evidence for the Casimir force. Sparnaay suggests the main issues in the experiment were that the potential differences between the plates could not be measured, and that there were problems like dirt and oxidation that needed to be overcome. The effects of these difficulties were previously outlined in [Experimental Considerations for the Casimir Force](#).

Demonstration of the Casimir Force in the $0.6\text{-}6 \mu\text{m}$ Range

It wasn't until 1996 when S. K. Lamoreaux experimentally demonstrated the unambiguous existence of the force [47]. The paper asserts that the Casimir force can be observed using a classical

macroscopic apparatus, in this case a torsion pendulum.

The paper gives the magnitude for Casimir force per unit surface area:

$$F(a)/A = \frac{\pi^2}{240} \frac{\hbar c}{a^4} \quad (9)$$

where a is the plate separation. Using the proximity force theorem [48], and taking the results of Brown and Maclay [49], and Schwinger *et al.*[50], temperature and finite conductivity corrections are adopted.

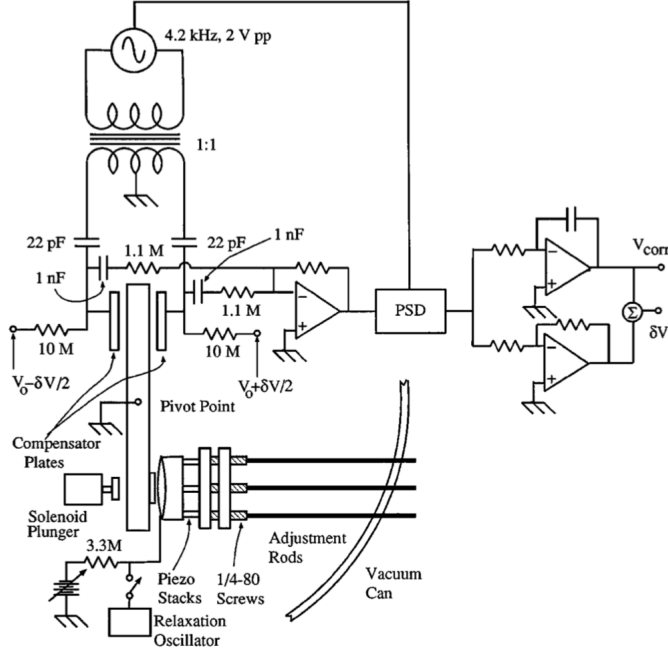


Figure 6: The apparatus used by Lamoreaux, where a solenoid plunger in a vacuum vessel was used to vary the distance of the plates. Reproduced from [47, Fig.1].

In the experimental apparatus, depicted in Fig. 6, a 0.5 cm thick quartz optical flat with a diameter of 2.54 cm, and a spherical lens with a diameter of 4 cm and radius of curvature of 11.3 ± 0.1 cm were used as the Casimir force plates. All plate surfaces were coated, by evaporation, with Cu of thickness $0.5 \mu\text{m}$, followed by a $0.5 \mu\text{m}$ gold (Au) coating onto the faces that would be brought together. Inside a 55 cm by 110 cm vacuum chamber, the flat plate was mounted onto a torsion pendulum, while the spherical plate was mounted onto a micro-positioning assembly. This comprised of $\frac{1}{4}$ -80 screws that were mounted on adjustment rods that could be used to make coarse adjustments to the spacing ($0.5 \mu\text{m}$ accuracy), and piezoelectric translators (PZTs) which were used to make fine adjustments. The uncertainty in the final relative displacement was measured to a $0.01 \mu\text{m}$ accuracy using a laser interferometer.

A vacuum of order 10^{-4} torr ($\sim 10^{-7}$ bar) was maintained in the chamber using a small oil diffusion pump. The experiment relied on a feedback system to maintain the angle of the torsion pendulum. Two "compensator plates" formed a capacitor with the pendulum body, and an AC bridge circuit was used to determine each capacitance. If found to be unequal, an error signal was sent to an integral-plus-proportional feedback circuit, as shown in Fig. 6. A DC correction voltage, δV was then applied to the compensator plates to keep the angle fixed. A 2.5 kG magnet was also used to over-damp all vibrational modes of the pendulum arm. This system has a sensitivity of $48 \text{ mV}/\mu\text{m}$. The restoring voltage δV applied at a given distance was used to determine the force being exerted on the torsion pendulum through the Casimir plate. The experiment cycled through 32 different distances using the PZTs, waiting 40 s for the feedback system to reach equilibrium before taking measurements of δV averaged for 7 s.

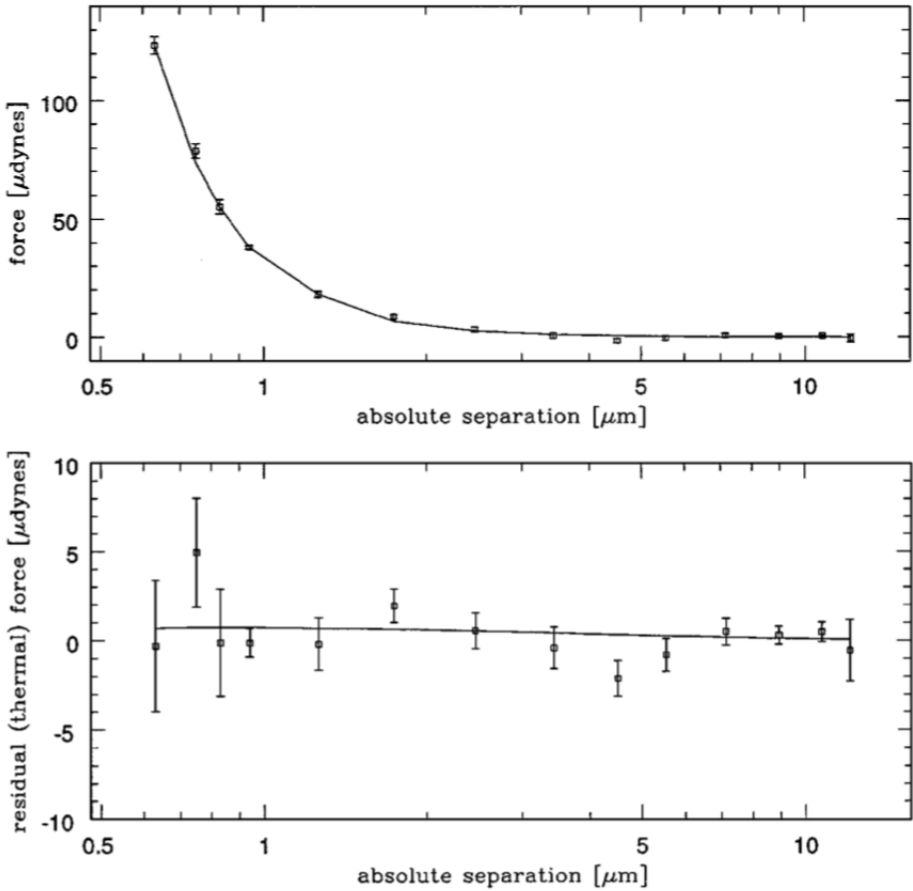


Figure 7: Top: The data with electric force subtracted. Bottom: The residuals for the theoretical Casimir force for a spherical plate without a thermal correction, and the experimental data. Reproduced from [45, Fig.4].

The data obtained by this experiment was an early unambiguous demonstration of the Casimir force, and is displayed in Fig. 7 where experimental data and theory is compared. Lamoreaux gives the data to an accuracy of 5%, which is rather inaccurate and reflective of the setup used. For instance, the feedback system is a large source of inaccuracy, becoming unstable at larger distances. Lamoreaux also found that there was a potential difference of 430 mV between the two 'uncharged' Casimir plates, which had to be corrected for in analysis. Furthermore, it was determined that there was a drift in the separation distances while sweeping through. This was attributed to environmental factors, most of which was temperature variations. 10% of sweeps were rejected due to anomalous drifts. This contributed to a large χ^2 in the final fit [47].

The fit shows that there is agreement with the data and the theoretical Casimir force with accuracy of order 5%. However, it is not accurate enough to demonstrate the finite temperature correction. Moreover, the experimental setup had its flaws, including the uncertainty due to the feedback system and temperature changes. Lamoreaux was unable to achieve separation distances less than 0.6 μm , attributing this limit to either dirt on the plates or instability of the feedback system.

Precision Measurement of the Casimir Force from 0.1 m - 0.9 μm

Building on the work of Lamoreaux, the next year U. Mohideen and Anushree Roy published their experiment [51] to more precisely measure the Casimir Force. This paper points that the two preceding experiments were not conclusive on account of their large uncertainties.

As can be seen in flat plate experiments [45], there is a considerable issue with keeping the plates parallel. Lamoreaux used a sphere with radius of curvature 11.3 ± 0.1 cm to overcome this issue [47]. This experiment used a far smaller sphere, with diameter $196 \mu\text{m}$, along with a flat plate. This allowed the two to be brought much closer together than previously possible.

The Casimir Force for this geometry is corrected to [47, 48],

$$F_c^0(d) = -\frac{\pi^3}{360} R \frac{\hbar c}{d^3} \quad (10)$$

Further corrections were made for the conductivity of the metal based on the free electron model of the reflectivity of metals (Drude model), the roughness of the surface and finally due to the finite temperature.

At room temperature, and a pressure of 50 mTorr (~ 66.7 mbar), an atomic force microscope (AFM) was used to measure the force between the sphere, and the plate. A 200 ± 4 μm diameter polystyrene sphere was mounted on a $300 \mu\text{m}$ cantilever, and a optically polished sapphire disk was used as the flat plate. Both were coated with 300 nm of Al by evaporation. Al was chosen due to high reflectivity at a sphere-plate separation of > 100 nm.

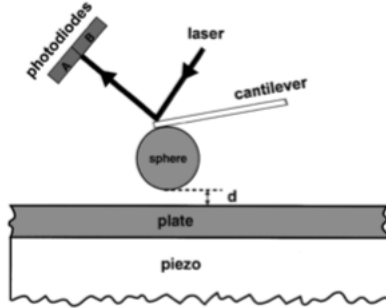


Figure 8: A schematic of the atomic force microscope setup used to measure the force applied between a Al coated sphere and flat Al plate. Reproduced from [51, Fig.1].

To prevent the patch charge effects due to oxidisation discussed by Lamoreaux [47], the surfaces were coated with 20 nm of 60% Au and 40% palladium. As shown in Fig. 8, a laser is used to detect a force on the cantilever using two photodiodes. Similar to the previous experiment, a piezo translation stage was used, and its hysteresis effects accounted for. 26 scans were taken at each height for different places on the flat plate, and averaged to produce Fig. 9.

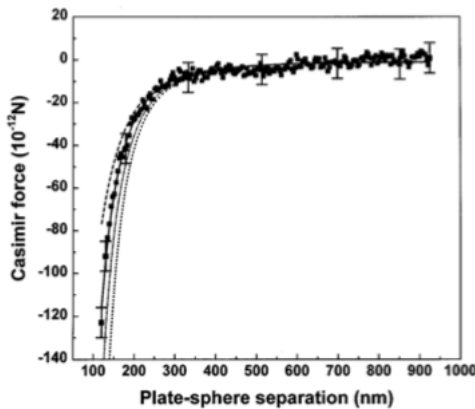


Figure 9: The average measured Casimir force for 26 scans are shown by the square points. The solid line is the fully corrected Casimir force, the dash-dot line is the Casimir force without corrections for conductivity, roughness and temperature. The dashed line includes only the finite conductivity correction, and the dotted line only the roughness correction. Reproduced from [51, Fig.4].

U. Mohideen and A. Roy found that they were able to perform precision measurements of the Casimir force to support the geometry, finite conductivity and roughness corrections introduced. This experiment was, however, limited by the cantilever apparatus. It is suggested that a cantilever

with a large radius of curvature might help increase precision, along with taking measurements at lower temperatures to reduce thermal noise.

5.3 Investigations into different geometries and the resultant Casimir Force

Measurement of the Casimir Force Between Parallel Metallic Surfaces

A return was made to the parallel plate method in 2002 by G. Bressi *et al.* [52]. This group undertook the challenge of measuring the Casimir Force without using the successful sphere-plate geometries of previous experiments [47, 51]. As parallel plates were the original subject of Casimir's theory, but no clear experimental result had been obtained, it was important to be able to demonstrate the force in this scheme.

A silicone cantilever with an optically flat surface of dimensions $1.9 \text{ cm} \times 1.2 \text{ mm} \times 47 \mu\text{m}$, covered in a 50 nm thick Cr layer, clamped onto a movable copper base was part of the setup. Another silicone arm, referred to as the source, with a thicker optically flat surface ($1.9 \text{ cm} \times 1.2 \text{ mm} \times 0.5 \text{ mm}$) was also covered in Cr, and mounted parallel to the first. The arms could be controlled by 1 nm step motors in all three directions and a PZT was used for fine adjustments to ensure the plates were parallel.

The relative displacement of the two surfaces was determined using a fiber optic interferometer with a resolution up to 50-100 nm, and capacitance measured by an AC bridge with a sensitivity of $\sim 0.4 \text{ pF}$. The previous challenges surrounding parallelisation were overcome by way of the step motors and PZT. The issue of maintaining the neutrality of the surfaces was resolved by inducing an offset voltage, V_0 , to counteract the inherent voltage caused by the different metals in the electrical circuit containing the plates using a precision voltage calibrator, shown in Fig. 10.

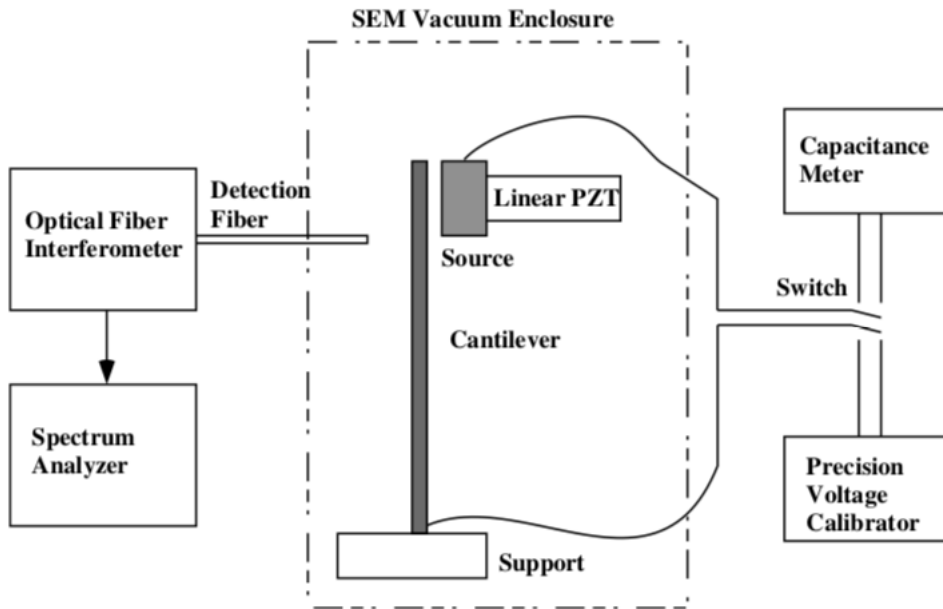


Figure 10: Experimental apparatus showing the cantilever and source enclosed in the vacuum chamber, while a optical fibre interferometer measures the cantilevers relative displacement. The plates are connected to either the capacitance meter or precision voltage capacitor for calibrating the offset voltage V_0 . Reproduced from [52, Fig.1].

To clean the surfaces, a filtered laminar air flow was used, as well as solvents, and an in-vacuum cleaning tool. This eliminates the previous problems of dust build up and oxidisation during repeated cleaning in air. These methods could clean dust down to approximately $0.5 \mu\text{m}$. Once the vacuum chamber reached a pressure of $\sim 10^{-5} \text{ mbar}$, and coarse parallelisation adjustments were made with the motors, the PZT and AC bridge were used for fine calibration. The plates were considered parallel when the capacitance was at a maximum and the uncertainty was 30 nm over 1.2 mm. The displacement of the cantilever due to an inherent voltage across the plates is

given by $\Delta x_i(V_c) = K_i(V_c - V_0)^2$ and was fitted against measured displacements to give an average $V_0 = -(68.6 \pm 2.2)$ mV. This was then applied as a counter-voltage to give a small residual voltage V_r , making the detection of superimposed distance dependent forces possible.

The superposition of the Casimir force and residual electrostatic forces contribution on the resonant frequency of the cantilever, ν , was determined by fast-Fourier transform of the interferometer signal. The squared-frequency shift is [53]:

$$\Delta\nu^2(d) = \nu^2 - \nu_0^2 = -C_{el} \frac{V_r^2}{d^3} - \frac{C_{Cas}}{d^5} \quad (11)$$

where $C_{el} = \epsilon_0 S / 4\pi^2 m_{eff}$, $C_{Cas} = K_C S / 4\pi^2 m_{eff}$ and S being the area covered by the cantilever. Additionally to the electrostatic calibration, the absolute distance between the plates was calculated by measuring the frequency shift at large distances and three different values of V_0 (-205.8 mV, -136.2 mV and +68.6 mV and fitting it to Eq. 11. At these large distances the d^{-5} is negligible compared to the electric component, so [52]

$$\Delta\nu^2(d_r) = -\nu_{offset}^2 - C_{el} \frac{V_r^2}{(d_r + d_0)^3} \quad (12)$$

where ν_{offset}^2 is the frequency offset taking into account long term drifts in the laser frequency. The last of these voltages was the quasicomplete cancellation voltage and was applied to find the residual frequency shift at short range, as shown in Fig. 11.

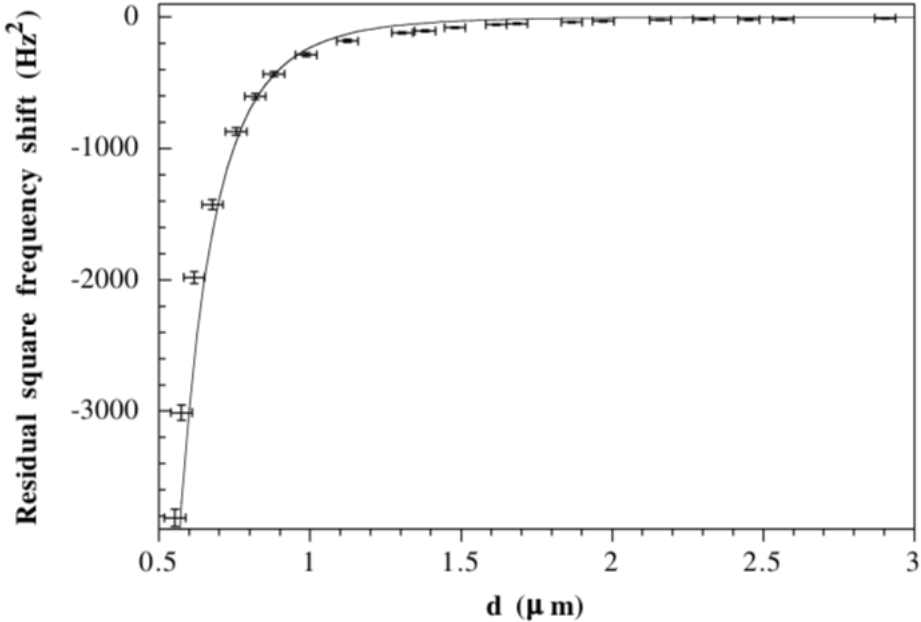


Figure 11: A graph showing the residual frequency shift with a correction voltage of 68.6 mV applied across the two plates. The fit was done by considering data from 0.5-1.1 μm , and includes errors derived from C_{el} , d_0 and V_0 . Reproduced from [52, Fig. 4].

The fit of this graph was the Casimir component of Eq. 11. The graph shows a good fit with χ^2 probability of 61%, though uncertainty in the distance is relatively large. The force coefficient was then calculated to be $1.22 \pm 0.18 \times 10^{-27} \text{ Nm}^2$.

Casimir Repulsion between Metallic Objects in Vacuum

Having finally unequivocally shown that the Casimir force is always attractive between two metal plates in a vacuum, M. Levin *et al.* concerned themselves with assessing whether this is generally true for dielectric or metallic objects, or whether the direction of the force could be changed by geometry [27].

Other papers have used inter-levered geometries combining attractive forces to give a 'repulsive'

interaction, but the sign is ambiguous [54]. However, the objects in Levin's paper, an ellipsoidal particle above a hole in a plate, lie either side of the $z = 0$ plane so any repulsion is unambiguous in reflecting the sign.

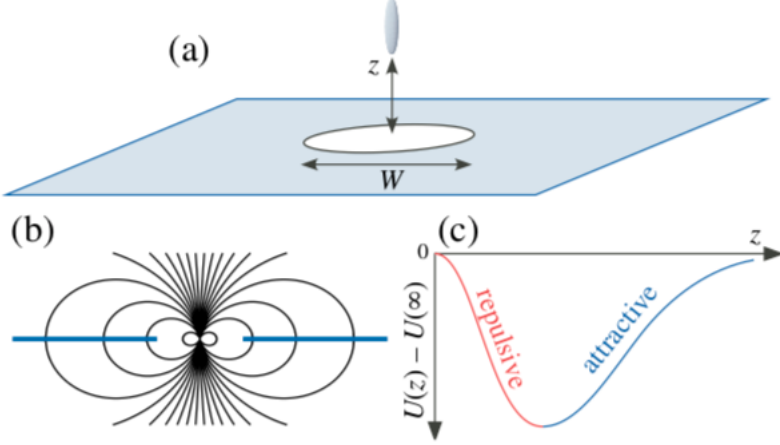


Figure 12: a) The ellipsoidal particle above the plate with a hole diameter W at distance z . The shaded area is the $z=0$ plane. b) side on view of the vacuum dipole fields centred at $z=0$. c) The interaction between the plate and the sphere, showing first repulsion then attraction as z increases. Reproduced from [27, Fig.1].

Levin argues that in an idealised geometry of an infinitesimal particle in an infinitesimally thin metal sheet with a hole, the Casimir energy is [55]:

$$U(\mathbf{x}) = -\frac{1}{2\pi} \int_0^\infty \alpha_{zz}(i\xi) \langle E_z(\mathbf{x})E_z(\mathbf{x}) \rangle_{i\xi} d\xi \quad (13)$$

where α_{zz} is the electric polarizability in the z direction, and $\langle E_z(\mathbf{x})E_z(\mathbf{x}) \rangle_{i\xi}$ is the mean-square z component of the electric-field fluctuations at \mathbf{x} and imaginary frequency $\omega = i\xi$. By using the classical mechanical Green's function via the fluctuation dissipation theorem, $\langle E_z(\mathbf{x})E_z(\mathbf{x}') \rangle_{i\xi}$ is proportional to the electromagnetic field produced by an oscillating z -directional dipole $\mathbf{p} = p_z \hat{\mathbf{z}} e^{i\omega t}$ at \mathbf{x} . Levin then states that there is a point where this dipole is unaffected by the metallic sheet with a hole, thus $U(\mathbf{x}) = U(\infty)$. It then follows that the energy varies monotonically between \mathbf{x} and ∞ so, using a symmetry argument, at some point the force must be repulsive. This condition is achieved at $z=0$ in Fig. 12.

The interaction energy $U(\mathbf{x}) - U(\infty)$ will therefore be zero at $z=0$, negative at small z , and positive at large z when the hole is negligible and the conventional Casimir force between a particle and a plate takes over.

A finite-difference time-domain (FDTD) method was used to compute the Casimir stress tensor via Green's function [56, 57], then the bound-element method (BEM) was used to solve directly for Casimir force via a path integral expression [58]. This was computed for a $20 \times 60 \times 320$ nm ellipsoidal gold and perfect metal particle above a $1 \mu\text{m}$ diameter hole in a 20 nm thick plate.

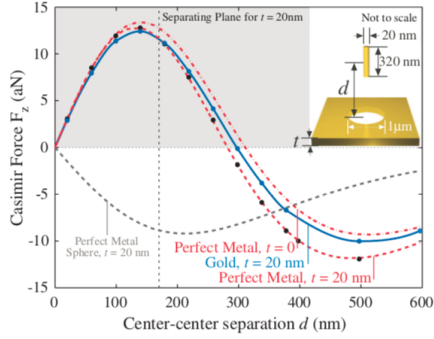


Figure 13: Casimir Force for the ellipsoid-plate interaction for perfect metals, computed using BEM, and gold computed using FDTD method. The force on the cylinder is repulsive in the shaded region and it is unambiguous between 170 nm and 300 nm where the ellipsoid is completely above the plate. This diagram also shows that the perfect metal sphere always experiences an attractive force. [27, Fig.3].

This simulation was the first to unmistakably show that based purely on geometrical changes, the sign of the Casimir Force may be changed as shown in Figures 13 and 14. Fig. 13 exhibits how the thickness of the perfect metal and gold affects the energy interactions, showing that a gold cylinder over a hole in a gold plate with thickness $t=20$ nm produces a considerable repulsive force. This is highly achievable in the real world and would be very interesting to test. Fig. 14 shows the dependence on the ellipticity of the particle, suggesting several geometries that could be manufactured.

Though the symmetry argument and mathematical methods have suggested this theory to be correct, it has not yet been proven. The paper suggests an experimental method consisting of a series of low permitted pillars connected to plates and an array of holes in a sheet of metal. According to their calculations, this only produces a maximum repulsive pressure of 10^{-6} Pa, which at the time was ~ 3 orders of magnitude beyond average experimental sensitivities.

Repulsive Casimir Force with Metallic Ellipsoid Structure

The geometries discussed in the previous paper [27] were expanded upon in a further simulation [2] based on a gold ellipsoid above a gold plate with a hole in it as depicted in Fig. 15.

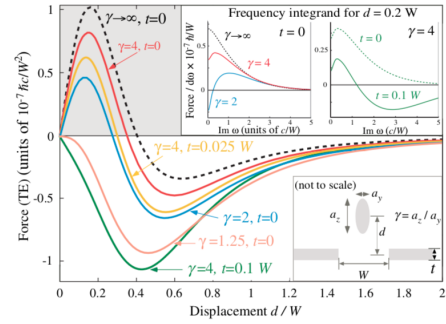


Figure 14: The Casimir Force was computed using BEM for cylinders with differing ellipticity, $\gamma = a_z/a_y$. The data shows that as ellipticity decreases, attractive contributions arise [27, Fig.4].

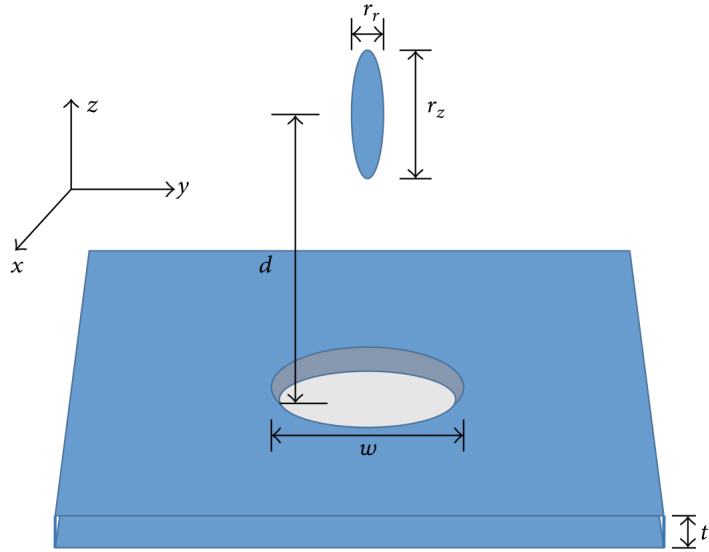


Figure 15: This is a diagram of the gold ellipsoid suspended above a gold plate with a hole in it, used to obtain the repulsive casimir force. The thickness of the plate t is 100 nm, the diameter of the hole was $2 \mu\text{m}$, and the ellipsoid had dimensions $r_r = 50 \text{ nm}$ and $r_z = 250 \text{ nm}$. Reproduced from [2, Fig.1].

Expanding on Eq.13, a modification of Maxwell's stress tensor [59, 60] was employed to calculate the Casimir Force in the time domain. Employing a FDTD calculation, where a source is placed on each point on the surface S of the gold ellipsoid, then calculating the entire frequency spectrum for each time domain, the final expression for the Casimir force is [2]:

$$F_i = \int_0^\infty \text{Im}[g(-t)] \cdot \sum_n \int_S d_{s_j}(r, z) f_n(r, z) \Gamma_{ij;n}(r, z, t) \quad (14)$$

where

$$\Gamma_{ij;n}(r, z, t) = \Gamma_{ij;n,m=0}(r, z, t) + 2 \sum_{m>0} \text{Re}[\Gamma_{ij;n,m}(r, z, t)]. \quad (15)$$

here $g(-t)$ is the geometry independent function derived by taking the Fourier transform of $g(\xi)$, the frequency spectrum in a single point on surface S and $\Gamma_{ij;n}(r, z, t)$ are functions of the electromagnetic fields on S . This was computed for a perfect metal and realistic gold for three different mediums: bromobenzene, ethanol and a vacuum.

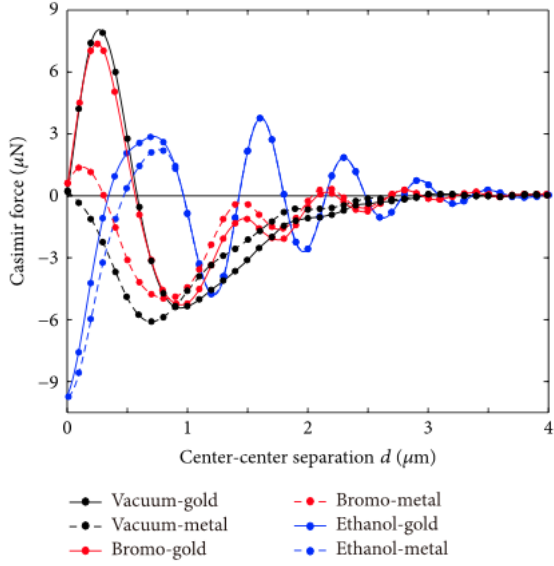


Figure 16: The Casimir force for a perfect metal, realistic gold ellipsoid and plate in three different media: bromobenzene, ethanol and a vacuum. The negative sign is a repulsive Casimir force. Reproduced from [2, Fig. 2]

Fig. 16 shows how the Casimir interaction is stronger between gold in the three mediums, agreeing with the results from [27]. The paper then proposes a new structure that may be very useful in MEMS (see [Applications of the Casimir Force](#)). This system involves the levitation of the ellipsoid between two identical plates, one above and one below (as before), see Fig. 17.

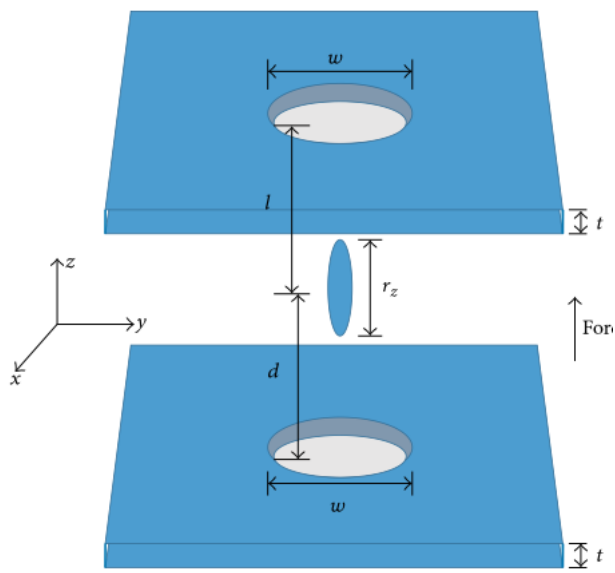


Figure 17: A new set up was proposed using the same dimensions as before, and including a second identical plate above the ellipsoid. It is suggested that this will have important uses in MEMS [2, Fig. 2]

With this setup, the distance l is kept constant and d is varied to see the Casimir force in both perfect metal and realistic gold. It is shown that at $l = 0.5 \mu\text{m}$ the repulsive force, shown in Fig. 18(a), can reach $10 \mu\text{N}$.

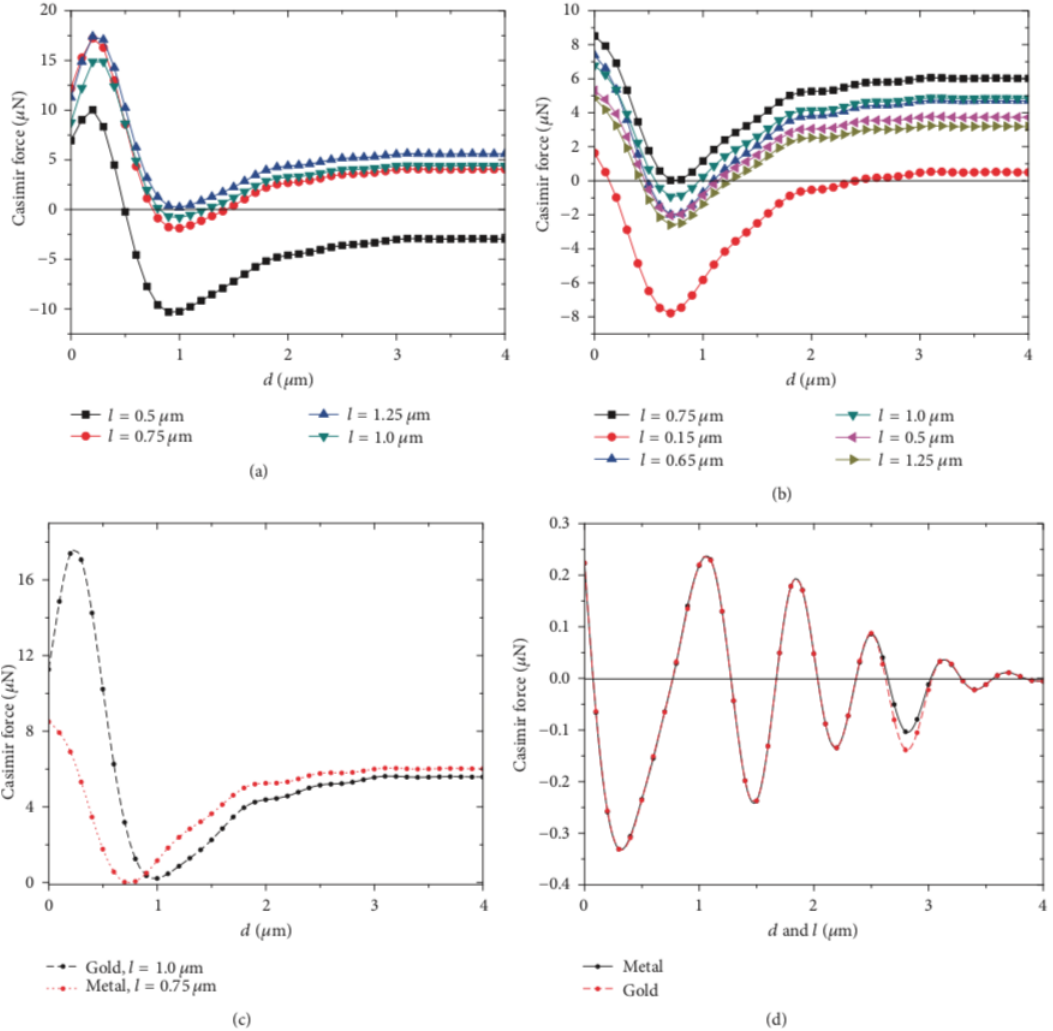


Figure 18: **a)** This shows the Casimir force in the proposed set up for a realistic gold over a variety of distances l . **b)** The Casimir force for a perfect metal over a variety of distances l . **c)** The two materials at two points where the repulsive force becomes attractive. **d)** The fluctuating Casimir force when the ellipsoid is fixed, and d and l are increased simultaneously. Reproduced from [2, Fig. 6].

It is clear in Fig. 18(a) that with the ellipsoid and top plate fixed, for $l = 0.5 \mu\text{m}$, the force becomes repulsive with an increase of d . However, for the separation $l = 1 \mu\text{m}$ the force is always attractive. Figure 18(b) also gives an insight into the materials investigated. The gold seems to be repulsive for a greater distance d before becoming an attractive force. Interestingly, in Fig. 18(d) the two materials act very similarly when both d and l are increased.

This paper not only provides a feasible way of computing the Casimir force, but also suggests an interesting setup that calls for further experimental investigation.

5.4 Novel Methods of Force Detection: Optical Levitation

Optical Rotation of Levitated Spheres in High Vacuum

More recently, the benefits of using optical traps for force detection experiments have become more and more evident. A research group from Yale has developed a technique for precision measurements using rotating optically levitated particles [61].

A trapping beam with wavelength $\lambda = 1064 \text{ nm}$ was used to levitate an amorphous SiO_2 sphere (diameter $10.3 \pm 1.4 \mu\text{m}$), and two linearly polarized beams at $\lambda = 532 \text{ nm}$ were used to image the 3D motion of the particle. The team also later levitated a vaterite sphere (diameter 4.9 ± 0.47

μm) which is a polymorph of CaCO_3 . The signals from the imaging beams were fed through a field-programmable gate array which then controlled the damping of the centre of mass degrees of freedom to maintain stable trapping [61].

The trapping beam is polarized by a LiNbO_3 electro-optic modulator which allows for control over the circular polarization of the beam. In turn, this applies a torque on the SiO_2 sphere. After the imaging beams pass through the particle, they go through a half wave plate before reaching a polarization sensitive sensor, comprising of polarizing beam splitter and a photo diode as shown in Fig. 19. The signal from the polarisation sensitivity sensor is modulated as the sphere turns round the axis [61].

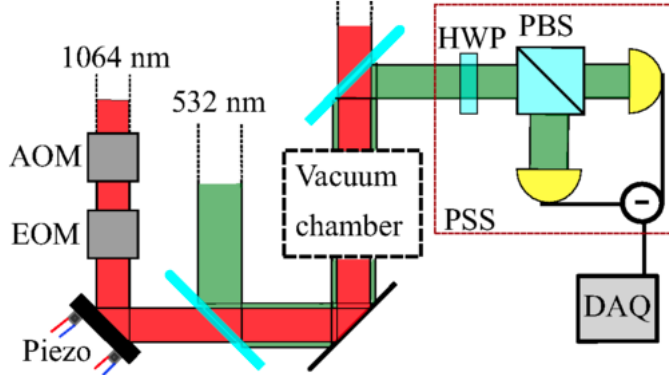


Figure 19: A schematic of the experimental set up, where 1064 nm light is fed through an acoustic optic modulator and the discussed electro-optic modulator. A piezo mirror is then used to modulate the position of the trapping beam. The 532 nm light is coaxial to the trapping beam. The 532 nm imaging beam passes through the half wave plate, and the polarizing beam splitted before reaching the photodiodes that determine its polarization. Reproduced from [61, Fig.1].

Two peaks of the rotational frequency for SiO_2 , and vaterite were measured at various pressures. The largest of these peaks, $2f_{rot}$, is caused by the polarization modulation from the rotation of the sphere. The other peak is observed at f_{rot} and is due to the modulation of the power reaching the sensor due to residual asphericity of the sphere. Higher harmonics are also observed but are much smaller in amplitude. These are shown for vaterite at $\sim 10^{-2}$ mbar in Fig. 20.

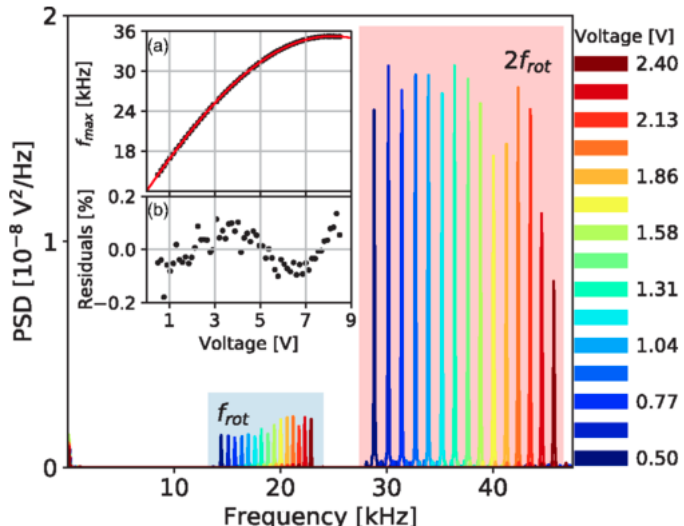


Figure 20: Power spectral density for the varetite sphere at a constant pressure of $\sim 10^{-2}$ mbar. f_{rot} and $2f_{rot}$ show the peaks observed and insert A shows the terminal velocity f_{max} achieved [61, Fig.2].

The terminal velocity f_{max} was caused by the torque from drag of gas in the chamber. The terminal velocity measurement, as well as power spectral density can be used to determine any other force on the particle. This can be achieved by measuring damping.

The optical levitation of dielectric spheres method has several advantages for precision sensors, as it allows the particles to be electrically neutralised and their charge can be controlled [5, 4]. This also allows precision control of the particles location. However, limitations are highlighted. For example, there are limitations such as the centrifugal stresses and trouble trapping at high vacuums.

Zeptonewton force sensing with nanospheres in an optical lattice

Researchers at the university of Nevada successfully used an optically levitated silicone nanosphere to measure zeptonewton force [62]. This suggests that this technology can be used to detect the Casimir force, along with applications in magnetic resonance imaging [63] and gravitational force detection [64].

The reported precision is achieved using two counter-propagating beams formed by splitting a 1064 nm laser. The beams foci are offset by 75 μm and form a waist size of 8 μm . The beam setup is shown in Fig. 21.

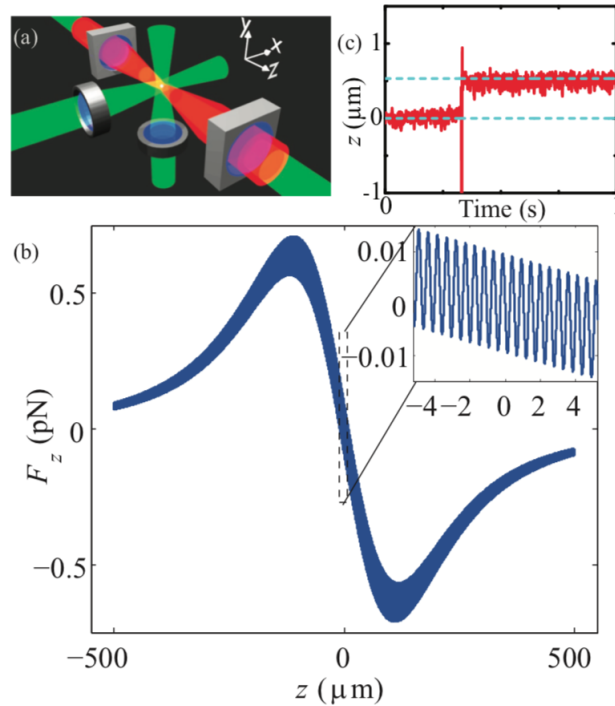


Figure 21: a) 1064 nm laser light is split using a polarizing cube beam splitter and produce a standing wave trap for a 300 nm nanoparticle. 780 nm lasers, shown in green, are used for cooling. b) The calculated force from superposition of the scattering and dipole forces from each beam. c) Time-trace of a 300 nm silicone nanoparticle as it changes trapping sites. [62, Fig.1]

Fused-silica spheres of diameter 300 nm are aerosolized by vibrating a glass substrate above the trap at 5-10 Torr ($\sim 6.67\text{-}13.33 \text{ mbar}$) of N₂ gas which is enough to damp the falling particles. The position of the nanoparticle is measured by using two quadrant photo-detectors (QPD) to detect the scattered light from the nanosphere.

At room temperature and 2 Torr ($\sim 2.67 \text{ mbar}$), the cooling laser is used to drive the nanospheres into an adjacent trap. This provides information about the half-wavelength of the trap to help with calibration, along with the signal from the QPD, achieving a scale factor for the voltage-displacement. Fig. 21 demonstrates the transition caused by perturbing laser light, the half wavelength between antinodes being $514 \pm 43 \text{ nm}$.

At a high vacuum, 5×10^{-6} (6.67 mbar), the average minimum force detectable is given by [62],

$$F_{min} = S_F^{1/2} b^{1/2} = \sqrt{\frac{4k_b T b k}{\omega_0 Q}} \quad (16)$$

Where b is the measurement bandwidth, $S_F^{1/2}$ s the F thermal-noise force spectral density , k is the spring constant of the oscillator, k_B is Boltzmann's constant, ω_0 . is the resonance frequency, and Q is the quality factor previously mentioned.

Fig. 22 shows the displacement spectral density in the x-direction of a nanosphere held at low vacuum with no cooling and at high vacuum with cooling. A Lorentzian fit shows that at high vacuum, the centre of mass motion was cooled to 460 ± 70 mK, with damping of 460 ± 49 Hz. In the y and z direction, the temperatures are 610 ± 190 mK and 7.9 ± 3 K with damping rates of 1.3kHz and 1kHz respectively. Using 16, the force sensitivity is $S_{F,x}^{1/2} = 1.63 \pm 0.37$ aN/Hz $^{1/2}$.

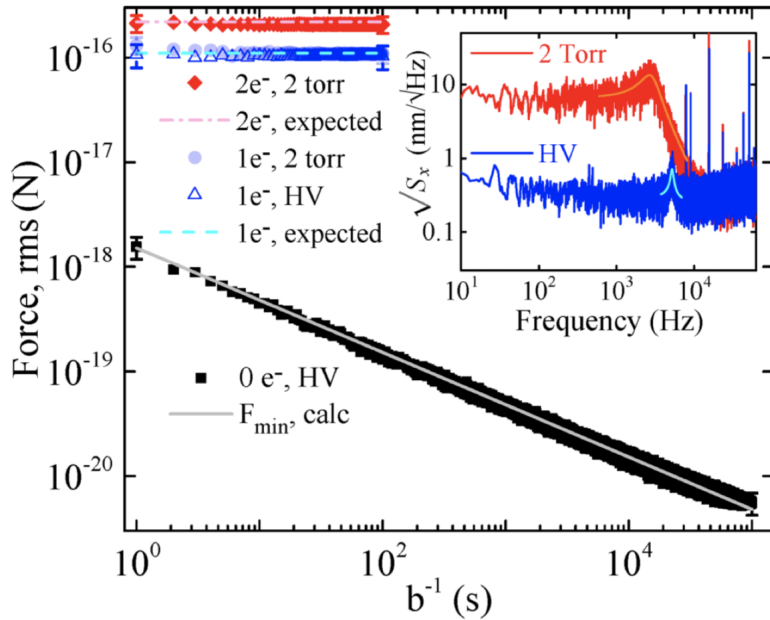


Figure 22: The force measured on charged and uncharged silicone nanospheres as a function of average time at 2 Torr an 5×10^{-6} Torr (HV). The insert is the x-displacement of the sphere at the two pressures with feedback cooling [62, Fig.2]

Fig. 22 shows that for average times of $\sim 10^5$ seconds, the signal due to thermal noise averages down to $b^{1/2}$, but this is limited by the noise in the QPD imaging electronics and trapping laser. At this timescale, the system is sensitive to 5.8 ± 1.3 zN, as indicated by the calculated line in Fig. 22. It was also found that 90% of the beads were neutral.

5.5 Summary

Through the years, a variety of experimental techniques have been employed to measure the Casimir force with varying degrees of success. From Sparnaay's original measurements [45] using levers to the newer experimental techniques, an improvement has been seen in the precision of the experiments, overcoming limitations such as electrostatic forces, static charges, measuring minute separations and thermal noise (see [Experimental Considerations for the Casimir Force](#) [Experimental Considerations for Casimir Force](#)).

Due to the ability to both control temperature using laser light and control the precise position of nanospheres, optical traps are the best of the available methods to detect the Casimir force. Furthermore, it was decided that we would employ these traps in order to experimentally recreate the geometry first proposed by M. Levin [27] and then expanded upon in [2].

6 Non-Newtonian Gravitational Force

The gravitational force has only been measured to a high degree of accuracy at distances greater than 1 cm. The inverse square law (ISL) for non-relativistic gravity is assumed to be valid for separations from infinity to approximately the Planck's length $R_P = \sqrt{\frac{G\hbar}{c^3}} = 1.6 \times 10^{33}$ cm [10], where G is the gravitational constant [65]. Modifications of the ISL in Newtonian gravity at sub-millimetre regimes (approx. 1 mm) is predicted by many theories [66]. One such example is string theory which uses ‘moduli’ fields to determine possible geometries of further dimensions [67]. As an example, if it is assumed $n = 2$ new dimensions, the Newtonian gravity law will transition from $\frac{1}{r^2} \rightarrow \frac{1}{r^4}$ [68].

An exponential decay of the interaction potential with distance is predicted by theories with non-zero gravitational force mediators. Therefore, short range Newtonian gravity corrections are commonly parametrized according to a Yukawa-type potential to embody this form of decay:

$$V(r) = \frac{m_1 m_2}{r} \left(1 + \alpha e^{-\frac{r}{\lambda}} \right) \quad (17)$$

where m_1 and m_2 are the masses separated by distance r . The range of interactions is given by the length λ and α is a dimensionless constant.

6.1 Measurement of the Non-Newtonian Gravitational Force

One of the greatest challenges faced when attempting to test gravity at these sub-millimeter ranges is the dominance of electromagnetic interactions i.e Casimir forces. These must be accounted for to a high degree of accuracy to allow detection of the weaker gravitational force signal [66]. Advantage can be taken of the fact that Casimir forces are solely dependent on material electrical properties, whilst gravity on the mass distribution. To distinguish between the two forces, objects having patches with the same electronic properties but varying density can be used to pinpoint gravitational interactions in short range experiments [66]. However, this method poses several problems due to the following difficulties:

- Making precise measurement of the Casimir forces for surface structures in this way is difficult due to its non-additivity.
- Electrostatic surface potentials can arise during the assembly process of the object.
- Taking measurements by moving a probe laterally over a surface whilst maintaining a constant distant from the surface is challenging.

6.2 Using Casimir Forces to Measure Non-Newtonian Gravitational Force

The Casimir effect overlaps with many ongoing questions in fundamental physics. One such interface is its connection with the mysteries of gravitational physics due to the problem of vacuum energy discussed earlier in [Vacuum Catastrophe/Cosmological Constant Problem](#) [9].

This short-range force can also help with the exploration of non-Newtonian gravitational forces at small separations. It is generally difficult to obtain background-signal free gravity measurements at scales less than 1 mm [10]. Gravitational force tests using dispersion forces can be carried out in the range $0.1 \mu\text{m} - 10 \mu\text{m}$ since this is where the Casimir force dominates the usual gravity force [9]. Measurements of gravity at these length scales can then be used to test string-theory predictions on gravity deviations formulated in part to tackle the cosmological problem.

These new variations of the gravity force would have a quantity equal to the measured difference between the experimentally determined, and theoretically predicted Casimir force [28]. It is therefore crucial that both theory and experiment are measured/conducted accurately since they must be assessed independently [9]. This indicates that theory-experiment comparisons to prove specific theoretical models or experimental results for the Casimir force are not possible. Through analysis of the experimentally allowed λ and α combinations in the Yukawa potential, at separations of $10 \mu\text{m}$ and below, gravity is no longer the dominant force between uncharged, non-magnetic bodies. Thus, there has been some level of success in constraining short range ISL deviations [66].

7 Optically Trapped Levitated Nanoparticles

7.1 Optical Traps

There are a variety of nanoparticle traps that are used for distinct purposes within different fields of science. While some traps, like the Paul Trap for instance, use various specific electrical currents and potentials to trap a particle, many modern systems use lasers and optomechanics instead.

Optomechanics offers a toolbox which allows us to study both classical and quantum mechanical oscillators in a highly controlled manner. Optical traps employ lasers to uniquely control the dynamics of small and nano-sized particles. These lasers are able to produce forces in the piconewton scale in order to move atoms and molecules of varying sizes.

A variety of different modern nanoparticle traps have been proposed and designed containing a range of flexibility, as well as efficiency [69]. Optical traps are used across fields of physics and biochemistry, particularly in modern research into high mass quantum physics [70]. Additionally, it has enabled experiments investigating protein characterization, laser induced fusion, and quantum information processing [71]. The ability of these traps to levitate and isolate particles in a vacuum, creating minimal contact with the environment, coupled with their power to cool particles in the order of 10^{-3} K, makes them an exciting tool in modern nanoparticle research.

The main component used in the employed particle trap is an optical tweezer. Optical tweezers use high frequency lasers which provide attractive or repulsive forces derived from the law of momentum conservation. The gradient trapping force is applied by bringing the laser beam to a diffraction limited focal spot through a large microscope objective [72]. These forces are used to slow down atomic sized particles and confine them to localized areas, and is able to lower the center-of-mass (COM) motion to significantly reduce thermal noise. A schematic of the employed optical trap is shown on Fig. 23 [73].

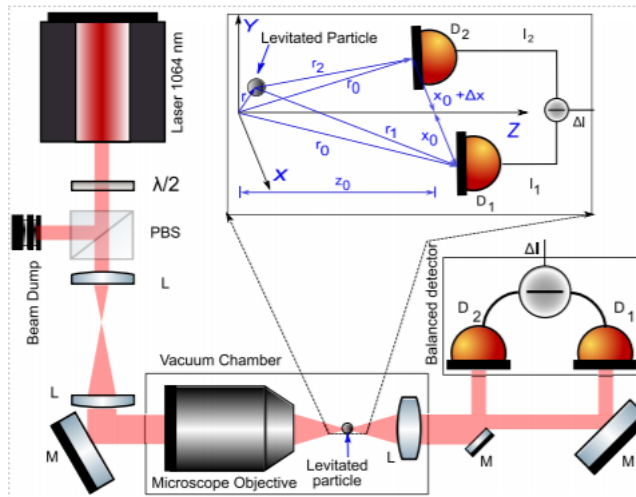


Figure 23: Schematic of Optical Tweezer Setup. The above symbols are defined as follows: L is a lens, M is a mirror, PBS is a polarizing beam splitter, $\lambda/2$ is a half-wave plate, and D are diodes. Reproduced from [73, Fig. 1]

The laser setup displayed in Fig. 23 is placed inside a strong vacuum chamber in order to lower the interaction with the surrounding environment.

7.2 Levitated Nanoparticles for Casimir Force Experiments

Various particles have been used across different experiments involving nanoparticle and optical traps. Whilst most experiments involving quantum levitation in optical traps have focused on low-absorption particles such as silicon [3], optical traps are able to trap particles ranging from metallic nanoparticles, to quantum dots.

One metallic particle that is commonly used in Casimir force experiments is the gold (Au) nanoparticle due to its benefits in nanoparticle trapping experiments. Firstly, the relatively large size of gold nanoparticles makes them significantly easier to trap and detect; one study finding a sixfold increase in trapping efficiency and detection compared to similarly sized polystyrene particles [74]. Previous investigations into Casimir forces using gold nanoparticles, like in the paper [2], would allow for comparisons to previously simulated and recorded data. These conditions, coupled with a reasonable accessibility to the particle, make the gold nanoparticle an optimal candidate for use in Casimir force experiments.

IV SIMULATIONS: SETTING THE TRAP

1 The Motivation

The motivation for simulating the nanoparticle system prior to starting experimentation is immediately apparent when you consider the delicate and expensive experimental equipment involved, and the limited number of laboratory hours available.

Not only does running a simulation provide a method by which to explore the properties of a system without risking jeopardising a carefully calibrated experimental set-up, but more usefully, it also allows for quick changes to initial conditions, testing of new interactions and pure experimentation without the fear of making mistakes.

“In real life mistakes are likely to be irrevocable. Computer simulation, however, makes it economically practical to make mistakes on purpose. If you are astute, therefore, you can learn much more than they cost. Furthermore, if you are at all discreet, no one but you need ever know you made a mistake.”

- John H. Mcleod in *Natural Automata and Useful Simulations* [75]

In this particular experiment, trapping the nanoparticle within the optical tweezers is no trivial task, it can take a number of hours and mistakes such as trapping multiple particles or losing the particle from the trap are easily made. Additionally, once the particle is trapped and a vacuum is pulled on the pressure vessel, no more alterations to the equipment are possible without repressurizing and starting from scratch. Furthermore, there are a host of experimental issues that can affect the experiment such as condensation formation and melting of the nanoparticle which can require the entire experiment to be restarted - a simulation is plagued by none of these issues.

An additional, but perhaps less tangible, advantage of simulating a physical system is that it often allows the observer to gain a more intuitive understanding of the underlying mechanics at play, more so than equations and theory alone can provide – if nothing else it allows the experiment to be started from a position of greater understanding.

The final and arguably most important motivation for building a simulation to run in tandem with the experiment was to provide a source of comparison for the experimental data collected. This source of comparison facilitates the expedient confirmation of behaviours that were expected, and equally valuable, the identification of those behaviours that were not.

1.1 The Basis of the Simulation

The initial step in producing the simulation consisted of forming a three-dimensional harmonic oscillator. The nanoparticle oscillates according to the harmonic potential produced by the laser that forms the optical tweezers [76].

We modelled the oscillator with three independent orthogonal axis of motion. Each with a different frequency of oscillation determined by the optical trap stiffness, k . The independent axis of motion x , y and z have k -values of 1.42×10^{-7} N/m, 5.68×10^{-7} N/m and 8.88×10^{-7} N/m, respectively. The equation of motion along the i^{th} axis can thus far be written as:

$$m\ddot{\mathbf{r}}_i(t) = -k\mathbf{r}_i(t) \quad (18)$$

where m is the mass of the nanoparticle and $\mathbf{r}_i(t)$ is the time dependent position along the i^{th} axis.

Numerical methods were used to solve this second order differential equation. To integrate the three independent equation's ($i = x, y, z$) numerically, we chose the velocity verlet integration scheme. This scheme was specifically chosen as it provides the important properties necessary for physical systems, such as time reversibility and energy conservation. The scheme uniquely implements energy conservation by allowing the integrator to stay on a surface of constant energy within the phase space. Where the phase space is a space defined by the nanoparticle's position and momentum. This type of integrator is known as symplectic and preserves this area of phase space [77].

The general form of the equations used in the velocity verlet scheme is shown below [1]:

$$\mathbf{r}_i(t + \Delta t) = \mathbf{r}_i(t) + \mathbf{v}_i(t)\Delta t + \frac{1}{2}\mathbf{a}_i(t)\Delta t^2 \quad (19)$$

$$\mathbf{v}_i(t + \Delta t) = \mathbf{v}_i(t) + \frac{\mathbf{a}_i(t) + \mathbf{a}_i(t + \Delta t)}{2}\Delta t \quad (20)$$

where \mathbf{v}_i and \mathbf{a}_i is the time dependent velocity and acceleration along the i^{th} axis, respectively and Δt is the time step. Thus, the algorithm that was implemented into our code goes as follows:

- The acceleration of the nanoparticle is calculated using the equation of motion.
- The position of the nanoparticle is then updated according to Eq. (19).
- Finally, the velocity of the nanoparticle is updated according to Eq. (20).

This verlet integration algorithm take place within a while loop where the time step iterates the simulation to produce a real time animation of the nanoparticle oscillating. Screenshots of the animation can be seen in Fig. 24.

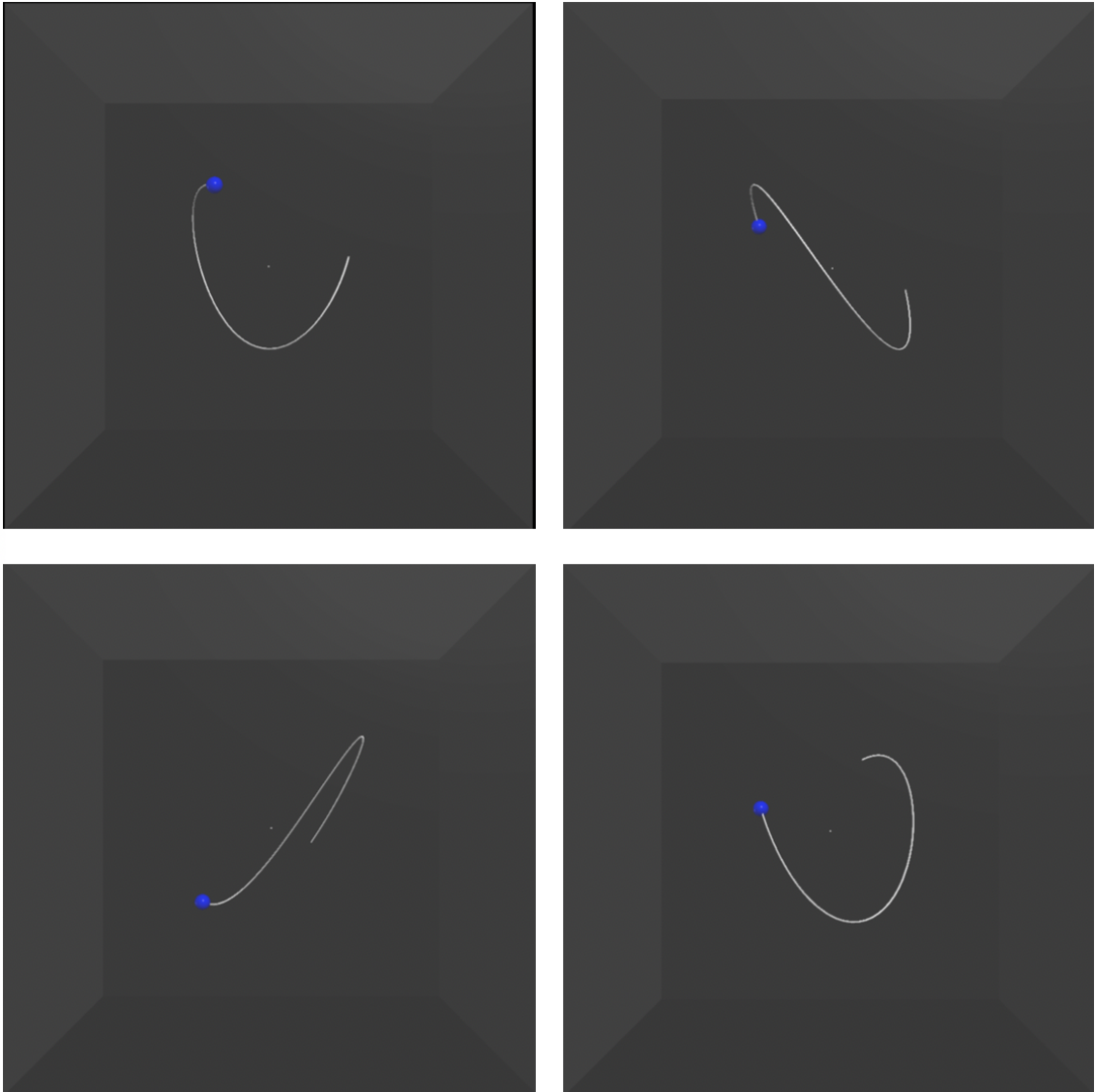


Figure 24: The nanoparticle oscillating according to the three-dimensional harmonic potential in a real time simulation shown in four images.

The motion of the nanoparticle is also illustrated by position-time and velocity-time graphs as shown in Fig. 25 and Fig. 26, respectively. These graphs are also plotted in real time as the nanoparticle oscillates in the simulation as was shown in Fig. 24. Each data point is plotted within the while loop and the graph is updated at the same time the animation is updated, to provide an accurate representation of the motion graphically.

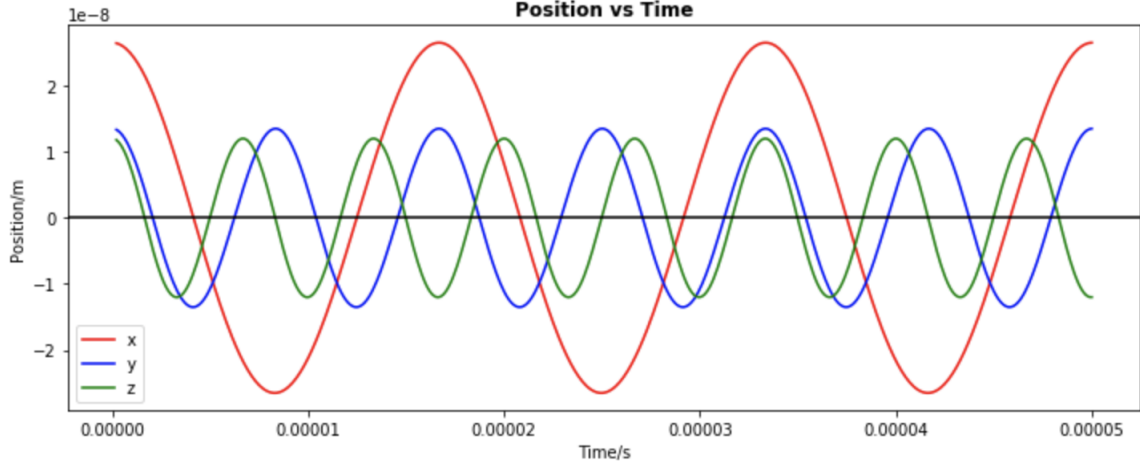


Figure 25: Position-time graph of the nanoparticle's motion.

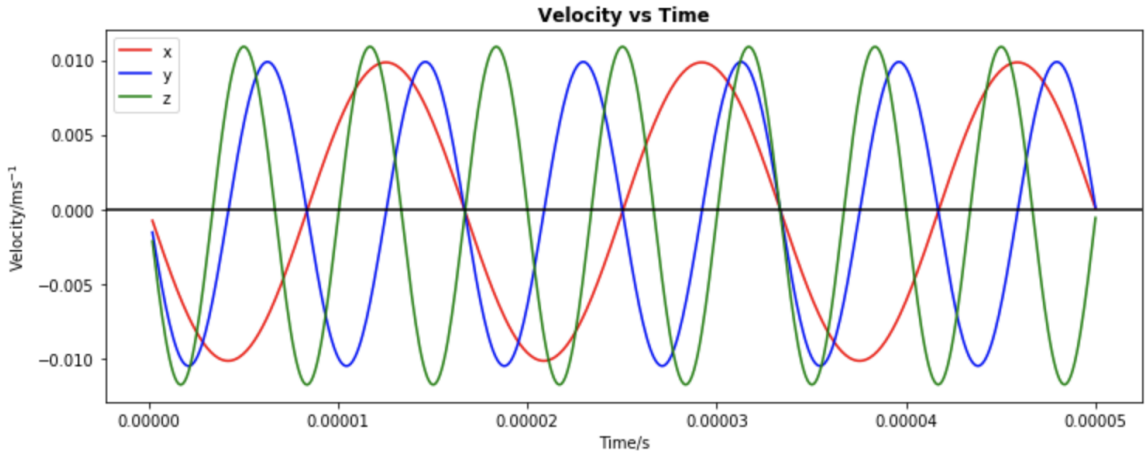


Figure 26: Velocity-time graph of the nanoparticle's motion.

To further progress with the simulation, the gas damping as a function of pressure was added. The damping rate, while assuming an equilibrium of the nanoparticle internal temperature with the background gas temperature, is given by Eq. (21) [78].

$$\gamma_{gas} = \frac{(1 + \frac{\pi}{8})\bar{c}P_g m_g}{k_b T_b a \rho} \quad (21)$$

where \bar{c} is the nanoparticle mean speed Eq. (22) [78], P_g the gas pressure, m_g the mass of the gas molecules, k_b Boltzmann's constant, a and ρ the nanoparticle radius and density respectively, and T_b the bath temperature.

$$\bar{c} = \sqrt{\frac{8k_b T_b}{m_g \pi}} \quad (22)$$

Under the following conditions: $P_g = 5$ mbar, $m_g = 5.46 \times 10^{-26}$ kg, $T_b = 293$ K, $a = 199$ nm, $\rho = 1850$ kg/m³, the gas damping term was evaluated to be 110 Hz.

The updated equation of motion with an additional gas damping term is shown below:

$$m\ddot{\mathbf{r}}_i(t) = -k\mathbf{r}_i(t) - \gamma_{gas}\dot{\mathbf{r}}_i(t) \quad (23)$$

Running the updated simulation demonstrates the effect of the gas damping term. The amplitude of the motion, on each of the three-independent axis, decays to zero with a characteristic envelope as determined by γ_{gas} . This is shown in Fig. 24.

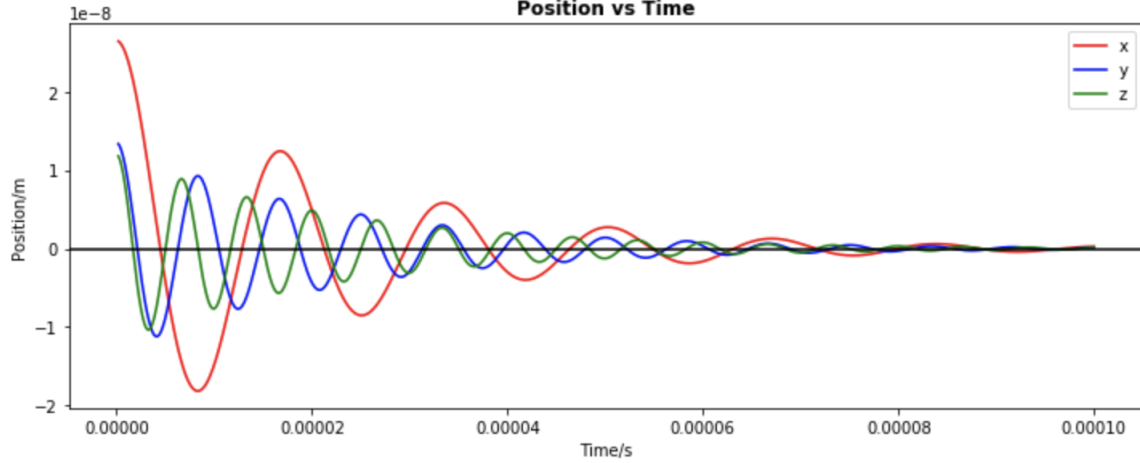


Figure 27: Position-time graph of the nanoparticle's motion with gas damping.

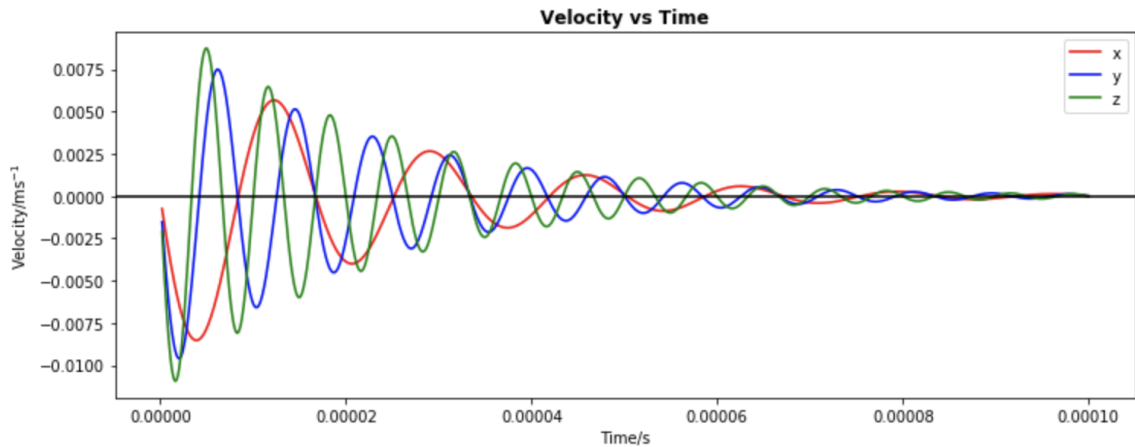


Figure 28: Velocity-time graph of the nanoparticle's motion with gas damping.

One initial problem with the simulation was that due to the damping force from the gas, the nanoparticle oscillations had a tendency to decay to zero over time. This was overcome by adding a driving term to the particles motion that set a limit on how small the oscillations could become. From the nanoparticles perspective there are two sources of energy input that could be considered to drive the oscillations to some extent. The first, and likely least significant reason, is that the nanoparticle is regularly colliding with gas particles within the pressure chamber and as such, it's momentum should be expected to equilibrate with the mean gas particle momentum over time. Therefore, if the nanoparticle's velocity drops too low, we should expect to see a net momentum transfer from the gas particles to the nanoparticle until they are once again in equilibrium.

It is reasonable, however, to suspect this factor is insignificant due to the large difference in the mass of the nanoparticle and the mass of the gas particles - an order of around a hundred million – which means this could only ever provide a very low floor to the amplitude of the nanoparticle oscillations, and therefore there must be a larger factor at play.

The second, more significant factor is that the nanoparticle is constantly being heated through the absorption and scattering of photons from the laser used to trap it [78], and indeed due to the low

pressures involved this heating effect can even lead to melting of the nanoparticle [78] if it is not adequately cooled.

The updated equation of motion with the additional thermal driving force term shown below [78]:

$$m\ddot{\mathbf{r}}_i(t) = -k\mathbf{r}_i(t) - \gamma_{gas}\dot{\mathbf{r}}_i(t) + \mathbf{F}_{th} \quad (24)$$

$$F_{th} = 4k_B T m \gamma_{gas} \quad (25)$$

where γ_{gas} is the damping value described by Eq. (21).

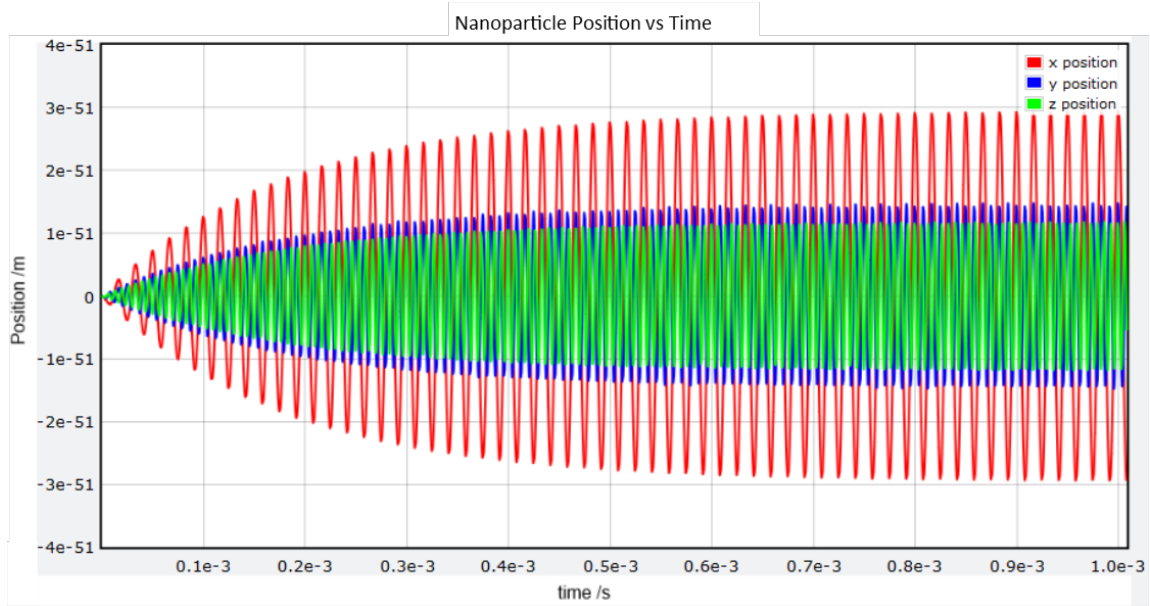


Figure 29: (a) Position-time graph of the nanoparticle's motion with gas damping and a thermal noise term.

It can be seen in Fig. 29 that after implementing the thermal noise term, even when the particle's initial position and velocity are set to zero, its amplitude still grows until the thermal noise and gas damping effects are in equilibrium. This is in contrast to the behaviour shown prior to the introduction of a thermal noise term in Fig. 25 where, had the particle started with zero velocity and placed at the origin, it would have stayed there without moving.

V EXPLORING COLLISIONS

1 Introduction

One avenue explored for measuring short ranged forces was calculating momentum and energy changes in collisions between a nanoparticle, and a range of incoming particles/molecules. The hypothetical experimental setup would involve an optically trapped and levitated nanoparticle. These calculated effects were then compared to simulations of the same system to see if there were any discrepancies. The hurdle to overcome with this method would have been the question of how to fire these particles/molecules at the target nanoparticle.

2 Field Ionisation of molecules

It is feasible to introduce the gaseous molecules to the chamber and let random motion take its course, however this surrenders a degree of control over the experiment, not knowing precisely when and how a collision will occur, especially when there may be other molecules in the chamber.

A solution to this is to ionise the gaseous molecules. Charged molecules are much easier to manipulate than neutral molecules, as it allows the use of electric and magnetic fields to control their motion.

Ionisation can be achieved through various means, but the simplest for this investigation is through the use of strong external electric fields [79, 80].

Electric fields, when applied to an atom or molecule, change the energy potential that keeps electrons bound to their nuclei. Normally, the main contributor to this potential is the coulomb force between the negative electrons and the positive nucleus - hence why an electric field is effective at perturbing it. Without the external field, the energy potential is similar to a well centred around the nucleus. The further out an electron orbits a nucleus, the less tightly bound it is, and thus less energy is required to free it, which can be inferred from the equation of electric potential energy between two point charges, and simplifying the molecule as such [81]:

$$V = \frac{q_1 q_2}{4\pi\epsilon_0 r} \quad (26)$$

where q_1 and q_2 are the charges of the point charges, r is the separation between the charges and ϵ_0 is the electric permittivity of free space.

When a strong electric field is applied to the molecule, the perturbed potential energy from the coulomb interaction can be expressed as [80]:

$$V(z) = -\frac{e^2}{4\pi\epsilon_0 z} - eF_z z \quad (27)$$

where e is the electron charge, z is the separation in z -axis and F_z is the force of the electric field in the z -axis.

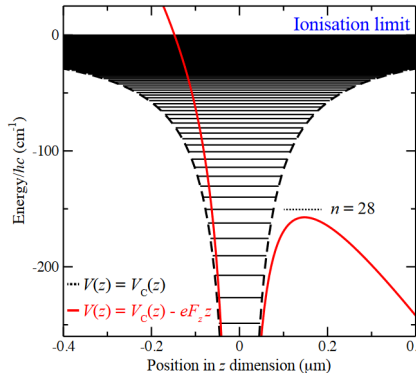


Figure 30: V_c is the pure coulomb potential experienced by the electron, represented by the black well. The red well shows how V_c is perturbed under a strong electric field. Reproduced from [80, Fig. 8.6]

By differentiating and setting the derivative to zero, the saddle point of the potential can be found, and thus the electron states it ionises. Rearranging the perturbed potential for the saddle point position gives:

$$z_{saddle} = \sqrt{\frac{e}{4\pi\epsilon_0 F_z}} \quad (28)$$

Which can be inserted into the perturbed potential equation, and further manipulated to get:

$$V(z) = -2\sqrt{\frac{e^3 F_z}{4\pi\epsilon_0}} \quad (29)$$

This can then be rearranged to find F_z , the electric field strength, needed to ionise a molecule of a chosen ionisation energy $V(z)$. Once this is known, the next concern becomes finding suitable apparatus to generate a possibly very large electric field strength.

Two methods were identified and covered over the course of the project. The first was the Dielectric Barrier Discharge setup, the other was the utilisation of electric fields at sharp points.

2.1 Dielectric Barrier Discharges

Dielectric Barrier Discharges (DBDs) are a relatively common tool used to create small, controlled bursts of plasma from a substrate gas. Initially used to create ozone, they are now used more commercially as well, such as indoor air treatment, or to clean and sterilise polymer surfaces [82].

In its most basic configuration, a DBD [83, 84] is essentially a high voltage (1 kV–100 kV) capacitor operated at room temperature (298 K), and standard atmospheric pressure (1 bar), with insulating dielectric and substrate gas placed between the plates. The dielectric can be formed with materials like glass or plastic, and the gas is the material that is required to be ionised.

The mechanism by which it works is via a strong uniform electric field, generated by the high voltage plates. This uniform electric field can be expressed via the following equation [81]:

$$E = \frac{\Delta V}{d} \quad (30)$$

where E is the strength of the uniform electric field, ΔV the potential difference between the plates and d the separation between the plates.

With the presence of the dielectric insulator, the potential difference between the plates is modified [81]:

$$\Delta V = \frac{\Delta V_0}{\kappa} \quad (31)$$

where ΔV_0 is the potential difference without the dielectric.

Inserting this new potential difference into the uniform electric field yields:

$$E = \frac{\Delta V_0}{d\kappa} \quad (32)$$

where κ is the dielectric constant or relative permittivity of the dielectric.

The electric field ionises the gas molecules by lowering the potential energy the bound electrons must overcome to become free electrons (and thus ionise the molecule). A more tightly bound electron, one that is in a shell closer to the nucleus, has less kinetic energy, so a stronger field would need to be applied to the molecule to free it than for an electron further from the nucleus. So for the goal of making a plasma - stripping a molecule of all of its electrons - a very strong electric field is needed, hence the high operating voltages.

Generally, DBDs operate in 1 bar of atmospheric pressure, but can work in lower pressures, down to at least 0.13 bar [85]. This is preferred as a lower pressure would mean less ambient molecules for the ionised particles to collide with, increasing the average distance over which they could travel, and the more often collisions will occur between an ion and the nanoparticle. Fig. 31 shows some basic DBD configurations.

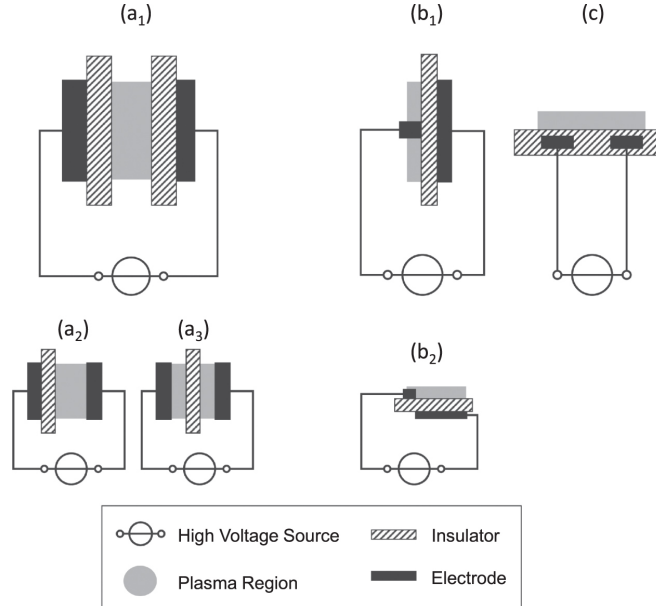


Figure 31: Basic planar configurations of DBDs: (a) volume DBD (1-symmetric, 2-asymmetric, 3-floated dielectric); (b) surface DBD (1-symmetric, 2-asymmetric 'actuator' design); (c) coplanar discharge. Reproduced from [83, Fig. 1]

In the a_1 setup, both electrodes are shielded by dielectric, preventing corrosion and extending lifetime of the setup. In the a_2 and a_3 setups, one or both of the electrodes are exposed, risking corrosion, but can also generate more plasma as it has more space for gas, and can operate at lower voltage magnitudes.

b_1 and b_2 are surface DBD designs – both electrodes are in contact with the dielectric barrier, plasma is formed in the gas at the exposed surface electrode, which propagates along the dielectric surface while the sheet or counter electrode is embedded in an additional dielectric layer (not shown in the figure).

c is a coplanar discharge model - both electrodes are embedded in the insulator and the discharge appears in the gas above the dielectric surface.

In theory, a setup similar to one of the basic configurations above could be used with a smaller electric field to only lightly ionise a desired molecule. This would also make such a setup safer by not having to use as high voltages.

The problem with this setup is that some molecules may require very large electric fields even for their first ionisation energy, which would necessitate extremely high voltages, or specially machined capacitor plates and dielectric in order to reduce separation distance to the order of microns. The issues with again with these solutions is the high danger such voltages pose, and the procurement time and expense of the latter, as well as raising the further question of how to inject a suitable amount of gas in between the plates.

2.2 Sharp Point Electric Fields

Another explored method for the ionisation of molecules was electric fields at a sharp point [86]. These exploit free charge density in conductors to generate large electric fields. The generated fields are strong enough to be utilised in apparatus such as MMR spectroscopy machines, in which the fields tear the molecules apart into pieces to be examined.

To explain the how the electric field at a sharp point can be so strong, consider two conductors with the same potentials, one is flat, the other has a sharp, highly curved end. A conductor must be an equipotential, due to charge carriers (electrons) repelling each other to the surface of said conductors (so the net field inside the conductor is always zero). This means that the field lines outside the conductor are always perpendicular to the surface. For the flat conductor, these field lines are equally spaced, but near the curved conductor the lines are more closely spaced close to

the conductor than further away – the electric field strength of the curved conductor is greater closer to it and decreases with distance.

Since the field is stronger near sharp points, gaseous molecules close to the surface will be affected by a strong electric field, inducing dipoles in them. These molecules will then be attracted to the conductor due to their dipoles, once they contact the surface they will be ionised to a like-polarity of the conductor. They will then be repelled due to the like charge – this happens for many particles at once, forming a kind of ion wind.

This effect could be used with a needle with high voltage flowing through it to ionise molecules and launch them at the trapped nanoparticle. The advantage is that this method means that lower voltages could be used, compared to a dielectric barrier discharge, as well as providing the means of propelling the ions at the nanoparticle. The setup would not require any specially machined parts or any dielectric, either.

3 Calculations

3.1 Particle Collisions

This experiment would involve creating a source of energised particles which could be fired with a known momentum to make the nanoparticle displace from its equilibrium oscillation within the optical trap. The main criteria in choosing the particle was both the availability and practicality of firing said particle, as well the ability to operate within an energy range which would suitably displace the trapped nanoparticle without completely removing it from the trap.

3.2 Trapped Nanoparticle

While the nanoparticle is located in the optical trap, it undergoes movement in the form of a simple harmonic oscillation around an equilibrium. The frequency of oscillation differs slightly depending on the spatial axis, but is approximately 100 kHz. Using this frequency in conjunction with the mass of the particle, it is possible to identify the restoring force of the particle trap, as well as the maximum displacement from equilibrium. These calculations are displayed below.

The trap's spring constant is given by [87]:

$$k = m\omega^2 = 4\pi^2mf^2 \quad (33)$$

where m is the mass of the nanoparticle, f the frequency and ω the angular frequency. In this case $f = 10^5$ Hz and $m = 3.79 \times 10^{-18}$ kg, giving $k = 1.496 \times 10^{-6}$ kg s^{-2} . The mean displacement of the nanosphere at its centre of mass temperature T is given by Eq. 34 [87]:

$$\bar{x} = \sqrt{\frac{2k_B T}{k}} \quad (34)$$

where k_B is the Boltzmann constant. Since the nanoparticle is cooled to a temperature of $T = 10^{-3}$ K, it has an average maximum displacement $\bar{x} = 1.32 \times 10^{-10}$ m. To detect a deviation from this motion, the particle must be displaced by a minimum of $2\bar{x}$, requiring an energy of $E_{2\bar{x}}$. This is calculated as follows [87]:

$$E_{2\bar{x}} = \frac{1}{2}k(2\bar{x})^2 = 2k\bar{x}^2 \quad (35)$$

Using the determined value of \bar{x} gives $E_{2\bar{x}} = 5.52 \times 10^{-26}$ J, which corresponds to a momentum increase of $p_s = 6.47 \times 10^{-22}$ kg m s^{-2} . As shown, the maximum displacement by the trapped nanoparticle is 13.2 nm. In order to confidently measure a kick induced by a particle collision, it requires a minimum displacement by the nanoparticle of twice its maximum displacement due to its oscillation about the equilibrium. This requires a minimum increase in momentum of 6.47×10^{-22} kg m s^{-2} for the nanoparticle. Using this value, particles of varying mass and charge were investigated to find an ideal particle which would reasonably transfer at least this amount of momentum to the stationary nanoparticle.

3.3 Incoming Particles

Below is a shortlist of particles identified as potential sources, as well as assumptions and reasons for including or omitting each particle. In the preliminary calculations performed on some of the particles, several assumptions were made about the interaction of the particles during the collision. These assumptions provide a very idealised version of the collisions and provide estimates to determine experimental feasibility.

Alpha Particles

The α particle consists of two protons and two neutrons closely bound together within a nucleus. Assuming an incoming energy of 4 MeV, the energy loss due to a collision with a stationary silicon dioxide (SiO_2) nanoparticle was found to be 20 keV. This value was found via Monte Carlo simulations, and was used to calculate the momentum change induced onto a SiO_2 nanoparticle. The velocity of the nanosphere prior to the collision v_s was taken to be 0 (by considering the collision in its initial reference frame). The velocity after the collision v'_s was then calculated and compared with the mean velocity of the nanosphere $\langle v_s \rangle$ for different temperatures (center of mass, not internal), to see whether the collision would be noticeable over the thermal motion of the nanosphere. The calculations are summarised below [88]

$$E_\alpha = \frac{p_{\text{alpha}}^2}{2m_\alpha} \quad (36)$$

$$v_s = \sqrt{\frac{2m_\alpha \Delta E_\alpha}{m_p^2}} \quad (37)$$

$$\langle v_s \rangle = \sqrt{\frac{k_b T}{m_s}} \quad (38)$$

Using Eq. 36 and Eq. 37, it is possible to calculate an average velocity of the trapped particle of $v_s = 0.0016 \text{ ms}^{-1}$. Using Eq. 38 which shows the average velocity for a trapped particle of mass m_s and temperature T , it is found that a SiO_2 particle moves with an average velocity of 0.0006 ms^{-1} , which is small enough to be distorted by the α particle collision. Thus the α particle was deemed a potentially suitable incoming gas particle for the proposed experiment.

Electrons

A central reason it was decided to investigate the usage of an electron for the collision is the accessibility of an electron gun. In order to simplify the calculations, the assumption was made that the electron would be absorbed by the nanoparticle. Though this is not an accurate model of the electron-nanoparticle collision, the approximate nature of these calculations allows for the assumption. This was begun by calculating the velocity required using a classical scheme, but due to the immense mass ratio to the order of 10^{13} between the electron and nanoparticle, this resulted in an electron velocity above the speed of light $v_e = 7.10 \times 10^8 \text{ ms}^{-1}$.

A further calculation was then performed using a relativistic scheme, using a Lorentz coefficient $\gamma = \frac{E_e}{m_e c^2}$ and relativistic kinetic energy $E_{KE} = (\gamma - 1)m_e c^2$. Propagating these equations using the mass of an electron m_e shows that in order to induce the necessary displacement, a minimum electron kinetic energy 836 keV is required. However, this greatly surpasses the 1 keV - 100 keV energy range of an electron gun [89]. As a result, the electron was not found to be a viable particle for this experiment.

Neutrons

Though a neutron would theoretically be a viable candidate due to its mass and neutral charge, the practical limitations of creating neutron emission proved to be too great. This is due to the safety regulations imposed on the highly penetrative particle, causing high security costs as well as risk [90].

Sulfur Hexafluoride (SF_6)

Unlike for the alpha particle, it was not possible to verify the energy shift due to a collision between an SF_6 and a gold nanoparticle. As a result, the calculation was simplified by assuming a perfectly

elastic collision, where no kinetic energy was lost. Though this is an imperfect assumption, it was predicted that the energy loss in an SF₆ collision would be small due to its spherical shape and lack of polarity [91]. Thus, the following equation was derived, where m_s and m_n are the masses of the SF₆ and the nanoparticle respectively. The velocities of SF₆ before and after collision are v_s and v'_s respectively whilst v_n is the velocity of the nanoparticle after the collision. This equation applies to all elastic collisions:

$$v_n = \frac{2v_s m_s}{m_s + m_n} \quad (39)$$

Inserting the relevant variables, it was found that a minimum incoming velocity of — was required for the SF₆ to induce an experimentally significant velocity change for the gold nanoparticle. Since this velocity is achievable through gas particle ionization, SF₆ was deemed to be a viable gas particle candidate.

Buckminster Fullerene (C₆₀)

The central issue involving the use of C₆₀ is the creation of the particle in a gaseous state. This is principally achieved using an electric furnace, which creates temperatures upwards of 1400 K, or through laser ablation. Laser ablation is a process in which particles are removed from a solid through irradiation by a high frequency laser beam [92]. This process allows a more controlled but smaller sample of particles to be removed as gas particles, however comes with several complications. Firstly, the mere laser ablation of C₆₀ in a solid state does not actually form C₆₀ gas particles, but rather reforms them into graphite particles. Instead, as outlined in a paper by Dasuke Kasuya *et al.* at the Meijo University in Japan, one would perform the ablation on graphite in the presence of a buffer gas (like He, Ar, or N₂) [93]. In the aforementioned experiment, the maximum yield of C₆₀ was found to be only 4% of that created by an electric furnace. Due to the evident complications in the formation of gaseous C₆₀ particles, as well as the lack of access to an electric furnace, it was decided not to use them for the purposes of an experiment.

3.4 Final Particle Chosen

From the benefits and issues of using the various particles discussed above, it was decided that the SF₆ and α particle were the two viable options for the experiment. From these choices, SF₆ was decided to be more ideal, principally due to its spherical shape which, as discussed earlier, is expected to lower the total energy loss in the collision. Additionally, the larger mass of the SF₆ particles mean a smaller energy is required to displace the trapped gold nanoparticle.

3.5 Simulating Gas Collisions

The gas collisions were modelled by drawing each velocity component from a Gauss distribution with variance [78]:

$$\sigma^2 = \frac{k_B T}{m} \quad (40)$$

where T is the temperature of the gas and m the mass of the gas particle. For the purposes of the simulation, the gas was assumed to be Nitrogen with a molecular mass of 28 atomic mass units.

The i_{th} velocity component of the n_{th} gas particle is then found by iterating over the following equation [78]:

$$v_{n,i} = \sqrt{\frac{k_B T}{m_n}} G(0, 1) \quad (41)$$

where G(0,1) is a Gaussian random number with a mean of zero and a variance of one.

Each velocity component of a given gas particle then follows a Gaussian distribution with equation:

$$\pi v_i dv_i \propto \exp\left(-\frac{v_i^2}{2\sigma^2}\right) dv_i \quad (42)$$

However, when the velocity vector distribution is written in spherical coordinates and integrated over the two angular components, a Boltzmann distribution is obtained with equation:

$$\pi v dv \propto v^2 \exp\left(-\frac{v^2}{2\sigma^2}\right) dv \quad (43)$$

When determining the frequency of gas particle collisions with the nanoparticle, it was important that the timing of these collisions was as random as possible. To achieve this, a dice roll was replicated by drawing a pseudo-random number and checking its size, this can be seen in line 161 of the code.

The three velocity components of the gas particle were then generated using Eq. (41) and these were used to find the momentum of the gas particle on each axis. These velocities were then converted to momenta and a random portion of this momenta on each axis was added to the momentum of the nanoparticle.

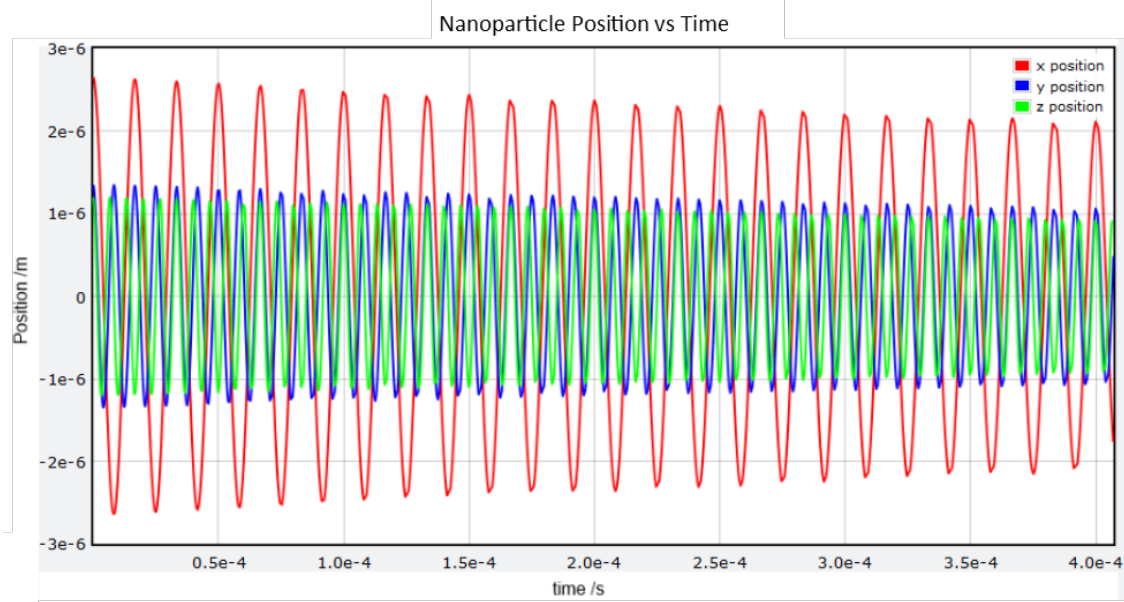


Figure 32: Position-time graph of the nanoparticle's motion with gas collisions, damping and thermal noise. Nanoparticle started with an initial velocity of zero and initial position coordinates of 2.65×10^{-6} m, 1.35×10^{-6} m and 1.2×10^{-6} m for the x, y and z axes, respectively.

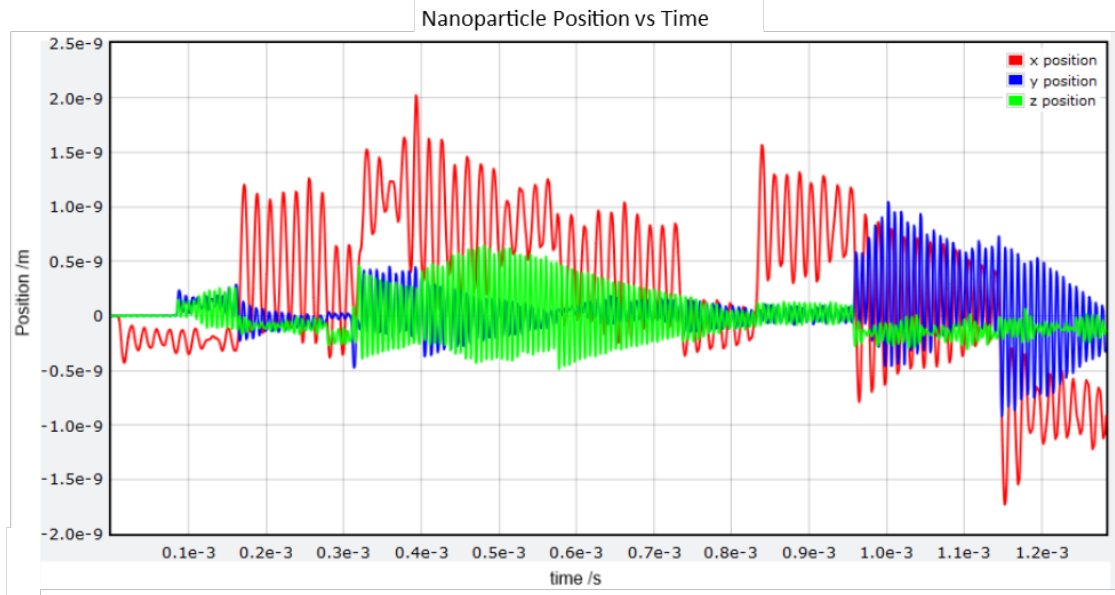


Figure 33: Position-time graph of the nanoparticle’s motion with gas collisions, damping and thermal noise. Nanoparticle started with zero velocity and initial position coordinates were (0,0,0).

It can be seen from the differences between Fig. 32 and Fig. 33 that the effect of the gas particle collisions on the motion of the nanoparticle is very sensitive to the average velocity of the nanoparticle. When the amplitude of the oscillations are small (on the order of nanometres rather than millimetres), and by extension the average velocity is also small, as in Fig. 33, the effect of the gas particle collisions is far more pronounced.

However, when the amplitude of oscillation is larger, as in Fig. 32, and hence the average velocity is also larger, the effect of the gas collisions on the motion of the nanoparticle is minimised and observing even a single collision becomes difficult.

3.6 Simulating Projectile Collisions

Collisions between the nanoparticle and both alpha (α) particles, and Sulfur Hexafluoride (SF_6) molecules were also simulated. The alpha particle mass was taken to be the accepted value [94] of 4 atomic mass units or 6.64×10^{-27} kg and its velocity was taken to be around 5% of the speed of light, or 15×10^6 m/s [95]. Likewise the SF_6 molecules were taken to have the accepted mass of ~ 146 atomic mass units [96] or 2.43×10^{-25} kg and it’s velocity 274 m/s, where the velocity was calculated using Eq. (22).

In the simulation, the projectiles were considered to be moving down the x-axis in the positive direction and so all collisions between the nanoparticle and projectile took place along this plane. In both cases, as with the gas collisions, the collision frequency was decided by a pseudo-random process. Once a collision was triggered, the projectile exchanged a random portion of its momentum in the x-direction with the nanoparticle. This was done in order to account for the range of possible collisions that could occur, from total reflections and glancing collisions, to situations in which the projectile stuck to the nanoparticle, imparting all of its momentum.

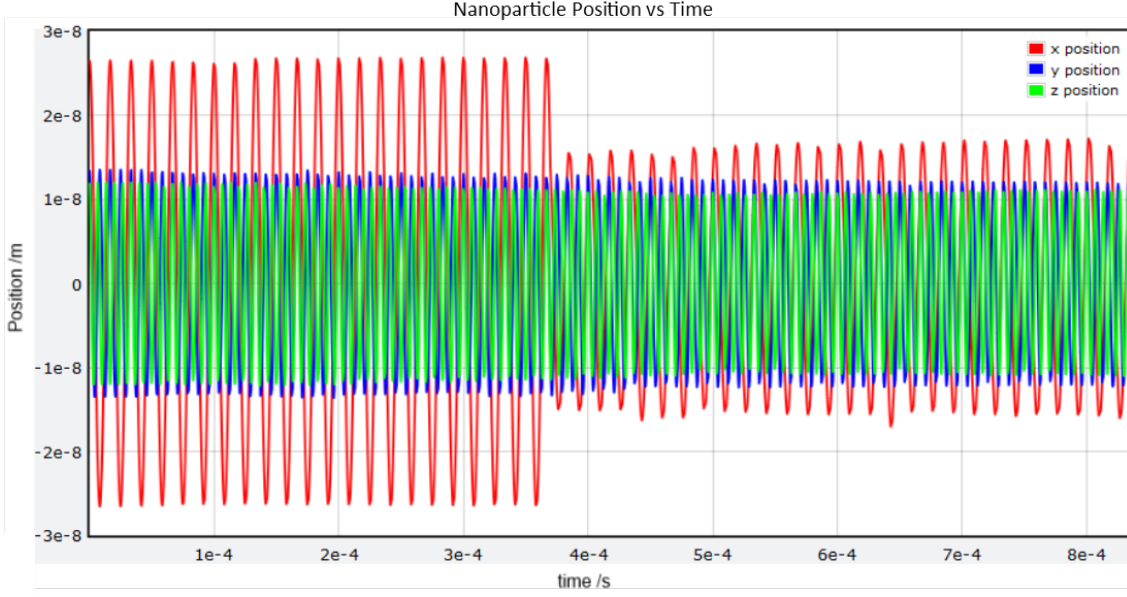


Figure 34: Position-time graph of the nanoparticle’s motion shows the particle being decelerated by a collision with an alpha particle.

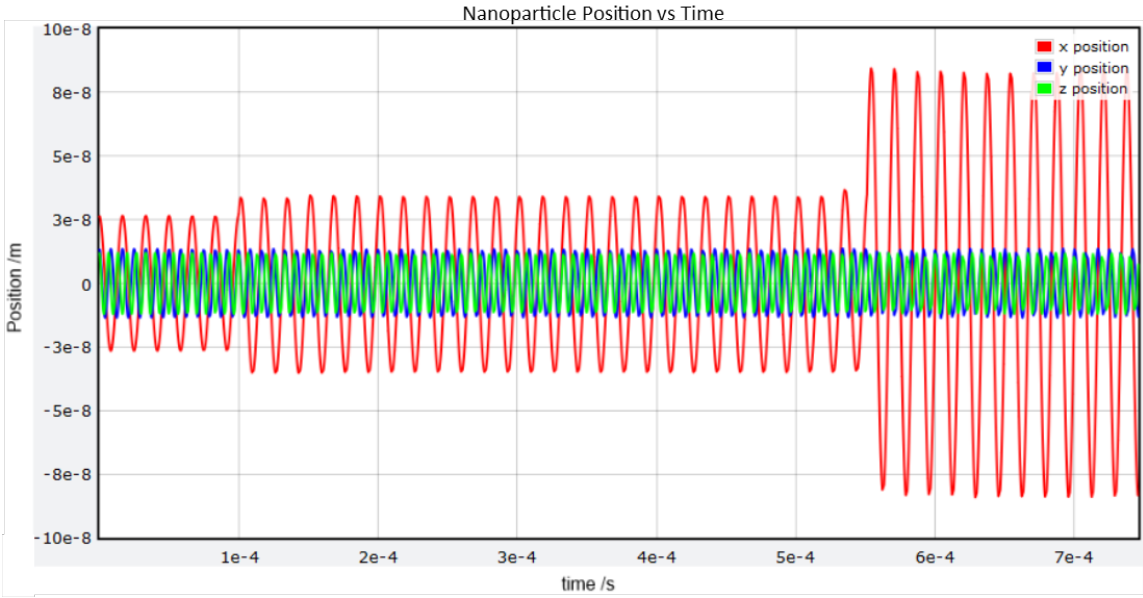


Figure 35: Position-time graph of the nanoparticle’s motion shows the particle being accelerated by a collision with an alpha particle.

As can be seen in Fig. 34 and Fig. 35, it is equally likely for any given alpha collision to accelerate or decelerate the nanoparticle, depending on what phase of the oscillation the nanoparticle is in at the time of collision. A successful projectile collision is therefore marked simply by a sharp change in the nanoparticle’s x -velocity, or an analogous sharp change in its x -position.

3.7 Assumptions and Approximations of the Simulation

Some assumptions were made in order to simplify the simulation, some of these were simplifications to reduce the computational demand and others were approximations in place of analytical solutions that may not exist, but in all cases, efforts were made to minimise the impact of these assumptions on the fidelity of the simulation.

The first assumption made was that each gas particle was considered to have the mass of a Nitrogen molecule, while strictly speaking the gas is actually a mix of Nitrogen, Oxygen and Carbon Dioxide with some other trace gases.

The second assumption made was that gas particles were equally likely to collide with the nanoparticle from all angles. While perhaps not strictly true, particularly if the particle were near the edge of the pressure vessel, this is a relatively innocuous assumption that was justified by the fact that the nanoparticle was never close to the walls of the vessel.

Ultimately, due to the enormous difference in mass and momentum between the gas and nanoparticles, even without these simplifications, the gas collisions would still have an insignificant effect on the overall behaviour of the nanoparticle. Additionally, by only generating the gas particle velocities at the moment of collision, this has the significant added benefit of saving computational time by avoiding the need to store information on the velocities and positions of the gas particles in the vessel at all times – and with thousands of gas particles involved, this is no small saving.

As a consequence of this simplification, it is also prudent to state that no effort was made to ensure the conservation of the total momentum of the nanoparticle-gas particle system, or put another way: when the nanoparticle gained momentum, an equal amount of momentum was not taken away from the surrounding gas. This was not deemed to be a necessary use of computational time due to the insignificant effect of the gas collisions on the nanoparticle's overall motion, i.e. there was no danger of the nanoparticle gaining so much momentum from the gas that it affected the fidelity of the simulation.

4 Conclusion of Findings So Far

After simulating and manually calculating the effect of a variety of collisions, the findings were in agreement with those of previous experiments [73] and shows that the levitated nanoparticle system is sensitive enough to detect forces on energy scales as small as individual alpha particle collisions. This holds promise for detecting even smaller scale forces, such as the influence of the particularly weak and illusive repulsive Casimir force.

VI REPULSIVE CASIMIR EXPERIMENT

While there are a lot of possible experimental setups to measure the Casimir force (see [Casimir Force Past Experiments](#)), it was decided to investigate the repulsive Casimir effect caused by the specific geometry of metal ellipsoid and hole in a metal plate. Specifically, this method was chosen due to the scale of the challenge and the possibility of doing novel research.

Building on the optical trap experiment required a gold nanoparticle in place of the standard silicon dioxide, and two gold pinhole plates to mount either side of the trapped nanoparticle [27, 2].

Using gold instead of silicon dioxide, as previously attempted [73], posed a few issues, the simplest of which are the procurement of useful specimens, and the separation of said specimens from each other, since these particles are small enough for Van der Waals forces to result in them clumping together.

An issue more pressing in the operation of the experiment is plasmonic resonance. This is when electrons on the material surface respond in a resonant manner to incident light of a particular frequency - in this case the laser light trapping the nanoparticle. The nanoparticle is small enough such that this wave can grow to encompass the entire surface of the particle, known as a localised plasmon resonance. Since gold is opaque to the laser light of the trap, this means that a significant proportion of the laser light is absorbed, and thus there is a risk of the particle melting if the heat is not dissipated quickly.

The simplest solution to this is to leave some air in the chamber. The gaseous molecules left inside act as a damping effect on the molecule's oscillations, transferring excess energy away from the particle. However, this introduces another problem in that the gas molecules may interfere with the particle's interactions with the pinhole plates, and may obscure the Casimir effect beneath their collisions with the particle.

It was decided to first do a preliminary experiment, without the pinhole plates to test the feasibility

of trapping the gold nanoparticles at a pressure of 5 mbar. Afterwards, using the data obtained, the optical trap could be further calibrated for the repulsive Casimir effect experiment, and compared against the data obtained from the Casimir effect simulation.

As mentioned previously, investigations into attractive and repulsive Casimir forces have been studied by groups such as Yujuan Hu et al. at the Anhui University of China [2]. However, in order to ensure that the potential resulting from the Casimir force is not negated by the optical trap forces, the data collected in the aforementioned study was used and compared with the optical trap forces. The following graphs display the Casimir and optical potentials for two different optical potentials; one centered at the origin, or at the plate, and one centered 1 μm from the plate.

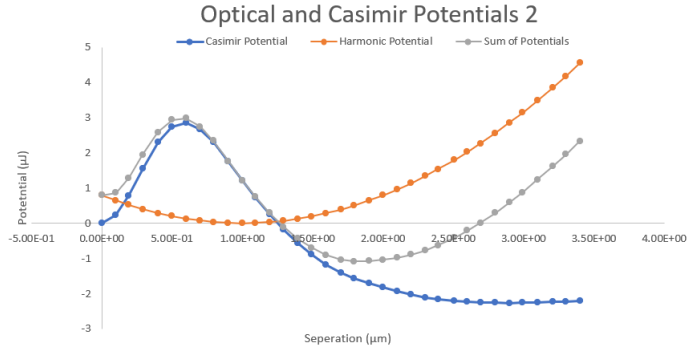


Figure 36: Comparison of shifted Optical Trap potential and Casimir potential for gold nanoparticle measured by Yujuan Hu *et al.* [2]

As shown from these graphs, the net potential due to the Optical and Casimir forces will still produce both an attractive and repulsive net force at different separations, demonstrated by the slope of the net potential being positive or negative, respectively. Thus we can predict that the forces due to the optical trap will still allow a measurement of a net repulsive force due to the Casimir effect.

1 The apparatus

The gold nanoparticles used for the experiment were from *nanopartz*. They were rod shaped, with dimensions 100nm height and 50nm diameter, and had their peak Spectral Plasmonic Resonance (SPR) at 600nm, and their Localised Spectral Plasmonic Resonance (LSPR) at 530nm.

The setup used was based upon the apparatus detailed in Fig. 37 [97]. A gold nanoparticle, of dimensions 100nm height and 50nm diameter, was suspended in an optical trap using infrared light of wavelength 1064nm. The laser that provided the trapping potential was a 500mW dyelaser pumped by an Elforlight I4-700 Neodymium-Yag laser. The dyelaser beam was first polarised using a polarising beam splitter, which could be altered to give a desired polarisation. The beam was then focused through an Aspheric lens with an effective focal length of 3.1mm as gaussian beams into the chamber, where the particle was trapped in the region of the beam with the highest intensity.

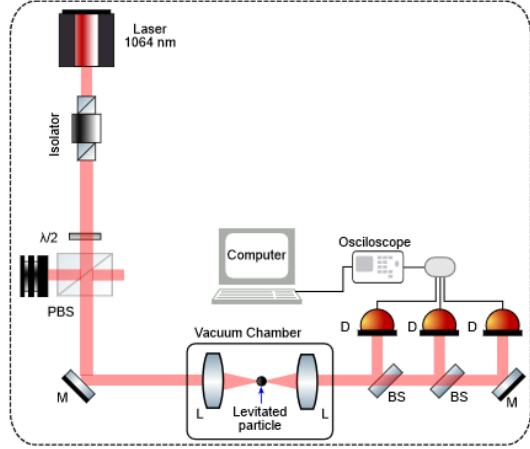


Figure 37: A layout of the apparatus. The different components are $\lambda/2$ = half plate, PBS = Polarising Beam Splitter, M = Mirror, BS = Beam Splitter, D = balanced photodiode and L = lens. Edited from [97, Fig. 2]

Light scattered from the nanoparticle was focused again through an identical lens and measured using the three balanced photodiodes, each of which gave a voltage proportional to the particle's position in their respective axis. These voltages were recorded and graphed as a function of time.

Two vacuums were operated to vacate the chamber, if required. One decreased the pressure inside the chamber to 10^{-2} mbar, and the other with a much higher operation frequency lowered it to a smaller 10^{-8} mbar. At higher pressures, gas inside the chamber could reliably cool the particle, collisions between it and the gas molecules siphoning energy from it. To cool the nanoparticle at pressures below 10^{-5} mbar, the particle could be charged and an electric field produced at the frequency of the particle oscillation observed by the computer from the voltage inputs of the photodiodes. This produced a force opposite to particle motion, slowing it down and thus cooling it [98]. Otherwise, the chamber was left at standard lab conditions of 1 bar of pressure, at a temperature of 298K.

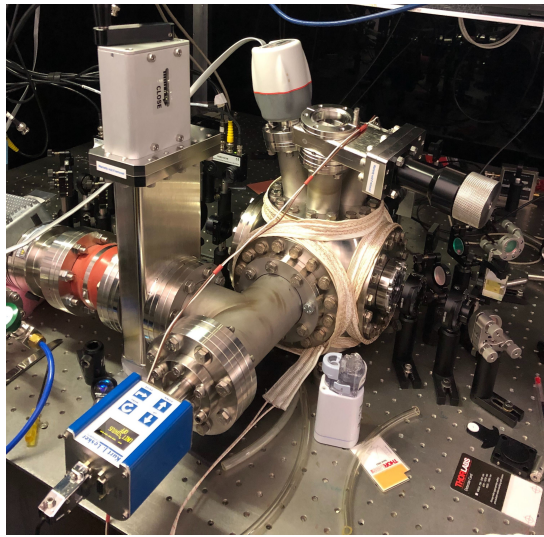


Figure 38: A picture taken of the chamber used in the experiment, wrapped in thermal wire to prevent condensation forming in the joints when operating at extremely low pressures

2 Preliminary Procedure: Trapping the Nanoparticle

The chamber was left at standard lab conditions, 1bar and 298K for initial trapping of the first nanoparticle. A nebuliser was used to insert a new nanoparticle into the trap, sprayed through a

valve that provided access to the inside of the chamber. However, multiple attempts were required before one of the nanoparticles was successfully trapped.

Once a nanoparticle was successfully trapped, shown by expected data being recorded by the computer and a camera setup to observe the trap, the pressure could be lowered using the vacuums, and the laser polarisation altered via the polarising beam splitter. The Voltage data for the x, y and z axes was plotted against time, and a fast Fourier transform was applied to get guideline data for the Power Spectral Density to be found in data analysis. Three nanoparticles were successfully trapped in all, and their oscillations measured at different pressures.

The first was trapped at 32 mbar and 22 mbar pressures, and for both was measured with linearly polarised (quarter 180) and circularly polarised (quarter 225) laser trap light.

The second was trapped at 24 mbar, 10mbar and 5.4mbar. At each of these pressures the nanoparticle was trapped and measured with linearly polarised (quarter 180) light, and only for the former two pressures was the nanoparticle trapped and measured with circularly polarised (quarter 225) light. 5.4 mbar was the lowest pressure a nanoparticle was successfully trapped and measured at, and the nanoparticle fell out shortly after.

The third was trapped at 18mbar only, and trapped and measured only with linearly polarised (quarter 180) light.

For the Data Analysis, only the data with linearly polarised laser light was used. This was due to most of the data taken being for linearly polarised light, specifically the 5.4mbar measurements. The measurements for the circular polarisation gives significantly different data to the linearly polarised measurements, and so would be unnecessary to compare. However, measurements with polarised light could be a potential subject for further experimentation.

3 Casimir Force Experiment

Unfortunately, due to the onset of the COVID-19 pandemic, there was not enough time to perform this experiment.

The intent was to modify the chamber in only adding two $25\mu\text{m}$ thick copper pinhole plates, one side surfaced with gold. The pinhole, centrally placed in the plates, would have diameters of $3\mu\text{m}$, so that they could be placed in planes perpendicular to the trapping beam such the light could pass through the holes, the gold plated side facing the nanoparticle.

Thereafter the procedure would be almost identical to the one used in the preliminary experiment, measuring the nanoparticle oscillations via the potentials produced from scattered laser light absorbed by photodiodes. These measurements would be taken at the same pressures as the preliminary experiment, however the trapping laser light would only be linear polarised, to best compare against the data of the trapped nanoparticle without the Casimir effect acting on it.

4 Experimental Problems

4.1 Probability of trapping the particle

Trapping the particle was difficult and mostly down to random chance, going entire runs without successfully trapping one that day. The nebuliser was a inconsistent method of introducing the nanoparticle to the chamber, requiring a manual opening of a valve at the top, disturbing the interior pressure created by the vacuums, as well as introducing other non-air molecules into the chamber. An additional consideration is that it is possible for multiple nanoparticles to become trapped at once, which can significantly compromise the reliability of the data collected and calls for the trapping procedure to be repeated.

The lowest pressure a nanoparticle was trapped at before falling was only 5 millibar. This could present a future problem in measuring the repulsive Casimir effect.

4.2 Mounting the pinhole plates

A concern with mounting such small plates is having them exactly parallel to each other, as them being askew would affect the Casimir potential. As of yet, no solution has been identified.

Another issue is the potential for the reflection of light scattered from the nanoparticle back and forth between the plates. This could possibly affect the accuracy of data acquired from the experiment, as the data comes from the scattered light absorbed by the photodiodes.

4.3 Electrostatic Patches

Due to improvements in technology and persistent research, the Casimir force is being measured between plates increasingly closer. However this means that any undesired and secondary effects will become more intrusive as their influence on measurements grows.

Electrostatic patches are potential differences that appear in the micrometer range between neutral conductors. The resulting force must be taken into account during Casimir forces measurements.

In basic Casimir measurements, it is often assumed that the metallic plates surfaces are equipotentials. However the crystallites on the surface of the material lead to different crystallographic orientations and different work functions [99].

The plates used in precision Casimir measurements subjected to ultra-high vacuum (pressure lower than 100 nanopascal [100]). In these conditions, the patches stemming from the different crystallites are lead to the topography. These patches can be measured using AFM, KPFM or EBSD microscopy [101]. However, contamination of the surface leads to an enlargement of the patch sizes and smoothing of the voltages. This discrepancy ultimately leads to uncertainty of the Casimir effect measurements.

The resulting pressure of the electrostatic patches can be modeled using the Poisson equation [102].

$$P = \frac{\varepsilon_0}{4\pi} \int_0^\infty \frac{k^3 dk}{\sinh^2(kL)} [C_{11}[k] + C_{22}[k] - 2C_{12}[k]\cosh(kL)] \quad (44)$$

A model of the spectra computing the correlations of the patch voltages is needed in order to solve the equation. Earlier models resulted in abrupt cutoffs for low and high-k [103]. However recent models tessellating the sample surface with randomized voltage assignment lead to a much smoother spectrum [104].

The better fit of the model allows more precise Casimir measurements, however certain questions remain. For example, the parameters of best fit correspond to the contamination of metallic surfaces model, and not the crystallites-patch model. Further research has been done to analyze the patches using Kelvin Probe Force Microscopy [105]. The forces of the patches has been modeled using a plane-sphere geometry structure [106]. Comparisons with ion traps are being made as they follow the same logic [107, 108].

4.4 Risk of Gold Melting

The lowest pressure used in the experiment was 5 millibar. Achieving lower pressures is important to maintain optimal measurement conditions and reduce background noise, however, it is important to be aware that the melting point of gold decreases with decreasing pressure and therefore at ultra-low pressures, the melting temperature of the nanoparticle can be significantly lowered. As the nanoparticle is heated by the laser, it is also radiating heat away in the form of infrared photons, this results in an equilibrium temperature at which the rate of these two opposing processes are equal. At ultra-low pressures, the melting temperature of gold may drop low enough that it is below this equilibrium temperature and this can lead to the nanoparticle melting, causing it to deform from its original rod shape. As a result, the data obtained would not be comparable with the model, as the nanoparticle's shape would have changed shape.

VII COMPARISON OF CALCULATIONS AND SIMULATIONS

1 Simulating the Casimir Potential

Using the experimental data shown in Fig. 36 for the Casimir force at various distances, a polynomial regression model was used to fit a trend line to the repulsive portion of the Casimir force-distance data. The equation for this trend line is shown below.

$$F_c(x) = -8 \cdot 10^{-13}x^6 + 9 \cdot 10^{-11}x^5 - 4 \cdot 10^{-9}x^4 + 9 \cdot 10^{-8}x^3 - 1 \cdot 10^{-6}x^2 + 5 \cdot 10^{-6}x - 4 \cdot 10^{-6} \quad (45)$$

Where $F_c(x)$ is the repulsive Casimir force in micro Newtons and x is the separation between the nanoparticle and gold plate in micro-meters.

A graph of the Casimir force data with the trend-line fitted is shown below:

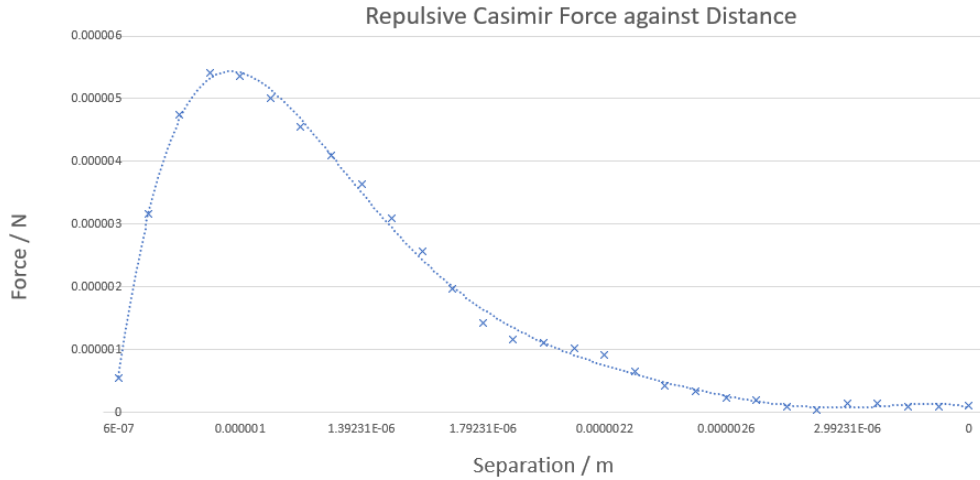


Figure 39: The Casimir force data with the calculated trend-line overlaid.

This potential was then simply added to the harmonic potential of the optical trap. Under normal circumstances, it is not good practice to fit high-degree polynomials to data, owing to the fact that they have a tendency to over-fit and lead to undulating patterns that are often nonphysical. However, it was justified in this case as the section of the curve being used was very small and the parts of the curve on either side - that would otherwise represent the attractive region of the Casimir force and those representing negative x-values - were excluded, as they were not of interest in this case and not physical respectively.

After implementing the repulsive Casimir force and running the simulation, the following graph was obtained:

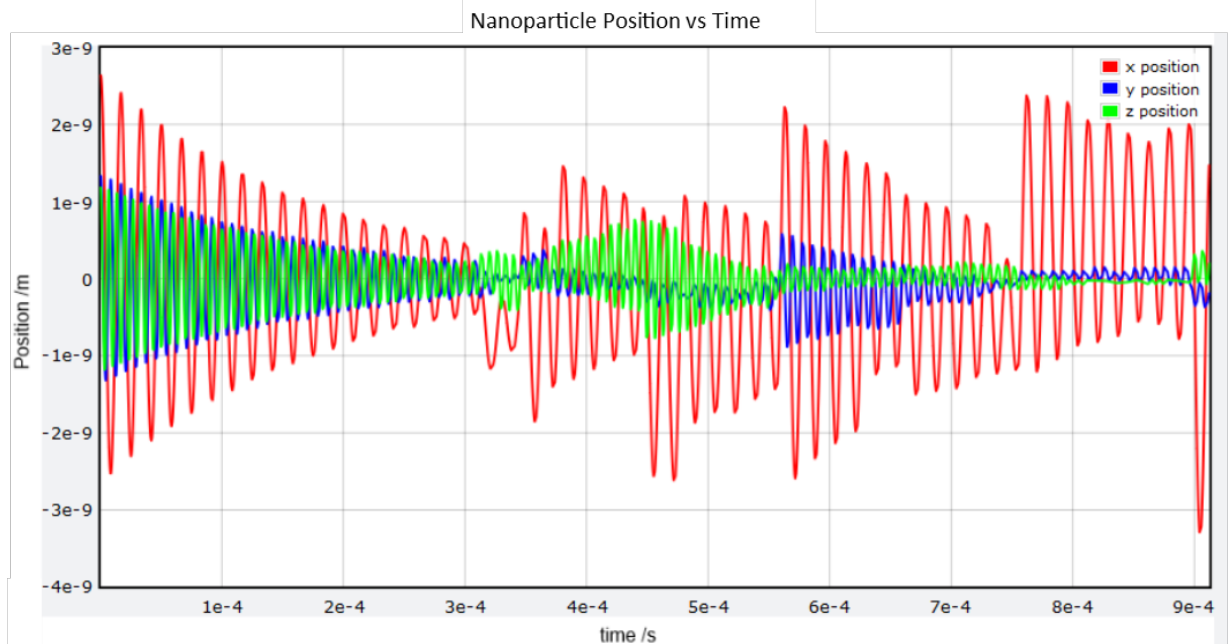


Figure 40: Nanoparticle position-time graph with gas collisions enabled.

After a brief examination it becomes obvious that any possible displacement due to the Casimir effect is completely hidden beneath the noise created by collisions with gas molecules. The Casimir force at its peak exerts approximately 5 micro Newtons of force on the nanoparticle, and that is over a distance of only a few micrometres, after which it quickly decays to zero.

2 Experimental Data

3 Comparison

VIII Data Analysis

1 Data Gathered

The data collected in the preliminary experiment took the form of a time series of voltage of the form $V(t)$ across 3 different channels. This data was gathered within *Picoscope*, a software based oscilloscope that can automatically record large quantities of data and output them in a .csv format for subsequent processing in Python. These channels are in theory meant to provide voltage data directly proportional to the position of the nanoparticle on each of the 3 axes, as gathered by 3 photodiodes, which should be centred around a common midpoint (a zero). For an example of what might be hoped for, refer to 26 in the simulations section, replacing in your mind the position label of the y axis with a directly proportional voltage. In practice however, the data must be processed significantly in order to get even this far. 41 shows an example of the raw data as recorded and graphed in *Picoscope*, using file 16 of 48.

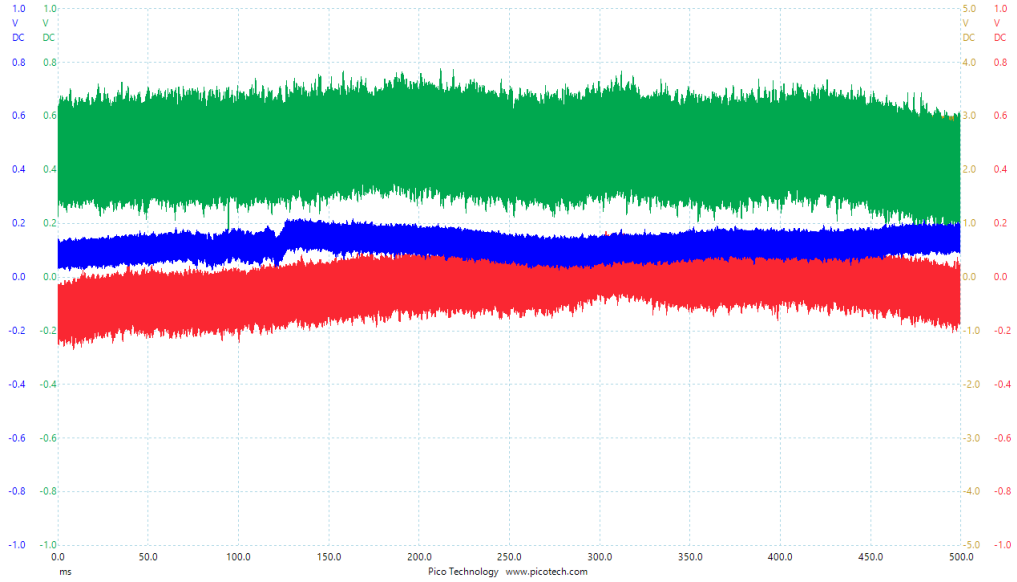


Figure 41: Raw data file as recorded in Picoscope, 16 of 48

Once the data has been processed so that a voltage channel can be taken as proportional to position, the desired outcome it to process this data to build a map of the potential experienced by the nanoparticle. The purview of this section is to explain how the full process from raw data to potential can be carried out using easy to use (that being a relative term) methods in python. For clarity this is carried out with a dataset from the preliminary experiment taken at 5.4 mbar pressure. The set consists of 48 consecutive data files in .csv format each providing a 500ms section of the time series with a timestep of $5.04 \times 10^{-7} s$.

2 Power Spectral Density

The power spectral density (PSD) is a distribution of the power in a signal across the frequency domain. This contains the information related to the strength of various frequency components in a signal. It is intimately related to a Fourier transform; in fact one way of finding a PSD is by squaring the Fast Fourier Transform (FFT). The PSD was computed in Python through the use of the `scipy.signal.periodogram` function to obtain the PSD for the overall time series as shown in 42:

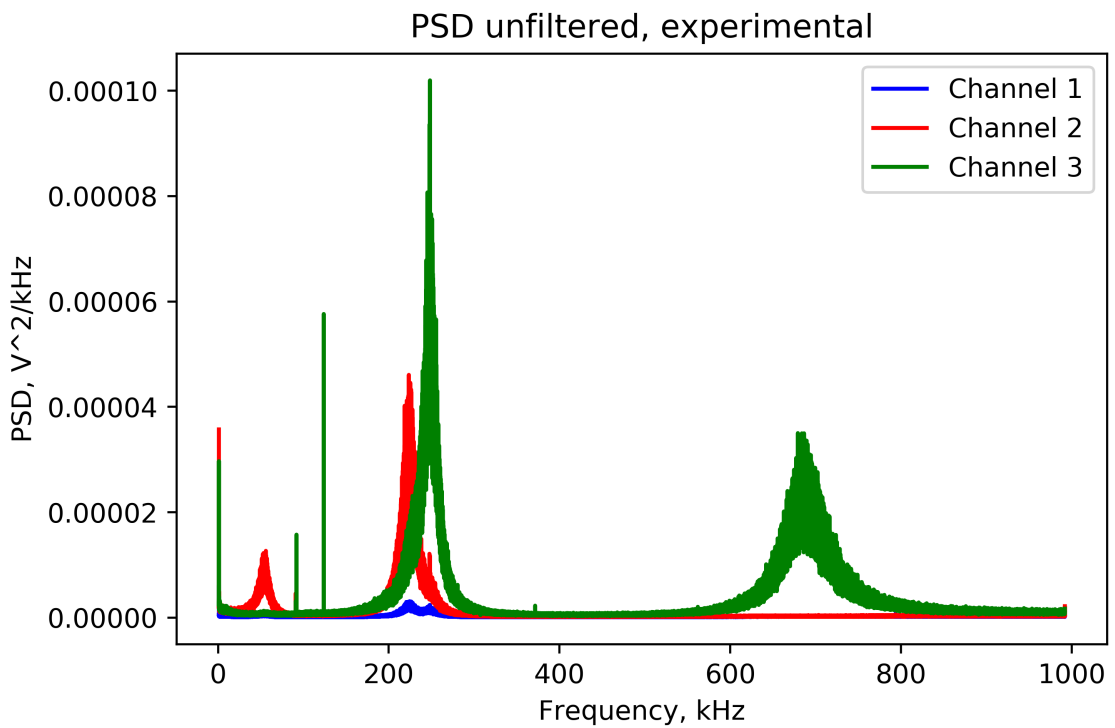


Figure 42: Graph of PSD, No filters

Additionally, the PSD code was run on a set of the simulated data, without the Casimir force, for comparison as seen in 43

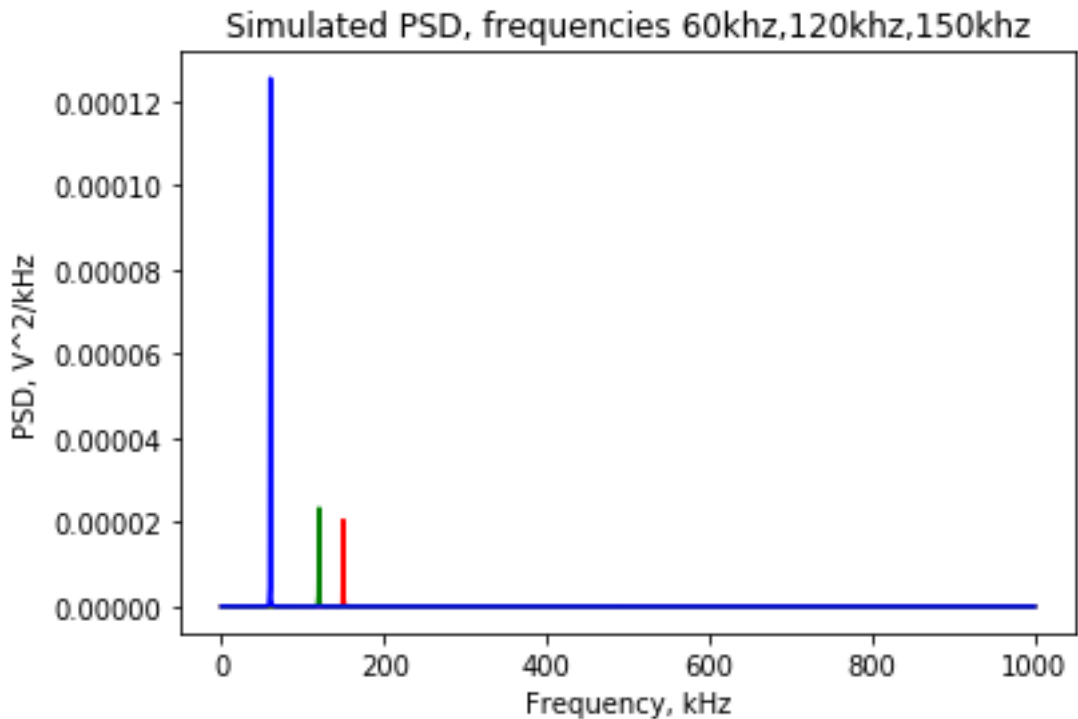


Figure 43: Graph of simulated PSD

There are a few differences of note here. Firstly, the wide gap peak between 600kHz and 800kHz in the experimental data. This is a systemic issue and is an artifact of the lasers own frequency,

creating an additional peak in the channel three photodiode, and is unrelated to the motion of the nanoparticle. Therefore, this frequency component can be safely removed from the overall channel 3 signal. Secondly, there is a significant difference in the widths of the peaks of the experimental and theoretical data and while the theoretical appear as straight lines, they are in fact very narrow peaks of a similar shape to the experimental peaks. This occurs due to the differences between the damping of the experimental and theoretical data, where the simulation of the gas collisions may not be a true representation of the underlying Physics. Lastly, whereas in the theoretical data there is one peak in each channel at the specific frequency of that axis' motion, in the experimental PSD, certain peak frequencies appear across multiple channels. This is more visible once band filters are introduced and is due to the problems discussed in the next section.

3 Signal Problems

In theory, the three voltage channels are supposed to provide voltage data corresponding to each axis independent of one another. Thus, each signal would be directly proportional to the position on a given axis and since each axis is tied to a specific frequency, each signal should show a single peak. However, in practice, the photodiodes can only be calibrated to show a *preference* for a particular axis and therefore still picks up (usually at a weaker level) some motion from the other axes. When discussing these with reference to the PSD plots it's best to refer to the positional axes by their characteristic frequencies (x,y and z being fairly arbitrary labels). In our case those 3 would be approximately 50kHz, 210kHz and 250kHz. The overlap of these frequencies on the same channel presents a problem as in order to map information about the potential, one needs independant position data for each axis.

A second problem with the signal is apparent when refering to the raw data as seen in [41](#). In principle the time series should all be centred around zero, with that zero representing the lowest point in the harmonic potentials in the x, y and z axes. However each series has a certain voltage offset, which is due to the photodiodes not neccesarily being caibrated around the midpoint of the oscillations. When constructing the potentials, this needs to be accounted for so that each potential is centred about the same point.

Both these problems can be solved by use of band filters, discussed in the next section.

4 Band Filters

Band filters are filters that remove parts of a time signal that correspond to any motion at any frequency not within the particular filters specified band. Use of these solves both of the problems previously discussed.

The first, the overlap in axes on the same channel is removed by examination of the PSD to see which bands on which channels contain a single peak at one frequency. In our case the channel bands are:

For channel 2: 10-100kHz, for the channel's preferred peak at 50kHz For channel 3: 100-400kHz, for the channel's preferred peak at 250kHz

While channel 1 could also provide a clean signal for the 50kHz axis, the signal is weaker than channel 2, so it wouldn't serve any purpose.

Originally, the channels were to be calibrated so that channel 1 would show preference for the 50kHz axis, channel 2 would show preference for the 210kHz and channel 3 would show preference for the 250kHz. However, channel 2 proved unable to show a clean preference for the the 210kHz axis (hence why it's signal has 2 peaks on the PSD in that frequency regions, the stronger one being at 210kHz. The secondary peak is most visible when applying a band filter of 100kHz-400kHz to channel 2 as seen in [44](#). Though the secondary peak is only slightly noticeable to the naked eye, the deviation prevents a clean fitting lorentian curve about the 210kHz frequency.

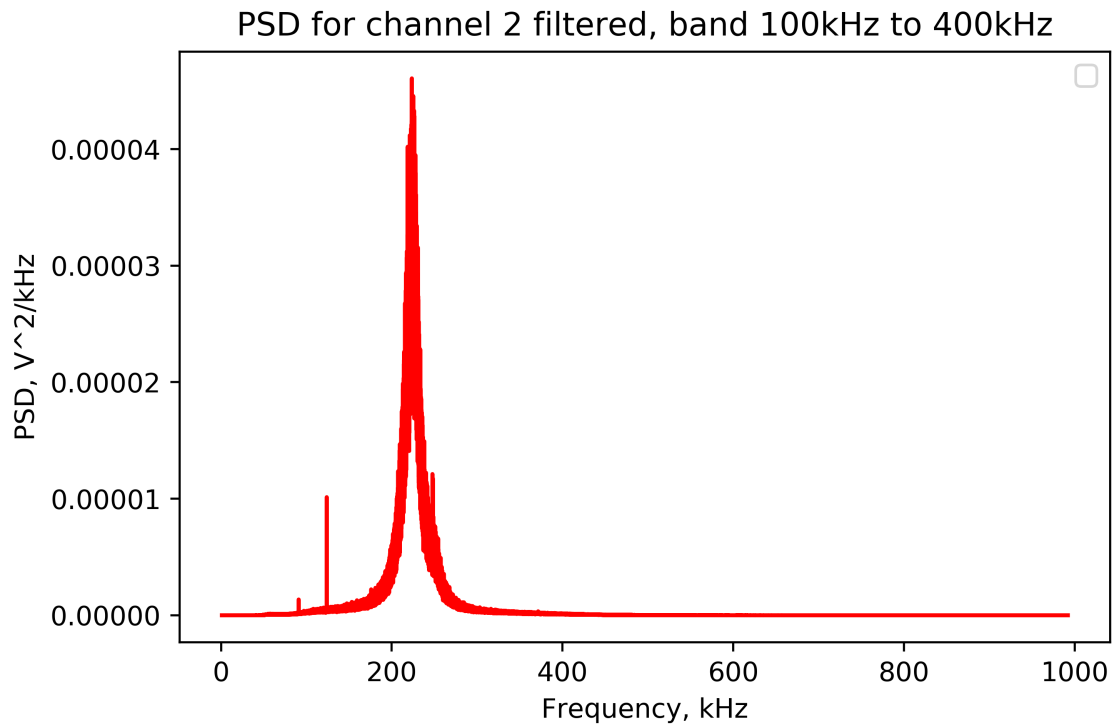


Figure 44: Graph of PSD for channel 2 with band filter 100kHz-400kHz

This unfortunately means that there's no way to get a clean time signal for the 210kHz axis for analysis, hence from this point on we will only be able to map the potential on 2 of the axes.

The second problem previously discussed, is the DC voltage offset that misaligns the potentials relative to one another. This handily is also solved by the implementation of band filters as the DC signal qualifies as a 0Hz signal which is removed from each of the channels, thus centering them all around zero

To implement the bands the `scipy.signal.butter` function is used to calculate Butterworth filter coefficients and the `scipy.signal.lfilter` function is used to process the channel 2 and 3 time series through the filters. A comparison of the unfiltered [45](#) and filtered time series [46](#) for file 16 shows the DC offset removed.

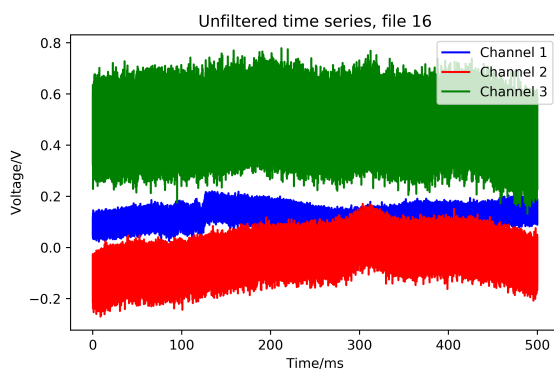


Figure 45: unfiltered time series, file 16

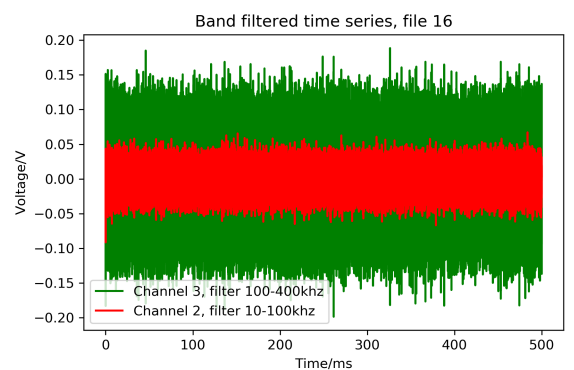


Figure 46: filtered time series, file 16

IX FINAL SUMMARY

The central aim set was to investigate and measure short range (sub-millimetre) forces, as well as their current and potential future uses, using an optical nanoparticle trap in a high vacuum. Various short range forces were explored through an extensive survey of literature ranging from short range dispersion forces to non-Newtonian gravity. Additionally, the associated momentum transfers of collisions between various projectile particles and the optically trapped nanoparticle were investigated, where calculations were undertaken in order to determine the expected changes in momentum and energy. While several projectile particles were considered, both the calculations and simulations of the single particle collisions supported the use of α particles and SF₆ molecules as the most viable candidates for this purpose. This decision was based on their respective masses and the range of velocities to which they could be practically accelerated using techniques such as field ionization.

These results were further explored through the application of computer simulations. The simulation produced a three dimensional dynamic animation by modelling the harmonic potential created by the optical trap. The collisions of α and SF₆ particles with the nanoparticle were also modelled, with the resultant changes in position and velocity illustrated graphically. The simulation was also extended to account for damping through the effects of pseudo-random gas collisions in addition to driving forces due to thermal energy input from the laser itself.

An investigation into the feasibility of experimentally measuring the repulsive Casimir force was subsequently explored. Using data from previously conducted Casimir force experiments, it was determined that the Casimir force would be theoretically detectable despite the much stronger influence of the harmonic potential due to the optical trap. An experimental setup was constructed employing two parallel pin-hole gold plates on either side of an optically levitated gold nanoparticle, inducing a plate separation-dependent Casimir force on the nanoparticle. Using an optical tweezer setup, a gold nanoparticle was successfully trapped, wherein a power spectral density was derived using the nanoparticle position-frequency data. (**PSD brief EXPLANATION + level of success with regard to vacuum level**). The accompanying simulation was also extended to implement the effects of the Casimir force to provide a basis for future comparisons.

The repulsive Casimir force experiment was not completed owing to the lack of laboratory access due to the outbreak of COVID-19. Instead, Casimir force-distance data from a previous experiment [2] was produced using a polynomial regression model in order to simulate the effect of the combined Casimir and optical potentials.

An understanding of short range forces, like the Casimir force, offer essential knowledge for fields such as nanotechnology, colloids, protein folding, as well as dark energy candidates. Despite the inability to complete the experimental investigation to measure the repulsive Casimir force, extensive research on the measurement of short range forces was conducted based on previous literature, simulations, as well as collected data. The central avenue of future research naturally involves conducting the gold plate Casimir force experiment, in order to compare collected results with theoretical results based on preceding studies [2]. Additionally, a further study could include the effect on the Casimir force of trapping by both linear and circularly polarized light.

References

- [1] D. Bowler, “PHAS0030: Further Practical Mathematics & Computing Session 7: Modelling with Particles,” pp. 3–4, Feb. 2019.
- [2] Y. Hu, R. Sun, Z. Huang, and X. Wu, “The repulsive casimir force with metallic ellipsoid structure,” *Journal of Nanotechnology*, vol. 2016, p. 1–5, 2016.
- [3] G. Winstone, M. Rademacher, R. Bennett, S. Buhmann, and H. Ulbricht, “Direct measurement of short-range forces with a levitated nanoparticle,” *Physical Review A*, vol. 98, no. 5, p. 053831, Nov 2018, arXiv: 1712.01426.
- [4] G. Winstone, R. Bennett, M. Rademacher, M. Rashid, S. Buhmann, and H. Ulbricht, “Direct measurement of the electrostatic image force of a levitated charged nanoparticle close to a surface,” *Physical Review A*, vol. 98, no. 5, p. 053831, Nov. 2018. [Online]. Available: <https://link.aps.org/doi/10.1103/PhysRevA.98.053831>
- [5] P. W. Milonni, “‘Nothing’s plenty. The vacuum in modern quantum field theory’ (1985) by I.J.R. Aitchison,” *Contemporary Physics*, vol. 50, no. 1, pp. 259–259, Jan. 2009. [Online]. Available: <http://www.tandfonline.com/doi/abs/10.1080/00107510802703017>
- [6] S. Reynaud, A. Lambrecht, C. Genet, and M.-T. Jaekel, “Quantum vacuum fluctuations,” *Comptes Rendus de l’Académie des Sciences - Series IV - Physics*, vol. 2, no. 9, pp. 1287–1298, Nov. 2001. [Online]. Available: <https://linkinghub.elsevier.com/retrieve/pii/S1296214701012707>
- [7] A. Einstein and A. Einstein, “The Swiss years writings, 1912 - 1914,” in *The collected papers of Albert Einstein*. Princeton, NJ: Princeton University Press, 1996, vol. 4, p. 134.
- [8] L. Galgani, “On Nernst’s deduction of Planck’s law and the problem of the Arnol’d diffusion,” *Il Nuovo Cimento B*, vol. 62, no. 2, pp. 306–314, Apr. 1981. [Online]. Available: <http://link.springer.com/10.1007/BF02721279>
- [9] A. Lambrecht and S. Reynaud, “Casimir and short-range gravity tests,” *arXiv:1106.3848 [gr-qc, physics:quant-ph]*, Jun. 2011, arXiv: 1106.3848. [Online]. Available: <http://arxiv.org/abs/1106.3848>
- [10] E. Adelberger, B. Heckel, and A. Nelson, “Tests of the gravitational inverse square law,” *Annual Review of Nuclear and Particle Science*, vol. 53, no. 1, pp. 77–121, Dec. 2003. [Online]. Available: <http://www.annualreviews.org/doi/10.1146/annurev.nucl.53.041002.110503>
- [11] K. A. Milton, “Local and Global Casimir Energies: Divergences, Renormalization, and the Coupling to Gravity,” in *Casimir Physics*, D. Dalvit, P. Milonni, D. Roberts, and F. da Rosa, Eds. Berlin, Heidelberg: Springer Berlin Heidelberg, 2011, vol. 834, pp. 39–95. [Online]. Available: http://link.springer.com/10.1007/978-3-642-20288-9_3
- [12] F. London, “ON THE THEORY AND SYSTEM OF MOLECULAR FORCES,” in *World Scientific Series in 20th Century Chemistry*. WORLD SCIENTIFIC, Mar. 2000, vol. 8, pp. 369–399. [Online]. Available: http://www.worldscientific.com/doi/abs/10.1142/9789812795762_0023
- [13] A. W. Rodriguez, F. Capasso, and S. G. Johnson, “The Casimir effect in microstructured geometries,” *Nature Photonics*, vol. 5, no. 4, pp. 211–221, Apr. 2011. [Online]. Available: <http://www.nature.com/articles/nphoton.2011.39>
- [14] H. B. G. Casimir and D. Polder, “The Influence of Retardation on the London-van der Waals Forces,” *Physical Review*, vol. 73, no. 4, pp. 360–372, Feb. 1948. [Online]. Available: <https://link.aps.org/doi/10.1103/PhysRev.73.360>
- [15] ——, “The Influence of Retardation on the London-van der Waals Forces,” *Physical Review*, vol. 73, no. 4, pp. 360–372, Feb. 1948. [Online]. Available: <https://link.aps.org/doi/10.1103/PhysRev.73.360>

- [16] S. J. Rahi, T. Emig, and R. L. Jaffe, “Geometry and Material Effects in Casimir Physics-Scattering Theory,” in *Casimir Physics*, D. Dalvit, P. Milonni, D. Roberts, and F. da Rosa, Eds. Berlin, Heidelberg: Springer Berlin Heidelberg, 2011, vol. 834, pp. 129–174. [Online]. Available: http://link.springer.com/10.1007/978-3-642-20288-9_5
- [17] D. Dalvit, P. Milonni, D. Roberts, and F. da Rosa, Eds., *Casimir Physics*, ser. Lecture Notes in Physics. Berlin, Heidelberg: Springer Berlin Heidelberg, 2011, vol. 834. [Online]. Available: <http://link.springer.com/10.1007/978-3-642-20288-9>
- [18] M. DeKieviet, U. D. Jentschura, and G. Lach, “Modern Experiments on Atom-Surface Casimir Physics,” in *Casimir Physics*, D. Dalvit, P. Milonni, D. Roberts, and F. da Rosa, Eds. Berlin, Heidelberg: Springer Berlin Heidelberg, 2011, vol. 834, pp. 393–418. [Online]. Available: http://link.springer.com/10.1007/978-3-642-20288-9_12
- [19] E. M. Lifshitz, “The theory of molecular attractive forces between solids,” *Sov. Phys. JETP*, vol. 2, pp. 3–83, 1956.
- [20] C. Genet, A. Lambrecht, and S. Reynaud, “Casimir effect and vacuum energy,” *arXiv:quant-ph/0210173*, Oct. 2002, arXiv: quant-ph/0210173. [Online]. Available: <http://arxiv.org/abs/quant-ph/0210173>
- [21] A. Lambrecht and S. Reynaud, “Recent Experiments on the Casimir Effect: Description and Analysis,” *arXiv:quant-ph/0302073*, Feb. 2003, arXiv: quant-ph/0302073. [Online]. Available: <http://arxiv.org/abs/quant-ph/0302073>
- [22] G. L. Klimchitskaya and V. M. Mostepanenko, “Experiment and theory in the Casimir effect,” *Contemporary Physics*, vol. 47, no. 3, pp. 131–144, May 2006. [Online]. Available: <http://www.tandfonline.com/doi/abs/10.1080/00107510600693683>
- [23] G. Bressi, G. Carugno, R. Onofrio, and G. Ruoso, “Measurement of the Casimir Force between Parallel Metallic Surfaces,” *Physical Review Letters*, vol. 88, no. 4, p. 041804, Jan. 2002. [Online]. Available: <https://link.aps.org/doi/10.1103/PhysRevLett.88.041804>
- [24] G. T. Moore, “Quantum Theory of the Electromagnetic Field in a Variable-Length One-Dimensional Cavity,” *Journal of Mathematical Physics*, vol. 11, no. 9, pp. 2679–2691, Sep. 1970. [Online]. Available: <http://aip.scitation.org/doi/10.1063/1.1665432>
- [25] H. Nikolić, “Proof that Casimir force does not originate from vacuum energy,” *Physics Letters B*, vol. 761, pp. 197–202, Oct. 2016. [Online]. Available: <https://linkinghub.elsevier.com/retrieve/pii/S0370269316304567>
- [26] R. L. Jaffe, “Casimir effect and the quantum vacuum,” *Physical Review D*, vol. 72, no. 2, p. 021301, Jul. 2005. [Online]. Available: <https://link.aps.org/doi/10.1103/PhysRevD.72.021301>
- [27] M. Levin, A. P. McCauley, A. W. Rodriguez, M. T. H. Reid, and S. G. Johnson, “Casimir Repulsion between Metallic Objects in Vacuum,” *Physical Review Letters*, vol. 105, no. 9, p. 090403, Aug. 2010. [Online]. Available: <https://link.aps.org/doi/10.1103/PhysRevLett.105.090403>
- [28] A. Lambrecht and S. Reynaud, “CASIMIR EFFECT: THEORY AND EXPERIMENTS,” *International Journal of Modern Physics: Conference Series*, vol. 14, pp. 171–180, Jan. 2012. [Online]. Available: <https://www.worldscientific.com/doi/abs/10.1142/S2010194512007313>
- [29] A. Lambrecht, A. Canaguier-Durand, R. Guérout, and S. Reynaud, “Casimir Effect in the Scattering Approach: Correlations Between Material Properties, Temperature and Geometry,” in *Casimir Physics*, D. Dalvit, P. Milonni, D. Roberts, and F. da Rosa, Eds. Berlin, Heidelberg: Springer Berlin Heidelberg, 2011, vol. 834, pp. 97–127. [Online]. Available: http://link.springer.com/10.1007/978-3-642-20288-9_4
- [30] A. O. Sushkov, W. J. Kim, D. A. R. Dalvit, and S. K. Lamoreaux, “Observation of the thermal Casimir force,” *Nature Physics*, vol. 7, no. 3, pp. 230–233, Mar. 2011. [Online]. Available: <http://www.nature.com/articles/nphys1909>

- [31] A. W. Rodriguez, F. Capasso, and S. G. Johnson, “The Casimir effect in microstructured geometries,” *Nature Photonics*, vol. 5, no. 4, pp. 211–221, Apr. 2011. [Online]. Available: <http://www.nature.com/articles/nphoton.2011.39>
- [32] A. W. Rodriguez, A. P. McCauley, D. Woolf, F. Capasso, J. D. Joannopoulos, and S. G. Johnson, “Nontouching Nanoparticle Dicusters Bound by Repulsive and Attractive Casimir Forces,” *Physical Review Letters*, vol. 104, no. 16, p. 160402, Apr. 2010. [Online]. Available: <https://link.aps.org/doi/10.1103/PhysRevLett.104.160402>
- [33] A. W. Rodriguez, D. Woolf, P.-C. Hui, E. Iwase, A. P. McCauley, F. Capasso, M. Loncar, and S. G. Johnson, “Designing evanescent optical interactions to control the expression of Casimir forces in optomechanical structures,” *Applied Physics Letters*, vol. 98, no. 19, p. 194105, May 2011. [Online]. Available: <http://aip.scitation.org/doi/10.1063/1.3589119>
- [34] L. Khine, J. M. Tsai, and J. Grandfield, *NEMS/MEMS Technology and Devices, ICMAT2011 Selected, Peer Reviewed Papers from the International Conference on Materials for Advanced Technologies (ICMAT2011), Symposium G: Nems/Mems and MicroTAS, 26 June to 1 July 2011, Suntec, Singapore*. Trans Tech Publications Ltd, 2011, oCLC: 1020550550.
- [35] J. Zou, Z. Marcet, A. W. Rodriguez, M. T. H. Reid, A. P. McCauley, I. I. Kravchenko, T. Lu, Y. Bao, S. G. Johnson, and H. B. Chan, “Casimir forces on a silicon micromechanical chip,” *Nature Communications*, vol. 4, no. 1, p. 1845, Oct. 2013. [Online]. Available: <http://www.nature.com/articles/ncomms2842>
- [36] M. Nawazuddin, T. Lammerink, E. Berenschot, M. Boer, K.-C. Ma, M. Elwenspoek, and R. Wiegerink, “Towards a Casimir Force Measurement between Micromachined Parallel Plate Structures,” *Challenges*, vol. 3, no. 2, pp. 261–277, Nov. 2012. [Online]. Available: <http://www.mdpi.com/2078-1547/3/2/261>
- [37] R. L. Forward, “Extracting electrical energy from the vacuum by cohesion of charged foliated conductors,” *Physical Review B*, vol. 30, no. 4, pp. 1700–1702, Aug. 1984. [Online]. Available: <https://link.aps.org/doi/10.1103/PhysRevB.30.1700>
- [38] H. E. Puthoff, “Advanced Space Propulsion Based on Vacuum (Spacetime Metric) Engineering,” *arXiv:1204.2184 [physics]*, Feb. 2012, arXiv: 1204.2184. [Online]. Available: <http://arxiv.org/abs/1204.2184>
- [39] D. A. R. Dalvit and R. Onofrio, “On the use of the proximity force approximation for deriving limits to short-range gravitational-like interactions from sphere-plane Casimir force experiments,” *Physical Review D*, vol. 80, no. 6, p. 064025, Sep. 2009. [Online]. Available: <https://link.aps.org/doi/10.1103/PhysRevD.80.064025>
- [40] K. Cahill, “Is Dark Energy a Cosmic Casimir Effect?” *arXiv:1102.5572 [astro-ph, physics:hep-ph]*, Mar. 2011, arXiv: 1102.5572. [Online]. Available: <http://arxiv.org/abs/1102.5572>
- [41] S. Ichinose, “Casimir Energy of the Universe and the Dark Energy Problem,” *Journal of Physics: Conference Series*, vol. 384, p. 012028, Sep. 2012. [Online]. Available: <http://stacks.iop.org/1742-6596/384/i=1/a=012028?key=crossref.453d5fecfb9ce609bd0cddfc9ed7f5c>
- [42] A. Balcerzak and M. P. Dąbrowski, “Randall-Sundrum limit of f (R) brane-world models,” *Physical Review D*, vol. 84, no. 6, p. 063529, Sep. 2011. [Online]. Available: <https://link.aps.org/doi/10.1103/PhysRevD.84.063529>
- [43] T. Can, M. Laskin, and P. Wiegmann, “Fractional Quantum Hall Effect in a Curved Space: Gravitational Anomaly and Electromagnetic Response,” *Physical Review Letters*, vol. 113, no. 4, p. 046803, Jul. 2014. [Online]. Available: <https://link.aps.org/doi/10.1103/PhysRevLett.113.046803>
- [44] P. H. G. M. van Blokland and J. T. G. Overbeek, “van der Waals forces between objects covered with a chromium layer,” *Journal of the Chemical Society, Faraday Transactions 1: Physical Chemistry in Condensed Phases*, vol. 74, no. 0, p. 2637, 1978. [Online]. Available: <http://xlink.rsc.org/?DOI=f19787402637>

- [45] M. Sparnaay, "Measurements of attractive forces between flat plates," *Physica*, vol. 24, no. 6-10, pp. 751–764, Jan. 1958. [Online]. Available: <https://linkinghub.elsevier.com/retrieve/pii/S0031891458800907>
- [46] V. A. Parsegian, *Van der Waals Forces: A Handbook for Biologists, Chemists, Engineers, and Physicists*, 1st ed. Cambridge University Press, Nov. 2005. [Online]. Available: <https://www.cambridge.org/core/product/identifier/9780511614606/type/book>
- [47] S. K. Lamoreaux, "Demonstration of the Casimir Force in the 0.6 to 6 μm Range," *Physical Review Letters*, vol. 78, no. 1, pp. 5–8, Jan. 1997. [Online]. Available: <https://link.aps.org/doi/10.1103/PhysRevLett.78.5>
- [48] J. Błocki, J. Randrup, W. Świątek, and C. Tsang, "Proximity forces," *Annals of Physics*, vol. 105, no. 2, pp. 427–462, Jun. 1977. [Online]. Available: <https://linkinghub.elsevier.com/retrieve/pii/0003491677902494>
- [49] L. S. Brown and G. J. Maclay, "Vacuum stress between conducting plates: An image solution," *Physical Review*, vol. 184, no. 5, p. 1272–1279, Aug 1969.
- [50] J. Schwinger, L. L. DeRaad, and K. A. Milton, "Casimir effect in dielectrics," *Annals of Physics*, vol. 115, no. 1, p. 1–23, Sep 1978.
- [51] U. Mohideen and A. Roy, "Precision Measurement of the Casimir Force from 0.1 to 0.9 μm ," *Physical Review Letters*, vol. 81, no. 21, pp. 4549–4552, Nov. 1998. [Online]. Available: <https://link.aps.org/doi/10.1103/PhysRevLett.81.4549>
- [52] G. Bressi, G. Carugno, R. Onofrio, and G. Ruoso, "Measurement of the Casimir Force between Parallel Metallic Surfaces," *Physical Review Letters*, vol. 88, no. 4, p. 041804, Jan. 2002. [Online]. Available: <https://link.aps.org/doi/10.1103/PhysRevLett.88.041804>
- [53] G. Bressi, G. Carugno, A. Galvani, R. Onofrio, G. Ruoso, and F. Veronese, "Experimental studies of macroscopic forces in the micrometre range," *Classical and Quantum Gravity*, vol. 18, no. 18, p. 3943–3961, Sep 2001.
- [54] A. W. Rodriguez, J. D. Joannopoulos, and S. G. Johnson, "Repulsive and attractive Casimir forces in a glide-symmetric geometry," *Physical Review A*, vol. 77, no. 6, p. 062107, Jun. 2008. [Online]. Available: <https://link.aps.org/doi/10.1103/PhysRevA.77.062107>
- [55] M. A.D., "Retarded dispersion forces in dielectrics at finite temperatures," *Proceedings of the Royal Society of London. Series A. Mathematical and Physical Sciences*, vol. 274, no. 1356, pp. 80–90, Jun. 1963. [Online]. Available: <https://royalsocietypublishing.org/doi/10.1098/rspa.1963.0115>
- [56] A. W. Rodriguez, A. P. McCauley, J. D. Joannopoulos, and S. G. Johnson, "Casimir forces in the time domain: Theory," *Physical Review A*, vol. 80, no. 1, p. 012115, Jul. 2009. [Online]. Available: <https://link.aps.org/doi/10.1103/PhysRevA.80.012115>
- [57] A. P. McCauley, A. W. Rodriguez, J. D. Joannopoulos, and S. G. Johnson, "Casimir forces in the time domain: Applications," *Physical Review A*, vol. 81, no. 1, p. 012119, Jan. 2010. [Online]. Available: <https://link.aps.org/doi/10.1103/PhysRevA.81.012119>
- [58] M. T. H. Reid, A. W. Rodriguez, J. White, and S. G. Johnson, "Efficient Computation of Casimir Interactions between Arbitrary 3D Objects," *Physical Review Letters*, vol. 103, no. 4, p. 040401, Jul. 2009. [Online]. Available: <https://link.aps.org/doi/10.1103/PhysRevLett.103.040401>
- [59] A. Taflove and S. C. Hagness, *Computational electrodynamics: the finite-difference time-domain method*, 2nd ed., ser. Artech House antennas and propagation library. Artech House, 2000.
- [60] J. L. Zhang, Z.-X. Huang, and X.-L. Wu, "Casimir force in anisotropic materials with ac kerr effect," *Progress In Electromagnetics Research M*, vol. 38, p. 165–173, 2014.

- [61] F. Monteiro, S. Ghosh, E. C. van Assendelft, and D. C. Moore, “Optical rotation of levitated spheres in high vacuum,” *Physical Review A*, vol. 97, no. 5, p. 051802, May 2018. [Online]. Available: <https://link.aps.org/doi/10.1103/PhysRevA.97.051802>
- [62] G. Ranjit, M. Cunningham, K. Casey, and A. A. Geraci, “Zeptonewton force sensing with nanospheres in an optical lattice,” *Physical Review A*, vol. 93, no. 5, p. 053801, May 2016.
- [63] D. Rugar, R. Budakian, H. J. Mamin, and B. W. Chui, “Single spin detection by magnetic resonance force microscopy,” *Nature*, vol. 430, no. 6997, p. 329–332, Jul 2004.
- [64] A. A. Geraci, S. B. Papp, and J. Kitching, “Short-range force detection using optically cooled levitated microspheres,” *Physical Review Letters*, vol. 105, no. 10, p. 101101, Aug 2010.
- [65] C. D. Hoyle, U. Schmidt, B. R. Heckel, E. G. Adelberger, J. H. Gundlach, D. J. Kapner, and H. E. Swanson, “Submillimeter Test of the Gravitational Inverse-Square Law: A Search for “Large” Extra Dimensions,” *Physical Review Letters*, vol. 86, no. 8, pp. 1418–1421, Feb. 2001. [Online]. Available: <https://link.aps.org/doi/10.1103/PhysRevLett.86.1418>
- [66] R. Bennett and D. H. J. O’Dell, “Revealing short-range non-Newtonian gravity through Casimir–Polder shielding,” *New Journal of Physics*, vol. 21, no. 3, p. 033032, Mar. 2019. [Online]. Available: <http://stacks.iop.org/1367-2630/21/i=3/a=033032?key=crossref.0d2ecc62a2d8499ca3002219a3f67950>
- [67] I. Ciufolini, D. Dominici, and L. Lusanna, “High precision gravity measurements by atom interferometry,” in *2001, a Relativistic Spacetime Odyssey: Proceedings of the Johns Hopkins Workshop on Current Problems in Particle Theory 25, Firenze, 2001 (September 3-5)*. World Scientific, 2003, pp. 147–158.
- [68] N. Arkani–Hamed, S. Dimopoulos, and G. Dvali, “The hierarchy problem and new dimensions at a millimeter,” *Physics Letters B*, vol. 429, no. 3-4, pp. 263–272, Jun. 1998. [Online]. Available: <https://linkinghub.elsevier.com/retrieve/pii/S0370269398004663>
- [69] J.-M. Fournier, F. Merenda, J. Rohner, P. Jacquot, and R. P. Salathé, “Comparison between various types of multiple optical tweezers,” in *Optical Trapping and Optical Micromanipulation V*, vol. 7038. International Society for Optics and Photonics, Sep 2008, p. 70381G. [Online]. Available: <https://www.spiedigitallibrary.org/conference-proceedings-of-spie/7038/70381G/Comparison-between-various-types-of-multiple-optical-tweezers/10.1117/12.796518.short>
- [70] G. Winstone, R. Bennett, M. Rademacher, M. Rashid, S. Buhmann, and H. Ulbricht, “Direct measurement of the electrostatic image force of a levitated charged nanoparticle close to a surface,” *Phys. Rev. A*, vol. 98, p. 053831, Nov 2018. [Online]. Available: <https://link.aps.org/doi/10.1103/PhysRevA.98.053831>
- [71] P. Mestres, J. Berthelot, M. Spasenović, J. Gieseler, L. Novotny, and R. Quidant, “Cooling and manipulation of a levitated nanoparticle with an optical fiber trap,” *Applied Physics Letters*, vol. 107, no. 15, p. 151102, Oct. 2015. [Online]. Available: <https://aip.scitation.org/doi/abs/10.1063/1.4933180>
- [72] P. A. M. Neto and H. M. Nussenzveig, “Theory of optical tweezers,” *EPL (Europhysics Letters)*, vol. 50, no. 5, p. 702, Jun. 2000. [Online]. Available: <https://iopscience.iop.org/article/10.1209/epl/i2000-00327-4/meta>
- [73] A. T. M. A. Rahman, A. C. Frangeskou, P. F. Barker, and G. W. Morley, “An analytical model for the detection of levitated nanoparticles in optomechanics,” *Review of Scientific Instruments*, vol. 89, no. 2, p. 023109, Feb. 2018. [Online]. Available: <https://aip.scitation.org/doi/full/10.1063/1.5008396>
- [74] Y. Seol, A. E. Carpenter, and T. T. Perkins, “Gold nanoparticles: enhanced optical trapping and sensitivity coupled with significant heating,” *Optics Letters*, vol. 31, no. 16, p. 2429, Aug. 2006. [Online]. Available: <https://www.osapublishing.org/abstract.cfm?URI=ol-31-16-2429>

- [75] Symposium on Fundamental Biological Models, H. H. Pattee, United States, Office of Naval Research, Stanford University, and Biophysics Laboratory, Eds., *Natural automata and useful simulations; proceedings.* Washington: Spartan Books, 1966, oCLC: 1144414.
- [76] A. T. M. A. Rahman and P. F. Barker, “Optical levitation using broadband light,” *arXiv:2002.04650 [nlin, physics:physics, physics:quant-ph]*, Feb. 2020, arXiv: 2002.04650. [Online]. Available: <http://arxiv.org/abs/2002.04650>
- [77] N. Grønbech-Jensen and O. Farago, “A simple and effective Verlet-type algorithm for simulating Langevin dynamics,” *Molecular Physics*, vol. 111, no. 8, pp. 983–991, Apr. 2013, arXiv: 1212.1244. [Online]. Available: <http://arxiv.org/abs/1212.1244>
- [78] N. P. Bullier, A. Pontin, and P. F. Barker, “Characterisation of a charged particle levitated nano-oscillator,” *arXiv:1906.09580 [physics, physics:quant-ph]*, Jun. 2019, arXiv: 1906.09580. [Online]. Available: <http://arxiv.org/abs/1906.09580>
- [79] M. Y. Ivanov, M. Spanner, and O. Smirnova, “Anatomy of strong field ionization,” *Journal of Modern Optics*, vol. 52, no. 2-3, pp. 165–184, Jan. 2005. [Online]. Available: <http://www.tandfonline.com/doi/abs/10.1080/0950034042000275360>
- [80] S. Hogan and D. Cassidy, “Phas0023: Atomic and molecular physics,” *UCL Dept. Of Physics and Astronomy*, Mar. 2019.
- [81] R. A. Serway, *Physics for scientists and engineers / Raymond A. Serway, John W. Jewett, Jr.*, 9th ed. Australia ; United Kingdom: Brooks/Cole Cengage Learning, 2014.
- [82] K. Shimizu, J. Kristof, and M. Gabriel Blajan, “Applications of Dielectric Barrier Discharge Microplasma,” in *Atmospheric Pressure Plasma - from Diagnostics to Applications*, A. Nikiforov and Z. Chen, Eds. IntechOpen, Apr. 2019. [Online]. Available: <https://www.intechopen.com/books/atmospheric-pressure-plasma-from-diagnostics-to-applications/applications-of-dielectric-barrier-discharge-microplasma>
- [83] R. Brandenburg, “Dielectric barrier discharges: progress on plasma sources and on the understanding of regimes and single filaments,” *Plasma Sources Science and Technology*, vol. 26, no. 5, p. 053001, Mar. 2017. [Online]. Available: <http://stacks.iop.org/0963-0252/26/i=5/a=053001?key=crossref.f87ae03ac97273ad527b1350b51838fc>
- [84] U. Kogelschatz, “Dielectric-Barrier Discharges: Their History, Discharge Physics, and Industrial Applications,” *Plasma Chemistry and Plasma Processing*, vol. 23, no. 1, pp. 1–46, Mar. 2003. [Online]. Available: <https://doi.org/10.1023/A:1022470901385>
- [85] J. Soni and S. Roy, “Low pressure characterization of dielectric barrier discharge actuators,” *Applied Physics Letters*, vol. 102, no. 11, Mar. 2013. [Online]. Available: <http://aip.scitation.org/doi/10.1063/1.4796176>
- [86] H. S. Fricker, “Why does charge concentrate on points?” *Physics Education*, vol. 24, no. 3, pp. 157–161, May 1989. [Online]. Available: <http://stacks.iop.org/0031-9120/24/i=3/a=309?key=crossref.d34f0db8f18e1887385037704e3fec10>
- [87] “Chapter 5: Harmonic Oscillator,” Feb. 2014. [Online]. Available: [https://chem.libretexts.org/Bookshelves/Physical_and_Theoretical_Chemistry_Textbook_Maps/Supplemental_Modules_\(Physical_and_Theoretical_Chemistry\)/Quantum_Mechanics/06._One_Dimensional_Harmonic_Oscillator/Chapter_5%3A_Harmonic_Oscillator](https://chem.libretexts.org/Bookshelves/Physical_and_Theoretical_Chemistry_Textbook_Maps/Supplemental_Modules_(Physical_and_Theoretical_Chemistry)/Quantum_Mechanics/06._One_Dimensional_Harmonic_Oscillator/Chapter_5%3A_Harmonic_Oscillator)
- [88] “Alpha Radiation - an overview | ScienceDirect Topics.” [Online]. Available: <https://www.sciencedirect.com/topics/biochemistry-genetics-and-molecular-biology/alpha-radiation>
- [89] “Electron Guns - an overview | ScienceDirect Topics.” [Online]. Available: <https://www.sciencedirect.com/topics/earth-and-planetary-sciences/electron-guns>
- [90] “Neutron Emission - an overview | ScienceDirect Topics.” [Online]. Available: <https://www.sciencedirect.com/topics/engineering/neutron-emission>

- [91] E. A. Mason and W. E. Rice, “The Intermolecular Potentials for Some Simple Nonpolar Molecules,” *The Journal of Chemical Physics*, vol. 22, no. 5, pp. 843–851, May 1954. [Online]. Available: <https://aip.scitation.org/doi/abs/10.1063/1.1740200>
- [92] “Laser Ablation - an overview | ScienceDirect Topics.” [Online]. Available: <https://www.sciencedirect.com/topics/materials-science/laser-ablation>
- [93] D. Kasuya, F. Kokai, K. Takahashi, M. Yudasaka, and S. Iijima, “Formation of C₆₀ using CO₂ laser vaporization of graphite at room temperature,” *Chemical Physics Letters*, vol. 337, no. 1, pp. 25–30, Mar. 2001. [Online]. Available: <http://www.sciencedirect.com/science/article/pii/S0009261401001397>
- [94] “CODATA Value: alpha particle mass.” [Online]. Available: <https://physics.nist.gov/cgi-bin/cuu/Value?mal>
- [95] curtis.supplee@nist.gov, “Stopping-Power & Range Tables for Electrons, Protons, and Helium Ions,” Oct. 2009. [Online]. Available: <https://www.nist.gov/pml/stopping-power-range-tables-electrons-protons-and-helium-ions>
- [96] “Sulfur hexafluoride.” [Online]. Available: <https://webbook.nist.gov/cgi/cbook.cgi?ID=2551-62-4&Type=IR-SPEC&Index=QUANT-IR,7>
- [97] A. T. M. A. Rahman and P. F. Barker, “Optical levitation using broadband light,” *arXiv:2002.04650 [nlin, physics:physics, physics:quant-ph]*, Feb. 2020, arXiv: 2002.04650. [Online]. Available: <http://arxiv.org/abs/2002.04650>
- [98] F. Tebbenjohanns, M. Frimmer, A. Militaru, V. Jain, and L. Novotny, “Cold Damping of an Optically Levitated Nanoparticle to micro-Kelvin Temperatures,” *Physical Review Letters*, vol. 122, no. 22, p. 223601, Jun. 2019, arXiv: 1812.09875. [Online]. Available: <http://arxiv.org/abs/1812.09875>
- [99] B. J. Ruck and T. Kemmitt, “Materials Science Forum,” in *Advanced Materials and Nanotechnology*. Zurich: Trans Tech, 2011.
- [100] A. G. Atkins and M. Escudier, *A Dictionary of Mechanical Engineering*. OUP Oxford, 2019, oCLC: 1110066129. [Online]. Available: <https://doi.org/10.1093/acref/9780198832102.001.0001>
- [101] W. J. Kim, A. O. Sushkov, D. A. R. Dalvit, and S. K. Lamoreaux, “Surface contact potential patches and Casimir force measurements,” *Physical Review A*, vol. 81, no. 2, p. 022505, Feb. 2010. [Online]. Available: <https://link.aps.org/doi/10.1103/PhysRevA.81.022505>
- [102] C. C. Speake and C. Trenkel, “Forces between Conducting Surfaces due to Spatial Variations of Surface Potential,” *Physical Review Letters*, vol. 90, no. 16, p. 160403, Apr. 2003. [Online]. Available: <https://link.aps.org/doi/10.1103/PhysRevLett.90.160403>
- [103] R. S. Decca, D. López, H. B. Chan, E. Fischbach, D. E. Krause, and C. R. Jamell, “Constraining New Forces in the Casimir Regime Using the Isoelectronic Technique,” *Physical Review Letters*, vol. 94, no. 24, p. 240401, Jun. 2005. [Online]. Available: <https://link.aps.org/doi/10.1103/PhysRevLett.94.240401>
- [104] R. O. Behunin, F. Intravaia, D. A. R. Dalvit, P. A. M. Neto, and S. Reynaud, “Modeling electrostatic patch effects in Casimir force measurements,” *Physical Review A*, vol. 85, no. 1, p. 012504, Jan. 2012. [Online]. Available: <https://link.aps.org/doi/10.1103/PhysRevA.85.012504>
- [105] A. Liscio, V. Palermo, and P. Samorì, “Nanoscale Quantitative Measurement of the Potential of Charged Nanostructures by Electrostatic and Kelvin Probe Force Microscopy: Unraveling Electronic Processes in Complex Materials,” *Accounts of Chemical Research*, vol. 43, no. 4, pp. 541–550, Apr. 2010. [Online]. Available: <https://pubs.acs.org/doi/10.1021/ar900247p>
- [106] R. O. Behunin, Y. Zeng, D. A. R. Dalvit, and S. Reynaud, “Electrostatic patch effects in Casimir-force experiments performed in the sphere-plane geometry,” *Physical Review A*, vol. 86, no. 5, p. 052509, Nov. 2012. [Online]. Available: <https://link.aps.org/doi/10.1103/PhysRevA.86.052509>

- [107] R. Dubessy, T. Coudreau, and L. Guidoni, “Electric field noise above surfaces: A model for heating-rate scaling law in ion traps,” *Physical Review A*, vol. 80, no. 3, p. 031402, Sep. 2009. [Online]. Available: <https://link.aps.org/doi/10.1103/PhysRevA.80.031402>
- [108] F. Chen and U. Mohideen, “Recent experimental advances in precision Casimir force measurements with the atomic force microscope,” *Journal of Physics A: Mathematical and General*, vol. 39, no. 21, pp. 6233–6244, May 2006. [Online]. Available: <http://stacks.iop.org/0305-4470/39/i=21/a=S14?key=crossref.7b6d346e52a3151eed4ab0ebc8ee700>

X APPENDICES

1 Code

Overleaf is the full code for the simulation. A visual animation of the simulation is available at:
<https://imgur.com/a/LhCxVYT>

```

1 from vpython import *
2 import numpy as np
3
4 # initialises the various arrays used
5 xPosData = np.array([])
6 yPosData = np.array([])
7 zPosData = np.array([])
8 timeData = np.array([])
9 velocityComponents = np.zeros(3)
10
11 # initialises the time counter and loop counters
12 i = 0
13 count = 0
14
15 # sets the canvas size
16 canvas(width=2400, height=1400) # slightly bigger than
   default, adjust if you have small screen.
17
18 # sets the time step
19 dt = 10e-8
20
21 # creates the canvas
22 box = box(pos=vector(0,0,0), length=10e-8, height=10e-8,
   width=10e-8, opacity=0.1) ## sets the size of the box
23
24 ## values for constants used in later equations
25 nanoM = 1e-18
26 gasM = 5.46e-26
27 alphaM = 6.644e-27
28 sf6M = 2.425e-25
29 c60M = 1.197e-24
30 T = 293
31 kB = 1.38e-23
32 P_gas = 500
33 nanor = 199e-9
34 rho = 1850
35
36 ## marks the centre where potential is zero, for reference
37 centrePos = vector(0,0,0)
38 Centre = sphere(pos=centrePos, radius= 10e-11, color=color.
   white)
39
40 # sets the nanoparticle's initial position
41 nanoxPos = 2.65e-6
42 nanoyPos = 1.35e-6
43 nanozPos = 1.2e-6 #-51

```

```

44 initNanoPos = vector(nanoxPos, nanoyPos, nanozPos)
45
46 ## sets the nanoparticle's intital velocity
47 nanoxVel = 0
48 nanoyVel = 0
49 nanozVel = 0
50 nanoVel = vector(nanoxVel, nanoyVel, nanozVel)
51
52 ## creates the nano particle with values defined above
53 nanoParticle = sphere(pos=initNanoPos, radius=10e-10, color
    =color.blue, make_trail=True, retain = 50, interval=1)
54 nanoParticle.trail_color = color.white # change the trail
    colour to white, or any colour you fancy
55 nanoVector = nanoParticle.pos
56 nanoVectorMag = mag(nanoVector)
57
58 ## creates a set of orthogonal arrows and labels to mark
    the co-ordinate axes
59 xArrow = arrow(pos=vector(box.length/2+0.1*box.length,0,0
    ), axis=vector(0.15*box.length,0,0), shaftwidth=10e-10,
    color=color.red)
60 xLabel= label(pos=vec(box.length/2+0.1*box.length + 1.1*
    xArrow.length,0,0), text='x', color=color.red)
61 yArrow = arrow(pos=vector(box.width/2+0.1*box.length,0,0),
    axis=vector(0,0.15*box.length,0), shaftwidth=10e-10, color=
    color.blue)
62 yLabel= label( pos=vec(box.width/2+0.1*box.length,1.1*
    yArrow.length,0), text='y', color=color.blue)
63 zArrow = arrow(pos=vector(box.height/2+0.1*box.length,0,0
    ), axis=vector(0,0,0.15*box.length), shaftwidth=10e-10,
    color=color.green)
64 zLabel= label(pos=vec(box.height/2+0.1*box.length,0,1.1*
    zArrow.length), text='z', color=color.green)
65
66 # defines the paramaters for vpythons dynamical graphing
67 graphpos = graph(x=2000, y=2000, width=1000, height=500,
    title='Position Vs Time', xtitle='time /s', ytitle='
        Position /m',
68                                     foreground=color.black, background=color.
    white)
69 graphVel = graph(x=2000, y=2000, width=1000, height=500,
    title='Velocity Vs Time', xtitle='time /s', ytitle='
        Velocity /ms^-1',
70                                     foreground=color.black, background=color.
    black)
71 graphKE = graph(x=2000, y=2000, width=1000, height=500,

```

```

71 title='KE Vs Time', xtitle='time /s', ytitle='KE',
72                                     foreground=color.black, background=color.
    black)
73 graphHist = graph(x=2000, y=2000, width=1000, height=500,
    title='Position Frequency', xtitle='Position', ytitle='
    Frequency',
74                                     foreground=color.black, background=color.
    black)
75
76 x_pos = gcurve(graph=graphpos, color=color.red, label='x
    position')
77 y_pos = gcurve(graph=graphpos, color=color.blue, label='y
    position')
78 z_pos = gcurve(graph=graphpos, color=color.green, label='z
    position')
79
80 x_vel = gcurve(graph=graphVel, color=color.red, label='x
    velocity')
81 y_vel = gcurve(graph=graphVel, color=color.blue, label='y
    velocity')
82 z_vel = gcurve(graph=graphVel, color=color.green, label='z
    velocity')
83
84 c = (8*kB*T/gasM/pi)**0.5 #Particle mean speed
85 b = ((1 + pi/8)*c*P_gas*gasM)/(kB*T*nanoR*rho) #gas
    damping term
86
87 gasMomentum = c*gasM
88
89 Sthermal = 4*kB*T*gasM*b # the thermal energy equation
90
91 thermalX = Sthermal
92 thermalY = Sthermal
93 thermalZ = Sthermal
94
95 def casimirForce(x):
96     casimirForceNewtons = (-8e-13)*x**6 + (9e-11)*x**5 - (
        4e-9)*x**4 + (9e-8)*x**3 - (1e-6)*x**2 + (5e-6)*x - 4e-6
97     if x < 6e-6 or 3e-6 < x:
98         casimirForceNewtons = 0
99     return casimirForceNewtons
100
101 ## the entire simulation takes place within this while
    Loop
102 while True:
103

```

```

104      ## sets the magnitude of the restoration force on each
105      #axis
106      restForceMagX = (1.42e-7)*abs(nanoVector.x)
107      dampingForceMagX = b * abs(nanoVel.x)
108
109      restForceMagY = (5.68e-7)*abs(nanoVector.y)
110      dampingForceMagY = b * abs(nanoVel.y)
111
112      restForceMagZ = (8.88e-7)*abs(nanoVector.z)
113      dampingForceMagZ = b * abs(nanoVel.z)
114
115      distanceToPlate = 1e-6 + nanoVector.z ## calculates
116      # the distance to the , with the plate set at -1e-6 m on the
117      # z axis
118
119      ## checks the position of the particle to decide in
120      # what direction the restoring force/ thermal energy input
121      # should act
122
123      if nanoVector.x > 0:
124          nanoVel.x = nanoVel.x - dt * restForceMagX / nanoM
125      else:
126          nanoVel.x = nanoVel.x + dt * restForceMagX / nanoM
127
128      if nanoVector.y > 0:
129          nanoVel.y = nanoVel.y - dt * restForceMagY / nanoM
130      else:
131          nanoVel.y = nanoVel.y + dt * restForceMagY / nanoM
132
133      if nanoVector.z > 0:
134          nanoVel.z = nanoVel.z - dt * (restForceMagZ -
135          casimirForce(distanceToPlate))/ nanoM
136      else:
137          nanoVel.z = nanoVel.z + dt * (restForceMagZ +
138          casimirForce(distanceToPlate))/ nanoM
139
140      ## checks the velocity of the particle to decide in
141      # what direction the damping force should act
142
143      if nanoVel.x > 0:
144          nanoVel.x = nanoVel.x - dt * dampingForceMagX + dt
145          *thermalX
146      else:
147          nanoVel.x = nanoVel.x + dt * dampingForceMagX - dt
148          *thermalX
149
150      if nanoVel.y > 0:

```

```

140         nanoVel.y = nanoVel.y - dt * dampingForceMagY + dt
        *thermalY
141     else:
142         nanoVel.y = nanoVel.y + dt * dampingForceMagY - dt
        *thermalX
143
144     if nanoVel.z > 0:
145         nanoVel.z = nanoVel.z - dt * dampingForceMagZ + dt
        *thermalY
146     else:
147         nanoVel.z = nanoVel.z + dt * dampingForceMagZ - dt
        *thermalX
148
149     ## simulates gas particle collisions
150     if np.random.randint(0,1001)>999: ## rolls a random
        number to decide if collision has occurred
151         i = 0
152         while i < 3:
153             velocityComponents[i] = np.sqrt(kB*T/gasM)*np.
        random.normal(0,1)
154             i = i + 1
155
156     # calculates the momentum associated with the gas
        particle velocity on each axis
157     xPortion = velocityComponents[0]*gasM
158     yPortion = velocityComponents[1]*gasM
159     zPortion = velocityComponents[2]*gasM
160
161     # updates the momenta of the nanoparticle
162     nanoXMomentum = nanoVel.x * nanoM + xPortion*np.random
        .randint(0,101)/100
163     nanoYMomentum = nanoVel.y * nanoM + yPortion*np.random
        .randint(0,101)/100
164     nanoZMomentum = nanoVel.z * nanoM + zPortion*np.random
        .randint(0,101)/100
165
166     nanoVel.x = + nanoXMomentum / nanoM ## adds an
        impulse to the velocity on each axis
167     nanoVel.y = + nanoYMomentum / nanoM
168     nanoVel.z = + nanoZMomentum / nanoM
169
170     ## simulates SF6/C60/alpha collisions. Delete as
        appropriate
171     if np.random.randint(0,10001)>9999: ## rolls a random
        number to decide if collision has occurred
172         Impulse = 0.01*(3e8)*alphaM      ## Alpha particle

```

```

173         #Impulse = 0.0001 * (3e8) * sf6M ## SF6 particle
174
175         nanoMomentum = nanoVel.x * nanoM + Impulse*np.
176         random.randint(0,101)/100
177         nanoVel.x += nanoMomentum/nanoM
178
179         nanoVector.x = nanoVector.x + nanoVel.x * dt + dt * dt
180         * restForceMagX/(2*nanoM)
181         nanoVector.y = nanoVector.y + nanoVel.y * dt + dt * dt
182         * restForceMagY/(2*nanoM)
183         nanoVector.z = nanoVector.z + nanoVel.z * dt + dt * dt
184         * restForceMagZ/(2*nanoM)
185
186         nanoParticle.pos = nanoVector # sets the new
187         nanoParticle position to the updated position vector
188         nanoVectorMag = mag(nanoVector)
189
190         # advances the times counter
191         count = count + dt
192
193         #dynamically displays the postion/velocity time graphs
194         # to the screen
195         x_pos.plot(pos=(count, nanoVector.x))
196         y_pos.plot(pos=(count, nanoVector.y))
197         z_pos.plot(pos=(count, nanoVector.z))
198
199         x_vel.plot(pos=(count, nanoVel.x))
200         y_vel.plot(pos=(count, nanoVel.y))
201         z_vel.plot(pos=(count, nanoVel.z))
202
203         timeData = np.append(timeData, count)
204         xPosData = np.append(xPosData, nanoVector.x)
205         yPosData = np.append(yPosData, nanoVector.y)
206         zPosData = np.append(zPosData, nanoVector.z)
207
208         # provides a visual counter for the number of data
209         # points saved that is printed to the screen
210         if i < 100:
211             i = i + 1
212
213         if i >= 100:
214             print("The number of xPosData points is: ",
215             xPosData.size)
216             i=0
217
218         # saves the position and time data as CSVs

```

```
211     np.savetxt('timeData.csv', timeData)
212     np.savetxt('xData.csv', xPosData)
213     np.savetxt('yData.csv', yPosData)
214     np.savetxt('zData.csv', zPosData)
215
216     rate(200) ## sets the animation rate
217
218
219
```

```

In [12]: import numpy as np
import matplotlib.pyplot as plt

In [13]: omega = np.arange(0,40,0.001)

In [18]: nanoM = 1e-18
gasM = (1.66e-27)*29 # Gas particle mass (from Prof Barker)
nanoR = 199e-9 # From Prof Barker paper
rho = 1850 # From Prof Barker paper
T = 293
kB = 1.38e-23
P_gas = 5

c = (8*kB*T/gasM/np.pi)**0.5 # Particle mean speed
b = ((1 + (np.pi/8))*c*P_gas*gasM)/(kB*T*nanoR*rho) # Gas damping term
beta = 10 #b/nanoM
# Prof Barker set this to 10 to get the correct shape of the
# So we need a b value that makes beta in the order of 10^1

#k_x = 1.42e-7
k_x = 377*nanoM

omega0 = (k_x/nanoM)**0.5

psd = (2*kB*T*beta)/(np.pi*nanoM*((omega0*omega0) - (omega*omega))**2 + (beta*beta*omega*omega))

print(b)
print(beta)
print(k_x)

plt.plot(omega,psd)
plt.title('PSD vs ω (x axis)')
plt.xlabel('ω')
plt.ylabel('PSD')

```

Figure 47: The code used to generate the power spectral density.

2 Finances

In order to complete the experiment, certain items had to be purchased as they were not available within the department.

Gold nanoparticles were necessary for the first experiment (optical traps). The nanoparticles were supplied by the research team led by Professor Barker. The cost for these particles was £400, and was reclaimed by the research group. For more information, please email Professor Peter Barker at p.barker@ucl.ac.uk.

In order to complete the second part of the experiment, a gold pinhole was necessary. Details are given in [The apparatus](#). A custom pinhole was designed with Thorlabs Inc. Thorlabs inc is available at <https://www.thorlabs.com>. The structure was copper with one gold plated face, and featured a 3um pinhole and a thickness of 25um. The price of the pinhole was £97.07. However due to the exceptional circumstances due to the Covid-19 pandemic, the experiment had to be cut short and the pinhole was not purchased.

No financing is needed for this experiment. The nanoparticles were bought by the research group led by Perter Barker, and the pinhole order was cancelled.

3 Contingency Plan

Due to the exceptional situation caused by the Coronavirus (Covid-19) pandemic, certain measures had to be taken to ensure a good continuation of the project and maximize our work within the best of our abilities.

Due to the outbreak, UCL decided to close access to a number of its facilities to protect the health and safety of its staff and students on the 13th of March 2020. In the context of our experiment, this meant that the members of this project no longer had access to the lab C.15 where our experiments were conducted. The preliminary experiment aimed at trapping the nanoparticles was successfully completed on the 11th of March 2020. A second experiment aimed at observing and trapping the Casimir effect was scheduled to take place the following week (16th of March 2020). As a direct consequence of not being able to perform the second experiment, the team focused instead on the direct comparison of the data from the preliminary experiment with the data obtained from the simulations. The focus of the team was also diverted onto perfecting the model for the simulations.

Prof Peter Barker was aware of the situation and supported the group's decisions in the given context.

Health and safety regulations enforced social distancing in an attempt to slow the spread of the virus. As a result, all communications, whether internal (within our group) or external (with our supervisor Prof Barker) had to be done virtually.

Slack was used during the full duration of the project to facilitate internal communications. Slack is an instant messaging app that uses channels and private messages to allow a clear and ordered flow of information. This proved essential due to the large quantity of information and was the backbone of the communication within our group. Microsoft Teams is a digital hub that merges instant messaging, file sharing and audio and video calls. This app was used to support live internal and external meetings. Prof. Barker was an experienced user of the app, which allowed a seamless transition from in-person meetings to virtual meetings. Live file sharing and screen sharing capabilities complemented the audio calls as they allowed access to any data that needed to be shared during the meeting.

The Covid-19 Pandemic caused a certain number of challenges, to which this group had to adapt to complete the project. Thanks to the reactivity of this team, as well as the support of our supervisor Prof. Barker and certain platforms such as Slack and Microsoft team, this team was able to adapt quickly and efficiently to overcome these challenges.

4 Risk Assessment

RISK ASSESSMENT OF LABORATORY WORK

**PHYSICS AND ASTRONOMY DEPARTMENT
UNIVERSITY COLLEGE LONDON**

HAZARD ASSESSMENT OF LABORATORY PROJECT

These forms must be completed for each new experimental project for undergraduate students, certified by the Supervisor and submitted to the Departmental Safety Officer

SUPERVISOR: Professor Peter Barker

PROJECT TITLE: Measuring forces using levitated nanoparticles

Apart from normal laboratory hazards that are covered in the Departmental Code of Practice, will the work involve any of the following special hazards?

- | | | |
|----|--|-----|
| 1. | Physical hazards arising from radiation, high voltage, high pressure,
ultrasonic, lasers, etc.? | YES |
| 2. | Special hazards of fire or explosion? | NO |
| 3. | Hazards arising from the use of known toxic or carcinogenic
compounds? | NO |

Please go to Page 2.

SUPERVISOR'S CERTIFICATION OF ASSESSMENT

If your answers to questions 1-3 are all NO and you are satisfied with the following statement, you should sign and date below.

If your answer to any of the questions 1-3 is YES, you should:

1. discuss with relevant Safety Officer (Laser,Radiation,Electrical or Departmental) precautions to be taken
2. append a sheet giving details of the special hazards, and explaining the precautions which you will take to protect the personnel involved and any other people such as College maintenance staff, cleaners or students who may enter the laboratory.
3. sign and date below, having read the following statement.

I have assessed the above project with respect to the Health and Safety Regulations as set out in the Departmental Safety Handbook and associated Safety Advisory Unit publications. The appropriate specialised Departmental Safety Officer has been notified of any work involving radiation, lasers, electrical, chemical or other identified hazards and precautions taken to protect personnel. I certify that the work will be carried out according to the Departmental Code of Practice and (if required) the further code that is appended, so that exposure to hazardous substances and other risks will be minimised. I undertake to review this assessment if the nature of the work should change, or if any unforeseen hazards should be encountered.

Signed: P. Barker

Date: 12/03/2020

PLEASE NOTE

One copy of this form should be retained by the supervisor, one copy sent to the Project Co-ordinator (Angelos Michaelides) and the original sent to the Departmental Safety Officer.

Department: Physics and Astronomy

Risk Assessment Form

WORK/PROJECT TITLE: Optical levitation of nanoparticles

LOCATION(S): C15

DESCRIPTION OF WORK: Observation of data collection by PhD student for 3rd year group project.

PERSONS INVOLVED: Omar Abbas, Peter Brown, Dorsa Nasrollahi Shirazi

HAZARD IDENTIFICATION (state the hazards involved in the work) Consider **Chemicals** (an additional assessment will also be needed), the **environment, equipment, manual handling, electrical equipment, fire and explosion, disposal of waste**.

Potential for stray laser light used for optical trapping experiments.

RISK ASSESSMENT (assess the risks involved in the work and state high, medium or low risk)

The risk of this is low as the optical setup was not adjusted by the students. They simply observed the data collection process carried out by a PhD student.

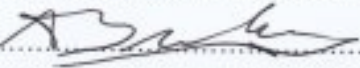
CONTROL MEASURES (say how you will reduce the risk to an acceptable level.)

Laser googles were worn to avoid all laser light. The room has an interlock to prevent unauthorized access.

DECLARATION

I the undersigned have assessed the work, titled above, and declare that there is no significant risk / the risks will be controlled by the methods stated on this form (delete as applicable) and that the work will be carried out in accordance with Departmental codes of practice.

Name.....Arthur Breabout.....

Signed..........

Supervisor... P. Barker.....

Date...4/03/2020....

Signed.....

Date.....

5 Safety Certificates



Nima Bagherzadeh Akbari

COURSE HISTORY

Course Name	Status	Enrolled	Completed	Score	Pass/Fail
Principles of Laboratory Safety at UCL	Completed	26/03/2020	26/03/2020	100%	Passed
Principles of Risk Assessment	Completed	26/03/2020	26/03/2020	0%	Passed



Arthur M C Breabout

COURSE HISTORY

Course Name	Status	Enrolled	Completed	Score	Pass/Fail
Principles of Risk Assessment	Completed	01/03/2020	01/03/2020	0%	Passed
Principles of Laboratory Safety at UCL	Completed	01/03/2020	01/03/2020	100%	Passed



Peter J Brown

COURSE HISTORY

Course Name	Status	Enrolled	Completed	Score	Pass/Fail
Principles of Risk Assessment	Completed	06/03/2020	06/03/2020	0%	Passed
Principles of Laboratory Safety at UCL	Completed	06/03/2020	06/03/2020	83%	Passed



UCL Certificate of Achievement

Alex Groth

has satisfactorily completed the course

Principles of Laboratory Safety

UCL Safety Services

Date



Generated by UCL Moodle



Yanek Nasiruddin

COURSE HISTORY

Course Name	Status	Enrolled	Completed	Score	Pass/Fail
Principles of Laboratory Safety at UCL	Completed	26/02/2020	27/02/2020	83%	Passed
Principles of Risk Assessment	Completed	26/02/2020	26/02/2020	0%	Passed



Dorsa Nasrollahi Shirazi

COURSE HISTORY

Course Name	Status	Enrolled	Completed	Score	Pass/Fail
Principles of Laboratory Safety at UCL	Completed	27/02/2020	01/03/2020	83%	Passed
Principles of Risk Assessment	Completed	26/02/2020	01/03/2020	0%	Passed
GDPR online training for all staff	Completed	24/10/2018	24/10/2018	80%	Passed



UCL Certificate of Achievement

Muhammad Usman

has satisfactorily completed the course

Principles of Laboratory Safety

UCL Safety Services

February 2, 2020

Date



Generated by UCL Moodle

MISSING: Omar

6 Agenda and minutes

Full Group Meeting 1 (Group 2)

21/01/2020

Agenda:

- Understanding of goals:
 - measurement of short range forces that can be measured with 100 nm nanoparticles levitated in high vacuum.
 - measuring the repulsive Casimir force, as well as thermal Casimir forces, in vacuum using optical levitation.
 - designing and carrying out the experiment in the laboratory
 - ways in which the forces can be calibrated using known processes such as Brownian motion induced by background collisions or by collisions with a single charged particle
- Possible suggested reading
- Experimental setup
- Times we can use labs
- Risk assessment for labs
- Budget - will we need to buy anything?
- Sub tasks - agree on some if there are any
- Deadlines - set up actions and milestones for next meeting

Present:

- Professor Barker
- Dorsa Nasrollahi Shirazi
- Peter Brown
- Alex Groth
- Nima Bagherzadeh Akbari
- Omar Abbas
- Raees Usman
- Yanek Nasiruddin
- Arthur Breabout

Tabled items:

- Risk assessment for labs
- Budget - will we need to buy anything?

Minutes:

Professor Barker presentation (sent via email to the group after the meeting)

- Levitate 100nm sized particle. Using optical or electrical field, can isolate particle from environment- interesting for work in QM. Use masses 10 -18 kg so it is massive for QM – unexplored. Does QM still hold? What may make it difficult to see?

- Cavity Optomechanics:
 - Cooling of oscillators to smaller scale. Control and cooling of light
 - Can fabricate and put in properties you can have
 - But since we are levitated- don't have that much engineering capability
- Interferometry
 - Mass wave interferometry- can use MF to separate out two components of spin
- Detecting quantum gravity – looking at interaction between two superposition of the two particles
- Can cool and hold in isolated vacuum for long time- useful for looking at short forces
- Holding to mirror and measuring gravity
- Gravitational frequency wave detector – as gravitational wave passes, trap changes in size
- Where we are now
 - Optical tweezers: trapping, cooling and manipulation in vacuum – 3D trap, harmonic at bottom. Can look at motion. Looking at motional temp not internal.
 - Heating and decoherence
- Prevent cooling: noise – if you don't take out gas, there is collisions with gas particles
- Recoil: if you trap particle in light, there is random scattering which is a kick. Direction it's scattered is different to direction it comes. Random and continuous momentum change.
- When cooling suppressing heating due to collision – like Brownian motion
- Blackbody radiation
- Charged particle trap (pole trap)- does not have scattering problem since it does not use light.

Understanding goals

- Preliminary calculations
 - Look at short range forces, collisions between levitated Nanospheres (electrical/pole trap or optical trap?)
 - Can we see a single collision from an atom or neutron for example – what range of momentum shift can we expect to see
 - K and m are all we need now for preliminary calculations
 - Look at interactions that occur between these collisions
 - Understanding how an oscillator works
 - Understand oscillators that we have. At specific temp, have and average amplitude. Defines how cold it needs to be to see something
- Simulations
 - Just do calculations first before looking at simulations.
 - stochastic simulations: divide it up after looking at essential physics. Can use matlab/ mathematica/ python
 - Only important things now: frequency and mass. Consider it as oscillators in all 3 dimensions. Choose frequency from: 100Hz – 100 KHz masses: 10 -18 to 10-12 kg.
- Experimental limitations

- calculate how much can we resolve to
- Conducting experiments
 - Do experiment in the lab on what looks promising and feasible
 - Particles are placed inside via a syringe, put particles in liquid (alcohol), liquid gets highly charged and expels itself so alcohol evaporates and you are left with particle. Vibration but only works with specific particles
 - Using silica dioxide Small particle: cross section small. Good to have a large array of small particles.
 - Other particles: can levitate He Nano droplets 155mK, YbLf
 - Looking at neutrons: may need to use light elements.
 - Charge trap: more sensitive on the charge, also easier to see a kick at lower frequency, lower the spring constant, the easier it is to see
 - Measuring: track optically with camera (is possible), moving interference pattern
 - Optical trap: since there are collisions, it is almost like having a bath of gas around it.
 - Repulsive force: have a pin hole, take a particle and it becomes repulsive.
 - Data points expected from one simulations: hold particles for a few months
 - Typically measure displacement.
- Look at dark matter candidates
 - Research possible major dark matter candidates

Possible suggested reading

- Look at Professor Barker's powerpoint presentation
- Read papers related to area of research
- Use textbooks for revision

Experimental setup

- We can use the existing experimental set-up UCL research group is using
- We will need to think about the particle source we will need after the preliminary calculations

Times we can use labs

- We will be shown the labs next week

Action points:

- Revise quantum harmonic oscillators
- Conduct calculations for changes in momentum, energy, charge, displacement etc for a chosen particle colliding with a silica particle (K and m are what we need for this)

(Feedback not provided)

Full Group Meeting 2 (Group 2)

28/01/2020

Agenda:

- Calculating momentum change (velocity), displacement, charge
 - what initial energy value do we use for the incoming particle- what energy will/can our source have
 - do we find a range of energies i.e. if it loses max energy or no energy at all
 - what is the value for the spring constant we use when calculating displacement
 - what particle sources do we actually have
- Preliminary simulations
 - How strong is the vacuum used? Needed to work out particle density
 - Show example of the simulation
- Risk assessment for labs
- Budget - will we need to buy anything?

Present:

- Professor Barker
- Dorsa Nasrollahi Shirazi
- Peter Brown
- Alex Groth
- Nima Bagherzadeh Akbari
- Omar Abbas
- Raees Usman
- Yanek Nasiruddin
- Arthur Breabout

Tabled items:

Minutes:

Calculating momentum change (velocity), displacement, charge

- Finding energy of incoming alpha particle collision
 - Americium
 - 4 MeV is typical alpha particle energy
 - Graph of energy deposited as a function of depth
 - Only 20Kev deposited, can be found online
 - Stopping power
 - Monte Carlo simulations
 - **Electron**
 - Energy can be controlled using electron gun
 - Choose an energy so that the 'kick' on the nanosphere is measurable

- K value
 - Frequency ~ 60kHz, 120kHz, 170kHz, (so about 100kHz)
 - Use mass and frequency to find k constant
- T in the order of 1mK
- The collisions causes a ‘kick’ which then decays into the original stochastic wavefunction
 - Using a high pass filter we can isolate the kick from the rest of the wavefunction
- Fluctuation dissipation theorem
- Bath uses average energy to compensate for cooling
- Its possible for nanoparticle to become ionised which needs to be avoided
- **Optical trap**
 - Different restoring force in different dimensions.
 - Due to light’s polarization in different directions and fluctuations in light intensity
 - 100kHz frequency range
 - Lasers used are NDYAG
 - Electrodes are used to slow down the motion of the particle to cool it down, however also speeds up the damping of the particle.
- Only actual particle is cooled down, the area around it (like a gas) will be at room temperature
- Vacuum strength
 - 10^{-8} mBar
- Sources
 - Cannot use neutron source but still worth exploring
 - Experimentally options are
 - Electrons
 - Alpha particles
 - Heavy gas particles
 - Avoiding having them stick to nanoparticle
 - ‘Accommodation coefficient’
- Ions
 - Neutrals are better
 - How to shoot particles (neutrals)
 - Valve with a magnet leading into a vacuum chamber
 - Can be opened and closed easily, only some particles will collide with target (ideal)
 - Accelerated particles to supersonic speed
 - Ex. Helium goes to 1800 m s^{-1}
 - heavier gases go slower
 - SF6
 - Ions
 - Instead of filament you have discharge in chamber

- Get a mix of neutrals and ions (issue)
- Amplification of data using potential difference (?)

Budget - will we need to buy anything?

- Nothing needed to buy currently

Risk assessment for labs

- Lasers are low energy
- Depends on the source used

Preliminary simulation

- Simulation
 - Acceleration term, damping term, spring term, and stochastic function $f(t)$
 - $F(t)$ will average to zero (can be ignored)

Action points:

- Look at different sources and find the maximum 'kick' (displacement) that can be expected at various energies
- Need to zero in on a specific experiment
- Continue simulations
- Divide up specific tasks

Feedback from board member:

- It is most important that all members of the group are equally engaged in this project
- The group needs to divide up the work
- This should be a broad exploration of potential interactions and modelling

Full Group Meeting 3 (Group 2)

11/02/2020

Agenda:

- Calculating momentum change (velocity), displacement, charge
 - NIST database for energy lost during interaction
 - PDG ionisation energies
- Preliminary simulations
- Explain electric field amplification in more detail
- Set up that will be used to investigate the casimir effect
- Refining of objectives

Present:

- Professor Barker
- Dorsa Nasrollahi Shirazi
- Peter Brown
- Alex Groth
- Nima Bagherzadeh Akbari
- Omar Abbas
- Raees Usman
- Yanek Nasiruddin
- Arthur Breabout

Tabled items:

Minutes:

- Delegated tasks between individuals of the simulation group

Calculating momentum change (velocity), displacement, charge

- Calculations carried out for electrons, alpha particles
- Density for silica, two values discussed, but ultimately the difference between the two would not have much of an effect on end results
- Discussed explicitly the calculations carried out – attempted in both relativistic and classical schemes, lead to very different but still wrong answers. Need to show step-by-step calculations to see what's going wrong
- Discussed what was needed from getting a value for ionisation energy
- Marked difference between collisions with neutral particles and charged particles regarding ionising the nanoparticle, charged particle ionisation stronger than neutral particle

- 6 - 9 MeV ionisation energy for electrons in silica
- Casimir effect – are we measuring change in the damping?
 - Casimir effect changes the shape of the oscillation curve
 - In practice, would be induced by bringing nanoparticle close to another object (e.g. glass gold), causes attractive interaction
 - Measure position as a function of time with effect active, make a histogram of results to give a probability distribution – can be used to measure the focus of experiment i.e. check how to optimise parameters of experiment
 - If material is gold, and nanoparticle placed close to a certain point on gold surface, gives a repulsive interaction
 - Attractive Casimir force more feasible to measure

Preliminary simulations

- Discussed the simulation details in depth, simulation now randomly gives a ‘kick’ to the nanoparticle, intend to tune further to lab conditions, each kick changes the mode of oscillation of nanoparticle
 - Found that lower energy particle kicks dampen the oscillation, while higher energy kicks impart energy to the oscillations
 - Approximation can be made to the mass of the nanoparticle due to relative size of nanoparticle
 - Advised to keep trying to simulate actual collisions with the nanoparticle, will give more insight into the effects of the kicks, should give rise to a thermal distribution consistent with the gas particles used

Set up that will be used to investigate the Casimir effect

- Explained the trap in more detail
- Collisions can be amplified via electric fields of the trap – gives rise to relatively large kicks, then a noticeable ring-down of the particle
- Larger number of gas particles gives higher pressure, vastly increases number of calculations
- Experiment pressure 10^{-5} milliBar
- Can compare the collision energy to the energy of the scattering laser to get an idea of how large a kick would be observed

Explain electric field amplification in more detail

- Can test for how much the nanoparticle has been ionised by collisions by changing the electric field strength to observe the response of the nanoparticle
- Going through details of optical trap
 - Lense with quadratic profile, illuminate with to focus very tightly
 - Capture light with another lense to collimate the light
 - Incident beam split into two beams
- Half Light goes to one detector, other half goes to another detector, signals compared

- If the particle moves the difference in signal changes, this is used to compensate for motion of the nanoparticle
- issue of nanoparticle becomes charged, coulomb interaction dominates the other interactions we may want to observe
- Coulomb interaction can be measured against strength of optical trap
- Should observe how much force acted upon nanoparticle under electric field for one unit of charge, i.e. nanoparticle with electron charge value, so that during experiment charge of the nanoparticle can be easily measured and accounted for
- Laser beam could be used to vaporise material to create gas particles we need
- Asked if the optical trap laser beams could be used to accelerate the gas particles – answer was no

Action points:

- Hand in step-by-step calculations done for necessary velocity of electrons
- Come to a conclusion on what particles we should use
- Divide up simulation objectives into individual tasks assigned to members

Feedback from board member:

“A good meeting and looks like more people are engaged in the project. But, perhaps not everyone. Please make sure this is the case.”

Full Group Meeting 4 (Group 2)

17/02/2020

Agenda:

- Calculations
 - Were there any errors in the calculations
 - Would we be able to use beta decay source as electron source
- Simulations
- The risk assessment is closed
- When can we start experiment

Present:

- Professor Barker
- Dorsa Nasrollahi Shirazi
- Peter Brown (unavailable)
- Alex Groth
- Nima Bagherzadeh Akbari (sick)
- Omar Abbas
- Raees Usman
- Yanek Nasiruddin
- Arthur Breabout

Tabled items:

Minutes:

Calculations

- Electron
 - Finding particle velocity
 - Assuming the electron is stationary
 - Considering that the electron collides with the nano particle
 - Electron absorbed into it
 - Electron has quite a low mass.
 - Need a pretty high energy electron to give it a decent kick.
- SF6
 - To make a beam of SF6
 - Valve, electromagnetic stopper

- Mix it with helium very high velocity
- Helium supersonic beam
- 5-10% helium
- SF6 dominated by helium and dragged along
- Inside chamber has its own thermal motion
- It accelerates as it's exiting
- 1-D Boltzmann distribution as all particles are going in the same direction
- Speed of sound in helium
- Library book: Molecular beam methods by Scoles
- Decided to use SF6
- Parker valves, supersonic expansion
- Look at the interface with the vacuum system
- Research The Casimir force
 - Have a look at Nima's Paper
 - See if Force is comparable to the optical force
- For SF6 no need to do the charge calculations

Simulations

- Current model presented
- Further work required

When can we start experiment?

- Look at Casimir first
- Complication with this molecular beam
- Use a Parker Valve
- Vacuum chamber
 - Want gas to flow
 - Using a skimmer, we can have a very directed beam
 - Want to give the particle a tap, depends on how short we can open the valve for (microseconds)
 - Want to open the valve for the shortest period of time
 - Do not want to leak too much gas
- Look at Parker Hannifin Valve series 99
- Contact BOC Gasses
 - What regulator is required
 - Mix of 10% SF6, 90% Helium
 - 5 Litres
- Look at Laser Ablation C60
- Electrons are bound by 9eV
 - If you keep the energy below that, then all the energy would transfer in the collision
 - If the energy is too high, internal processes
 - Ion Beam may be suitable
- Sharp pin: Creates field ionisation
 - Put metal or C60 on the tip

- Field emission around a sharp tip

Action points:

- Research The Casimir force
 - Have a look at Nima's Paper
- Contact BOC Gasses
 - What regulator is required
 - Mix of 10% SF6, 90% Helium
 - 5 Litres
- Look at certain papers
 - Look at Laser Ablation C60
 - Look at dielectric Barrier Discharge
 - Look at Field emission around a sharp tip
- Compare SF6 and C60 and see which would be better to use

Next Week timetable

- Group meeting Tuesday 2pm in Prof Barker's office
- 1 on 1 meetings after the group meeting next Tuesday

Full Group Meeting 5 (Group 2)

25/02/2020

Agenda:

- Reviewing and completing SF6 and C60 calculations
- Adjusting simulations
- Research in:
 - Casimir force experimental set up
 - Laser ablation C60
 - SF6 regulator mix with H2 (10:90 ratio)
 - Dielectric barrier discharge
- The lab course is closed - we must complete this course to be able to start experiment
- Risk assessment
- When can we start experiment

Present:

- Professor Barker
- Dorsa Nasrollahi Shirazi
- Alex Groth (ill)
- Nima Bagherzadeh Akbari
- Omar Abbas
- Raees Usman
- Yanek Nasiruddin
- Arthur Breabout (away, family emergency)
- Peter Brown

Tabled items:

Minutes:

Reviewing and completing SF6 C60 Calculations

Yanek: Looked over calculations found K is wrong but cancels out. Old calculations apply for SF6, not done for C60 yet.

Adjusting Simulations

Graphs showing real time for displacement and velocity.

Next sophistication: background gas collisions and collisions we are interested in. Even with gas collisions, unless it's really low pressure you'll have continuous collisions.

Gold hole experiment decided upon

Research plasmonic resonance in gold.

Include the measurement and the simulation.

Focus on this paper:

<https://www.hindawi.com/journals/jnt/2016/1746908/>

<http://www.jpier.org/PIERM/pierm38/17.14072111.pdf>

How much do we talk about other papers in the final report?

Talk about all of them:

- This is what they've done
- This is why they're useful

Give background and show research

Chosen experiment is useful because it fits the best with what our equipment is.

Do we want to completely rip all the ions away?

Won't be easily done- **you should look at it because it should be interesting.**

Research how we could use a pin with SF₆ on it that has a very high electric field where you can actually extract ions (field emission).

What's the effect on the potential caused by the Casimir force? Measure the motion of the gold particle and invert to find the potential.

Question is : you've got this potential, how much will the distortion be, how sensitive does the experiment have to be. For example, you might want the aperture closer, or further away to see if you can measure the difference. Calculate energy distribution and then overlap them.

Peter has trapped gold before, any absorption can actually melt it.

Would we need to take any systematic errors into account?

The plate needs to be neutral. You can ground the plate. You can also neutralise using UV light.

The lab course is closed

Lab course: can't be accessed.

Must contact Angelos Michaelides for info

Risk assessment

Review will be done by Professor Barker

Meeting later in the week: Friday 1pm

Action points:

Look at pin holes

Look for a translation stage – calibrate with an interference pattern

Add leapfrog integration to the course – Peter send an email to Peter

<https://arxiv.org/abs/2002.04650>

Continue looking at how you would get atoms, either discharge or pin method

Trap something, measure the potential.

Check if Potential is big enough from Casimir compared to the optical potential.

Research plasmonic resonance in gold.

SF6 regulator mix – if Arthur can send details, Peter can let him know what we need

Atoms- Full Group Meeting 6 (Group 2)

28/02/2020

Agenda:

- Possible questions on the 2 research papers
- Research
 - Look at pin holes
 - Look for a translation stage – calibrate with an interference pattern
 - Plasmonic resonance in gold
 - Electrostatic patches
- Continue looking at how you would get atoms, either discharge or pin method
- Add leapfrog integration to the course
- Check if Potential is big enough from Casimir compared to the optical potential.
- SF6 regulator mix
- Details of gold
- When can we start experiment

Present:

- Professor Barker
- Dorsa Nasrollahi Shirazi
- Alex Groth
- Nima Bagherzadeh Akbari
- Omar Abbas
- Raees Usman
- Yanek Nasiruddin
- Arthur Breabout (away, family emergency)
- Peter Brown

Tabled items:

Minutes:

Research

Atoms – pin and discharge

Omar's transit idea (flow of charge between 2 plates, mediated by C60 charge carriers moving back and forth) – barker says unlikely

Dielectric barrier discharge discussed

Want to maintain vacuum, that's advantage of the pin method, disadvantage of using high flow rate discharge?

Comparing effective potential to optical potential

Group - Not sure how to start calculations

Response - 1st stage is to overlap the two potentials and see how the new shape looks

2nd Stage – Experimental - you build up a histogram of the position and invert the histogram to change back to potential

Plasmonic resonance

Surface electrons in macroscopic conductors but because nanoparticle, all electrons oscillate due to an electric field.

Occurs at certain frequencies so want to avoid those to prevent heating

Electrostatic patches

Force depends on size, need to see if they are significant or negligible
They can be factored into calculations, if necessary.
Barker - Want to find ways of cleaning the nanoparticle to remove the dielectric impurities.
Laser may heat it sufficiently to do this
Translation stage – Barker is handling it
Leapfrog integration
Raees did it, also added damping term, reported that had little to no effect
Barker - Find power spectral density to compare with damping term

SF6 regulator mix

Barker - SF6 – downselect (deprioritise) for now

Gold size

– just been sent apparently

When can start experiment

– probably next week

Lit review – should we do one?

Apparently more of a background review of topics considered and ideas discussed:

Casimir force, optical tweezers, measuring small forces at short range, things that have been discussed, options that were considered and why they weren't used

Other stuff to include in report- comparison between simulations and measured data.

Query: How many people in lab?

– 1 operating, 2-3 present, post doc supervision

Assembly line style – people in lab get data --> pass on to others for data analysis

Action points:

- **TOP PRIORITY: Look at gold pinhole – where to order, NEEDS TO BE DONE EARLY NEXT WEEK - Arthur**
- Potential Comparison – alex, nima, dorsa, yanek
 - Process potential-position curve for Casimir
 - Process potential-position curve for elastic
 - Plot Sum (potentially use a slider in python to toggle position of Casimir potential) and elastic. Barker advised just a “by eye” analysis of whether Casimir potential stands out
- Start writing the report – headings at least – ?Everyone?
- Power spectral density – compare damping? – Raees + Peter
- Pin electrostatic discharge - Omar

Next meeting

12:15pm Tuesday – Barker's room

Full Group Meeting 7 (Group 2)

03/03/2020

Agenda:

- Casimir and optical potential calculations
- Buying:
 - Pin holes
 - Gas mixture
- Simulations
- Set date to start experiment
- Discuss writing of formal report + poster

Present:

- Professor Barker
- Dorsa Nasrollahi Shirazi
- Alex Groth
- Nima Bagherzadeh Akbari
- Omar Abbas
- Raees Usman
- Yanek Nasiruddin
- Arthur Breabout
- Peter Brown

Tabled items:

Minutes:

Casimir and optical potential calculations

- Will the thickness change the potential?
- There is no analytical expression
- Barker told us not to worry about that, use the quadratic potential and Casimir potential and sum them up
- Compare with and without potential
- There is no analytic expression for the anharmonic potential
- Choose a point that will make a biggest difference to the potential
- Possible use of a slider to shift the Casimir potential
- Use the information from the paper we have been looking at

Simulations

Power spectral density

- The strongest frequency we observe will be the resonant frequency

- Find what frequency components are within the noise
- See where the noise is within the spectrum

Damping

- Gamma is a function of pressure
- We can vary damping rate by changing the pressure or temperature
- At a high temperature the distribution of the potential will spread out
- Plot of the combinations of the two potentials for next time

Gas

- Downselected the SF6 gas
- We will use what we have available in the lab, nitrogen or helium.

Pinholes

- Pinhole can be purchased from Thorlabs
- Custom pieces are available
- Approach them for a custom piece

Histogram

- Use the position as a function of time graph from the simulations group
- Divide the axis into increments
- Everything that falls into those increments you can put into a bin for the histogram

Histogram for the two potentials

- We know the values of k and T
- Calculate $U(x)$ which is defined as $U(x) = -kT(\ln(p(x))) - \ln(c)$
- C is an offset which means the DC component is not important
- Set c, so the midpoint of the trap is zero in the potential

Report

- Doesn't need to be as long as the reports completed in the previous years
- We are measuring small forces not just short range forces
- Talk about experimental history of Casimir force

Calculations

- Casimir effect - what happens if you have a charge, see the effect on the potential
- The particle may not have a net charge but may have a dipole moment
- Do a calculation of the possibility of a torque due to the moment
- Check how this will effect of general calculations

Dielectric barrier discharge

- Barker says 10KPa of pressure will work
- Minimum separation distance of 1.5mm
- Redo the calculations for next time
- Look at the needles with field emissions
- Even though we are not using needles just write about it for the review

- Traps are custom made so there is no name or make

Low pressure will result in the gold deforming

High temperature will cause the gold to melt

With the gold there was no shrinking in size only a change in shape

Action points:

- Send a plot of the potential to Prof Barker this week
- Plan a meeting with the group this week to start writing the report
- Implement the power spectral density equation that was shown to Barker after the meeting and compare with the data

Next meeting

Monday at 6:00pm – Prof Barker's room

Full Group Meeting 7 (Group 2)

09/03/2020

Agenda:

- Casimir and optical potential calculations- share findings
- Simulations
- Buying pin holes
- Starting the experiment
- Formal report- go through outline of the final report
- Poster- discuss specific titles that we should include

Present:

- Professor Barker
- Dorsa Nasrollahi Shirazi
- Alex Groth
- Nima Bagherzadeh Akbari
- Omar Abbas
- Raees Usman
- Yanek Nasiruddin
- Arthur Breabout
- Peter Brown

Tabled items:

Minutes:

Casimir and optical potential calculations- share findings

- Using the spring constant and numbers from the Chinese paper, still quite prominently below the x axis
- New implementations make a big difference at small distances.
- Check that same numbers in the other paper (PRL 2010)

Simulations

- Damping value from the paper sent implemented.
- Changed to another number to see the damping.
- Velocity Verlet Method
- C60 collisions damping to absolute 0 every time.
- Bring a video of the running simulation next time.
- Compare with the numbers.
- Do an interpolation at a very fine level.
- Also look at classic fit, but may not be as effective.

Buying pin holes

- Structure and dimensions
 - The piece would be copper based with one gold face
 - It would have a 3um pinhole and a thickness of 25 um
- Thickness:
 - Thickness of the custom piece will have to be bigger than what was requested
 - However there will still be an attractive Casimir effect
- Deadline: Need the piece for next week

Starting the experiment

- On Wednesday
- 3 people

Formal report- go through outline of the final report

- *Aims and objectives*
 - Talk about discussions and thought process behind it
 - Exploring the possibilities of using this apparatus to measure forces.
 - Start really generally.
 - Other forces: Collisions: collisions with ions, electrons, etc.
 - Certain approximations and assumptions were made.
 - Need to map it out and relate to what happened but not exactly.
- *Lit review*
 - Add Gravitational short range forces to small ranged forces
 - Background gas: Momentum kicks, Brownian motion.
 - How is this useful? How could we use this to measure things.
 - We've been tasked with this apparatus that works in this particular way.
 - What people use it for: Short range forces.
 - What we've considered: Pros and cons for each of those.
 - Show the path.
- Early next week: comparison between the simulations and what we've measured

Poster- discuss specific titles that we should include

- Not really doing quantum stuff: don't really need to talk about trapped quantum states
- Graphs and explain them. Going through each and explain the story.
- A0 poster size

Action points:

- Calculations
 - Check that same numbers in the other paper (PRL 2010)
- Simulations
 - Do an interpolation at a very fine level.
 - Also look at classic fit, but may not be as effective.
- Pinhole
 - Deadline: Need the piece for next week
- Report
 - Changes for aims and objectives, as well as the literature review
- Experiment
 - Prof Barker will email for the time on Wednesday for the lab group
- Next group meeting
 - Meeting with Prof Barker on Monday at 6pm

Feedback from board member:

“The group appears to be operating very well with a high level of co-operation.”

Full Group Meeting 9 (Group 2)

16/03/2020

Agenda:

- Casimir and optical potential calculations- share findings
- Simulations
- Experiment continuation?
- Formal report- go through progress
- Poster- how will we make one with no findings

Present:

- Professor Barker
- Dorsa Nasrollahi Shirazi
- Alex Groth
- Nima Bagherzadeh Akbari
- Omar Abbas
- Raees Usman
- Yanek Nasiruddin
- Arthur Breabout
- Peter Brown

Tabled items:

Minutes:

Casimir and optical potential calculations- share findings

- Position of 0?
- Can move the harmonic potential away from the zero point
 - > 1 micron away or half a micron away
- That way you can see both sides of the harmonic potential

- Pressure seems a bit high at 250.
- Lowest pressure attained was 5 millibar.

Prof Barker will have a look at the experimental results.

Simulations

- Y and z axis no collisions.
- Constant driving force to stop it from decaying completely.

- Add in the Casimir potential
 - See how that changes the displacement and the shape at the graph
- Pressure: 5 millibar
- Feedback: looks good.
 - Visualization would be good for the poster session.
- Much better for 5.4 millibar
- 3 frequencies available

- Use the lower frequency to compare with the simulations 0.055MHz

Experiment continuation?

- Useful to see this data and analyze.
- Will not be able to do any further experimentation.
- The second part (interaction with the pinhole) will have to be explained in the report.
—> How we would have proceeded with the experiment and what we would have done with the data.
- Purchase of the pinholes has been canceled

Formal report- go through progress

- Must link to the Casimir effect
- Bring together into one big section
- Send Prof. Barker a draft of the whole thing.
- Call in a couple of days
- Need to write about the experiment that we will no longer be able to do.
- Was about to put the aperture in from Thorlabs.
- Give a prediction on how the experiment would've proceeded.
- How we would've analyzed the data, and what we expected.
- With the data get a histogram
- Calibrate the data (pressure given in the filename)
- Look at significant gravitational force between the pinhole and the particle
- Introduce a section about how we dealt with consequences from the pandemic.
- Compare the Power spectral density of the simulation with that of the data.
- Try and commit to sending a rough draft by Wednesday.
- Talk afterwards on Wednesday at 5pm.

Poster- how will we make one with no findings

- Format: Pdf or powerpoint. Prezi?
- Maybe use a link?
- Format of live Q&A will be given in days to come.
- Would be interesting to have an animation running during the presentation.

Action points:

- *Calculations*
 - Try moving the harmonic potential away from the zero point

- *Simulations*
 - Add the Casimir potential
- *Data Analysis*
 - Use the lower frequency to compare with the simulations for 0.055MHz
- *Formal report*
 - Various comments on different sections
 - Detail can be found in Formal report section of the minutes

Full Group Meeting 10 (Group 2)

18/03/2020

Agenda:

- Casimir and optical potential calculations
- Simulations
- Formal report- go through progress
- Formal report and poster split up
- More meetings as a group

Present:

- Professor Barker
- Dorsa Nasrollahi Shirazi
- Alex Groth
- Nima Bagherzadeh Akbari
- Omar Abbas
- Raees Usman
- Yanek Nasiruddin
- Arthur Breabout
- Peter Brown

Tabled items:

Minutes:

Casimir and optical potential calculations

- Put a filter across the data (using the picoscope software)
 - Tools -> Math channels -> Create -> Advanced -> Filters -> High, Mid or Low Pass
 - High pass filter (allows frequencies higher than 20k Hertz)
 - Need to setup a new filter around the peak (13 kiloHertz up to 92 kiloHertz)
 - That will give info around that peak
- Easiest thing to do is to get a histogram
- Once data is filtered, will be easier to fit histogram
- Want to use all 66 time stamps

Simulations

- Take data and do a power structure density of it
 - Will help broaden spectrum
- Will need to have a longer time series to have a broader frequency spectrum

Formal report progress

- Add sections as soon as possible so that Prof Barker can have a look and give feedback
- Dorsa's Lit Review
 - Too broad, a lot of historic context
 - Would give the current view of the Casimir force and how it generally works
 - Keep the different models
- Gas Particle Production
 - Don't need to add unnecessary equations, unless it is complicated
 - It's fine to have it as text
- Simulations part
 - Need to talk about what method you're using to solve it
- Chosen Experiment
 - Reference the article sent by Prof Barker that uses the same apparatus (but different light source)
- Experimental problems
 - If the experiment is done at too lower pressure, risk of gold melting
 - As gas pressure decreases, cannot cool it as much
 - Even if they get hot, their center of mass motion increases as well
 - Using that, can look if we need to take this into account
- Final summary
 - Get the other stuff done first

Poster

- Once the bulk of the report has been written, will separate the group into two groups of four: one for the poster, one for finishing up the writeup of the report.

Meeting at 11am on Thursday to separate the groups

Action points:

Data analysis

- Put filter on data (Instructions are given in the minutes)
- Fit a histogram on the filtered data

Simulations

- Do a power structure density of the simulation data

Formal report

- Breakdown of individual sections given in minutes

Poster

- Internal meeting on Thursday 19/03 at 11am to discuss separation of tasks for poster

MISSING: MEETING 11

XI ACKNOWLEDGMENTS